Faculty of Engineering of University of Porto

University of Sheffield

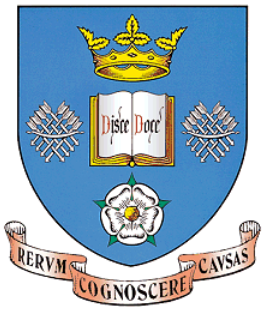

Influence of hydrodynamic conditions on bacteria physiology and behavior

by

Leonam Vieira Gonçalves

Dissertation held under the Master Degree in Bioengineering – Major in Biological Engineering

Advisors: Prof. Manuel Simões; Prof. Lucia Simões and Prof. Catherine Biggs
Supervisor: Dr. Esther Karanukaran
September 13th 2013

© Copyright by Vieira Gonçalves, Leonam, 2013

Abstract

The hydrodynamic conditions have been shown to have a significant impact on bacteria swimming, collective motion and cohesive structure formation. Those are notable aspects of microbial dynamics and were shown to be relevant for wide range of applications. Nevertheless, the need for a deeper insight about the direct influence of hydrodynamics on microbial behavior and physiology at planktonic state remained latent. Aiming to overcome that, the present study focused on the characterization of bacterial growth and physicochemical properties of cell surface grown under different agitations speeds.

The influence of distinct hydrodynamic conditions on growth of *Acinetobacter calcoaceticus* was evaluated by growth and substrate consumption curve elaboration. It was observed that cells under slower agitation speed presented a significant lower growth rate with higher biomass yield in terms of reducing sugars (substrate) consumption. Moreover, the metabolic activity of microbial cultures was evaluated by respirometry, which showed higher total respiratory activity in mid-exponential growth phase was achieved for cells grown under higher agitation speed. Thus, it was concluded that observed differences in terms of cell growth and respiratory activity across different agitation speeds could be the result of distinct cellular dynamics, which are the product of an interplay between physical (mass transfer issues) and biological (energy uncoupling between anabolism and catabolism) phenomena.

In terms of cell surface properties, suspensions of *A. calcoaceticus* cultivated in distinct hydrodynamic conditions were examined by Microbial Adhesion to Hydrocarbons (MATH) assay, electrophoretic mobility measurement, Fourier transform infrared spectroscopy (FTIRS) and X-ray photoelectron spectroscopy (XPS). These experiments showed that bacteria cells cultivated under distinct agitation speeds possess different cell surface chemistry as well as hydrophobicity and cell surface charge differences. The influence of hydrodynamics on those properties is important as cell-cell and cell-abiotic surface interactions were reported to rely on it. For instance, it was found in this study that microbial cells at lower agitation speed had a higher trend to auto-aggregate, which demonstrates enhancement at the level of cell-cell interactions. It was also shown that polysaccharides and proteins account for most changes at cell surface level across different agitation speed, where higher content of those macromolecules were attained for

bacterial cells cultivated under higher agitation speeds. It was hypothesized that lipopolysaccharides (LPS) with long O-antigen structure could be more abundant at surface of cells cultivated under higher agitation speeds. This was explained by LPS physicochemical properties like hydrophilicity and cell mechanical stability enhancement.

Since the influence of hydrodynamics on *A. calcoaceticus* dynamics was the main goal of the present study, proteomic studies through tandem mass spectrophotometry (LC-MS/MS) were carried out to verify differences in terms of outer membrane protein (OMP) expression. It was reported that cells cultivated at higher agitation speed had a higher number of proteins linked to transport and receptor mechanisms. Hence, it was concluded that cells under higher agitation speed may have a more complete apparatus to sense the environment, and may present higher metabolic response to environmental changes. Besides, differences at the level of iron metabolism and pathogenicity factors were reported. That suggests cells cultivated at higher agitation speeds may present higher cellular adaptation capability in different hosts.

The present study showed that hydrodynamics can be regarded as an important cell cultivation parameter at planktonic state as it was reported that cell surface chemistry and growth dynamics seem to be affected. The differences observed for cells at planktonic state help to understand differences found in the literature in terms of bacteria collective behavior and coherent structure formation across different hydrodynamic conditions.

Acknowledgements

First of all, I would like to deeply thank my advisor in the University of Porto, Prof. Manuel Simões for all the scientific advices, constructive suggestions and for believing I would be capable of achieving interesting results throughout the project by means not only of hard work, but by positive thinking as well. Of course, I would also like to deeply thank my advisor in the University of Sheffield, Prof. Catherine Biggs, for advising and giving me the opportunity to work in such a great environment like the Department of Chemical and Biological Engineering (CBE). Thanks to her I was able to contact and perform a wider range of experiments, which made this work to become even more interesting to me.

I would also like to extend my gratitude to my supervisor, Dr. Esther Karunakaran, who guided me through the many experiments (even in holidays) and helped me to overcome a lot of problems with patience. Thanks to her I was introduced to great people like Dr. Narciso Couto, Dr. Henriette Jensen and Dr. Bharathi Ramalingam, who also gave me valuable advices throughout the project and showed me that a lab can also be a fun place.

I believe my adaptation and accommodation in Sheffield would not be possible without the help of two people who were my first true friends in United Kingdom, Jennifer Dick and Simon Vardy. They were really nice to me even when I was unfairly complaining about the city.

Last, but not least, I would like to thank and dedicate this dissertation to my beloved parents, José Manuel and Francisca for the unconditional support, love and care throughout the entire course. I owe them every challenge I was able to overcome.

Table of Contents

List of Figures

List of Tables

Symbols and Abbreviations

List of symbols

A (%)	Auto-aggregation index
A_A	Optical density at 600 nm at 1h after suspension preparation
A_B	Optical density at 600 nm at 0h after suspension preparation
A_C	Optical density at 600 nm of control suspension
A_M	Optical density at 600 nm of test suspension after mixing with *n*-hexadecane
D_M	Diffusion rate of molecule
E	Rate of strain of the flow field
e	Swimming direction
f	Angular velocity
h	Wave amplitude
H (%)	Hydrophobicity index
J	Oseen tensor
k	Wave number
k_e	Empirical factor
L	Biofilm thickness
M	Signaling molecule concentration
p	Probe value
p_s	Dipole strength
r	Distance to dipole
S_f	Reducing sugars concentration at the end of exponential phase
S_i	Reducing sugars concentration at the beginning of exponential phase
S_m	Bacterium surface
t	Time
t_j	Traction force
U	Translation velocity
u_y	Vertical velocity
X_f	Biomass concentration at the end of exponential phase
X_i	Biomass concentration at the beginning of exponential phase
$Y_{X/S}$	Yield of biomass in terms of reducing sugars consumption
β	Hydrolysis rate
γ	Cell aspect ratio
ζ	Detachment rate
ζ_{max}	Maximum detachment
μ	Specific growth rate
μ_f	Fluid viscosity
τ	Shear stress
Ω	Rotation velocity

ω	Vorticity of flow field

List of abbreviations

ATP	Adenosine triphosphate
ATR-FTIR	Attenuated total reflectance Fourier transform infrared
ATR-FTIRS	Attenuated total reflectance Fourier transform infrared spectroscopy
CID	Collision induced dissociation
DNS	3,5 dinitro salicylic acid
EPM	Electrophoretic mobility
EPS	Extracellular polymeric substances
FTIR	Fourier transform infrared
HPLC	High performance liquid chromatography
LB-A	Luria-Bertani medium with agar
LC-MS/MS	Liquid chromatography couples with tandem masss spectrometry
LC/MS	Liquid chromatography coupled with mass spectrometer
LPS	Lipopolysaccharides
MATH	Microbial adhesion to hydrocarbon
OD	Optical density
OMP	Outer membrane proteins
PCA	Principal component analysis
rpm	Rotation per minute
TOC	Total Organic Carbon
SDS-PAGE	Sodium dodecyl sulphate polyacrylamide gel electrophoresis
TSB	Tryptic Soy Broth
XPS	X-ray photoelectron spectroscopy

1. Introduction

1.1 Background information

It is well known that many abiotic physical and chemical factors influence metabolic activity, growth of microorganisms and even survival. Nutrient availability, temperature, pH and water activity are the main factors and the impact of each of them is substantially different from organism to organism (Madigan et al., 2000; Atlas and Bartha, 1987). Another important factor is related to hydrodynamic conditions, which are shown to influence collective behavior of bacteria, mainly swarming, turbulent-like motion and coherent aggregation, such as biofilm formation. These behaviors are part of bacteria dynamic system and are regarded as protective mechanisms, which lead to effects on foraging, transport of metabolites and signaling events (Drescher et al., 2011; Copeland and Weibel, 2009).

The role of hydrodynamic conditions on bacterial adhesion to surfaces and biofilm formation has been widely studied due to many problems regarding biofilm control and application of biofilms in the environmental technology field, more specifically wastewater treatment (Nicolella et al., 2000). It was verified that hydrodynamics possess great impact on biofilm structure, activity (Pereira et al., 2002) and heterogeneity in terms of bacterial community (Rochex et al., 2008). There are two main ways by which hydrodynamic stress is known to affect biofilm formation and development: i) mass transport effect involving transport of dissolved solutes into and out of the biofilm and ii) shear stress, which is associated to the application of force that may cause biofilm to move and detach (Stewart, 2012). The latter is mathematically defined by Equation 1-1, as follows:

$$\tau = \mu_f \frac{dv_x}{dy} \quad \text{(Equation 1-1)}$$

Where τ stands for shear stress (Pa), which is proportional to the fluid velocity profile with fluid viscosity (μ_f) as proportionality constant (de Campos, 2003).

The velocity field of the fluid in contact with microbial layer and the shear stress developed under certain flow regimes influence formation, structure and stability of biofilms. Those parameters are interlinked and may influence diffusion rate of cells and nutrients as well as formation of detachment force. For instance, it is known that biofilms which are grown under turbulent flow have a distinct architecture in such way they are thinner, denser and have higher content of extracellular polymeric substances (EPS) (Pereira et al., 2002). It is expected that microbial metabolism will be affected at some level, since density and thickness will influence resistance to diffusion of nutrients and affect microenvironment surrounding cells (Liu and Tay, 2001a).

Despite the influence of hydrodynamics on biofilm structure has been attributed in the literature mainly to physical phenomenon, biological phenomenon has played a role as there are evidences that microbial cells can respond to hydraulic shear by changing morphology, growth rate, cell size and metabolic activity (Chen and Huang, 2000; Simões et al., 2007). For instance, it was reported that as shear stress increases, cell growth yield reduces and 2-(p-iodophenyl)-3-(p-nitrophenyl)-5-phenyl tetrazolium chloride (INT) dehydrogenase activity increases concomitantly. Hence, shear stress influenced metabolism at both catabolic and anabolic levels (Liu and Tay, 2001b). Besides, Stoodley et al. (1999) showed that hydrodynamic conditions have greater impact on biofilm formation and structure than cell signaling events (known as quorum sensing). Although those evidences about the effect of hydrodynamic conditions on biofilm development and cell metabolism are experimentally verified, the mechanisms by which those phenomena occur are not fully understood yet and models that describe the influence of hydrodynamic parameters on cell behavior are still required.

Large-scale coherence processes such as biofilm formation and co-aggregation has an initial step composed by physical movements to initiate bacterium-to-bacterium contact and/or bacterium-to-surface contact, which involves mainly cell mobility and hydrodynamic force (Pratt and Kolter, 1998). Thus, several theoretical models at microscopic level focusing physical aspects of bacterial dynamics in suspension have been developed and they are based on flow field around a bacterium. It is believed that long-range hydrodynamic interactions are important for cell-cell/surface interactions (Najafi and Golestanian, 2010). Despite that, Drescher et al. (2011) observed that stochasticity (mainly associated to thermo- and chemotaxis) drowns the effects of long-range hydrodynamic for cell-cell interactions. However, they discovered that hydrodynamics play a role on cell-surface interaction when bacterium is within few

microns of the surface, which may influence the collective behavior (Drescher et al., 2011). A macroscopic evidence of this phenomenon was achieved by Lecuyer et al. (2011) that showed shear stress increased significantly the residence time of *Pseudomonas aeruginosa* adhesion, where there is formation of specific (known as catch-bonds) and non-specific bonds.

In order to have a deeper insight on the influence of hydrodynamics at a micro- (interaction between single cells), meso- (collective motion) and macroscopic levels (biofilm formation) and predict cell distribution as well as steady-state profile of adsorption, models that describe the physical phenomenon of attraction have been developed (Berke et al., 2008). These models can assume bacteria as non-Brownian particles for study of near-field interactions and describe bacteria movement and noise of the system (mainly associated to collision and roughness of surfaces) (Metzger and Butler, 2010). Hence, these models are useful analytical tools at different levels since they tend to describe bacteria collective motion and behavior, which can be used to obtain important parameters for development of models that account for hydrodynamic effect on biofilm formation for example.

In this context, the present section aims to review the current state-of-the-art on the influence of hydrodynamics on microbial cell behavior with emphasis on biofilm formation and metabolic induced changes. Furthermore, hydrodynamic models at microscopic scale and description of bacterium flow field will be presented.

1.2 Physical aspects: Long-range hydrodynamics

As discussed earlier, bacterial collective motion and behavior at microscopic scale are triggered by biochemical and physical events where hydrodynamics may play a major role. An example of biochemical event is the quorum-sensing phenomenon, where quorum-sensing bacteria produce and release auto-inducers which can be detected by other bacteria and alter their gene expression and behavior (Waters and Basslers, 2005). On the other hand, long-range hydrodynamic forces and far-field hydrodynamic interactions represent physical events related to bacterial dynamics (Najafi and Golestanian, 2010). For instance, Ishikawa and Hota (2006) showed that hydrodynamic forces instead of biological reactions mainly induced changes in direction between two swimming cells, which may impact collective motion.

In order to better comprehend the role of these interactions in bacterial collective behavior, models have been developed to predict bacteria walk, diffusion and collision with surfaces. Unlike chemo- and thermotaxis, which considers bacterial movement as random and net movement caused by gradients of nutrient concentration and temperature (Adler, 1966), the models for long-range hydrodynamics are deterministic and have been successful to describe experimental data (Drescher et al., 2011; Ishikawa and Hota, 2006). These models are continuum, since microorganism is generally much smaller than the flow field under analysis and variables are mainly volume-averaged quantities (Metcalfe et al., 2004). Despite the fact hydrodynamic coupling for cell-cell and cell-surface interaction has been almost exclusively described in terms of far-field interactions; Ishikawa et al. (2006) found out that near-field interactions also play a role on the stability of swimming motions and trajectories. Thus far-field and near-field interactions should be analytically described.

1.2.1 Bacteria movement and cell-surface interaction

Bacteria locomotion often arises from flagella rotation, which is capable to proper them forward or promote changes in direction. Basically, the flagella rotation is driven by an inward ion current across the cell membrane through an embedded motor which can lead to bidirectional rotation (clockwise and counter-clockwise) and changes in direction. Some bacteria can change their direction by variation of flagella rotation speed (Armitage and Schmitt, 1997).

In terms of modeling, one of the most commonly used bacterial models is the one presented by Phan-Thien et al. (1987). It was developed by means of boundary-element analysis of flagellar propulsion for spherical and ellipsoidal bodies that allowed attaining optimum aspect ratios. Figure 1-1 represents the bacterial model commonly used and respective shape parameters:

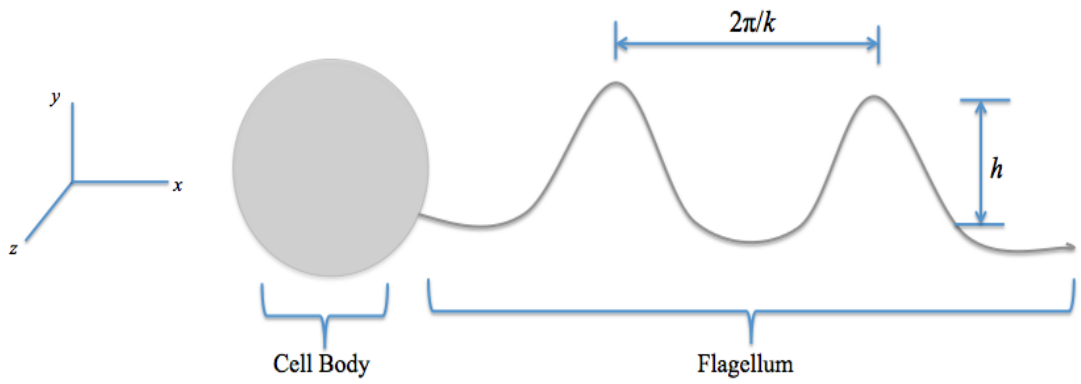

Figure 1-1: Bacterial model and shape parameters commonly used for flow field and hydrodynamic modeling. According to this model, bacteria swims by performing a helical wave down its flagellum, where h is the wave amplitude and k the wave number (adapted from Ishikawa et al., 2007)

For modeling purposes, it is assumed that a single bacterium is a neutrally buoyant particle due to the fact sedimentation velocity is much less than swimming speed. In addition, it is assumed that center of buoyancy associated to the bacterium is the same as the geometric center, which makes it to be force and torque free (Ramia et al., 1993). The most relevant assumption underlying hydrodynamic models is that self-propelled bacterium can be seen as a force dipole, since the drag force exerted by the cell body and flagellum is balanced by a rearward flagellar thrust (see Figure 1-2 A) (Pedley and Kessler, 1992).

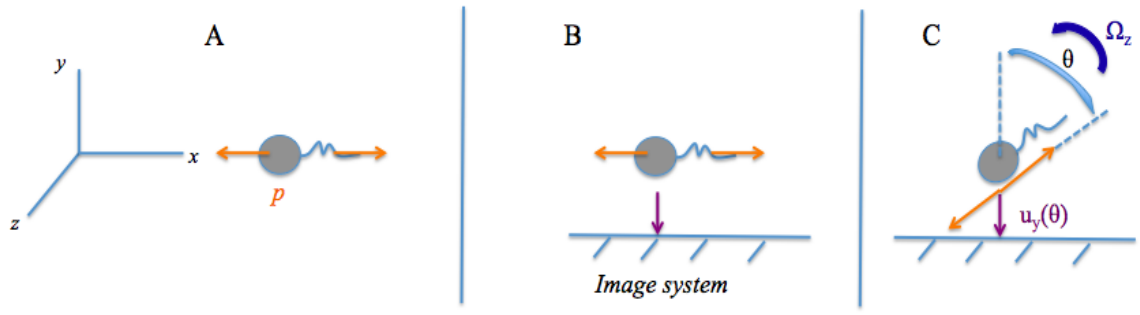

Figure 1-2: Representation of different cases of bacterial swimming and forces developed as it moves in a fluid. (A) Represents the flow-field around bacterium as a force dipole; (B) the cell surface hydrodynamic interaction and development of image system and (C) Swimming trajectory changes and hydrodynamic interaction with no-slip surface (adapted from Berke et al. (2008))

The flow around a single bacterium can be approximated by force dipole and a derivation of the Stokes flow field gives rise to Equation 1-2 which relates fluid velocity (u) with

swimming parameters like dipole strength (p_s), swimming direction (e) and distance to the dipole (r), as follows:

$$u = \frac{p_s}{8\pi\mu_f r^3}\,(-1 + 3 \times \frac{(r.e)^2}{r^2})r \quad \text{(Equation 1-2)}$$

It is important to take into account that this model is only valid for distances significantly larger than the length of swimming cell. Thus, it is classified as a far-field model (Berke et al., 2008).

As bacterium gets closer to a surface, the flow field induced by the cell is the net result of a superposition of a force dipole plus image flow field generated by an image system. Since bacterium is assumed to promote a force dipole parallel to a no-slip surface (condition at which fluid possess zero velocity relative to the boundary), the image system for this type of force is mainly composed by force dipole, force quadrupole and source quadrupole (Blake, 1971). The resultant of these forces induces a velocity component towards surface, which is directly proportional to dipole strength and inversely proportional to the square of distance between bacterium and surface (see Figure 1-2 B). The generated velocity component can be seen as an explanation in physical terms for attraction phenomenon (Hernandez-Ortiz et al., 2005). The image system represents a symmetric dipole on the other side of the surface and therefore, dipole-dipole attraction takes place.

Although dipole-dipole attraction describes a physical mechanism by which cells interact with surfaces, it is not ideal since collisions and Brownian motion may disturb the alignment of bacteria trajectory and nearby surface states. Consequently, force dipole is not aligned with no-slip surface and attraction can turn into repulsion, thus it must be considered in the model. In the case of Figure 1-2 C, a vertical velocity (u_y) away from the surface is formed and can be computed through Equation 1-3, as follows:

$$u_y\,(\theta, y) = -\frac{3p}{64\pi\eta y^2}\,(1 - 3cos^2\theta) \quad \text{(Equation 1-3)}$$

Where θ is angle of dipole position with respect to the vertical direction. From Equation 1-3, repulsion (positive u_y) is verified for very small angles.

The image system on the no-slip surface does not only induce attractive and/or repulsive velocities, but it also has nonzero velocity gradients that promote rotation of the cells. The rotation rate (Ω) is computed by the following set of equations, as follows:

$$\omega = \nabla \times u \quad \text{(Equation 1-4)}$$

$$E = \frac{1}{2}\,(\nabla u + \nabla u^T) \quad \text{(Equation 1-5)}$$

$$\Omega = \frac{1}{2}\omega + \left(\frac{\gamma^2-1}{\gamma^2+1}\right) e \times (E.e) \quad \text{(Equation 1-6)}$$

Where ω is the vorticity of flow field, E is the rate of strain of the flow field due to the image system and γ is the aspect ratio of the cell according to the bacterial model. The Equation 1-6 shows that cell rotates at half the vorticity induced by the image system plus a term, which takes into account shape parameter and flow field strain (Kim and Karilla, 1991).

Allison et al. (2008) demonstrated that far-field hydrodynamic interactions of swimming cells with solid surfaces lead to cell reorientation in a plane parallel to the surface as well as attraction by the nearest surface. Despite that evidence, Drescher et al. (2011) reported that noise due to Brownian motion and intrinsic swimming stochasticity drown long-range hydrodynamic effects between two bacteria beyond small length scale of few microns. This evidence implies that hydrodynamic effects between cells are only relevant in dense suspensions. On the other hand, they discovered that near-field hydrodynamic effects might play a role within few microns of the surface, which may lead to bacteria trapping onto surface. Lecuyer et al. 2011 showed that shear stress increases residence time of adhesion of *Pseudomonas aeruginosa* and that none of the bacterial surface features (flagellum and extracellular matrix production capability) is responsible for the observed trend. They also hypothesized that longer residence time is a direct consequence of less motile cells due to high shear stress. Therefore, physical interactions rather than chemical ones may be responsible for the increased residence time. Nevertheless, the role of cell appendages and surface chemistry on the adhesion process and the influence of hydrodynamics are not fully understood yet.

1.2.2 Cell-cell interaction and near-field analysis

The cell-cell interaction is an important factor for cohesive structure formation like granules (through aggregation phenomena) and biofilm. Additionally, the effects of hydrodynamic interactions between two bacteria on the rheology and diffusivity of suspensions have been investigated (Ishikawa et al., 2007; Hernandes-Ortiz, 2005; Ishikawa et al., 2006b). By modifying suspension fluid mechanics, individual cell and collective behavior may be altered. According to Ishikawa et al. (2007), stability of swimming motion dominates the length and timescales of these coherent structures formation. The near-field hydrodynamic interactions play a major role on the stability of swimming motion and cell-surface interaction within few micrometers. Thus, it must be

treated precisely and included in hydrodynamic models (Ishikawa et al., 2006a; Drescher et al., 2011).

For discussing far-field hydrodynamic interactions, models can assume bacteria as a single point force or stresslet, since moments decay rapidly when distance between particles is significantly great. Nevertheless, multipole moments must be taken into account in the context of near-field interaction analysis, which makes models at this level to have different assumptions. For instance, bacteria cannot be seen as particles with Brownian motion due to their size (between 2-10 μm), *i.e.*, they are significantly large for Brownian motion to be considered in near-field interaction. Besides, the swimming trajectory for near-field interaction analysis is only seven times the body length, which makes hydrodynamic interactions to be dominant over Brownian motion (Brennen and Winet, 1977).

The hydrodynamic interactions between two swimming bacteria are computed in an infinite fluid and since the flow field around bacteria can be described as a Stokes flow, the flow field around bacteria that interacts with another one can be given by Equation 1-7, as follows (Ishikawa et al., 2007; Vicsek et al., 1995):

$$u_i(x) = -\frac{1}{8\pi\mu_f}\sum_{m=1}^{2}\int_{S_{mo}}^{S_{mf}} J_{ij}(x-y)t_j(y)\,dS_y \qquad \text{(Equation 1-7)}$$

Where S_m stands for bacterium surface; J the Oseen tensor and t_j is the traction force (Youngren and Acrivos, 1975). Since it is assumed that bacteria possess the center of buoyancy at the same position as the center of gravity, a force and torque free model is developed and the velocity field on the surface of the body (including spherical body plus flagellum) is given by the following set of equations which includes translation velocity (U) and rotation velocity (Ω) (Ishikawa et al., 2007):

$$u(x) = \begin{cases} U+\Omega & if\ x\ is\ a\ positin\ on\ the\ cell\ body \\ U+(\Omega-f) & if\ x\ is\ a\ position\ on\ the\ flagellum \end{cases} \qquad \text{(Equation 1-8)}$$

Where f is an angular velocity. These equations are normally solved numerically by using the boundary element method. Ishikawa et al. (2007) observed that there is an unstable parallel motion of bacteria by applying the mentioned boundary element method, which breaks down easily in three-dimensional space. Besides, as two bacteria approach each other near-field interactions like lubrication forces can change their orientations. Although Ishikawa and Hota (2006) already verified experimentally that hydrodynamic interaction play a role on the cell-cell interaction, the effect of near-field lubrication forces remains to be observed experimentally. In this context, Drescher et al. 2011 verified experimentally

that collision models are more suitable than long-range hydrodynamics, but hydrodynamic interactions may still play a role in near-field. In order to obtain the complete physic picture of the bacterium dynamics and influence of hydrodynamics, models should include both far-field and near-field interactions as well as the impact of biochemical events and cell surface features.

Lega and Passot (2003) developed a hydrodynamic model, which integrates continuum equations involving reaction and diffusion of nutrients and bacteria with velocity field of bacteria-water mixture. The model was able to describe successfully the dynamics of microorganisms within colony and a mechanism for collective motion towards fresh nutrients. Their study shows that incorporation of reaction-diffusion equations for nutrient concentration (like in chemotaxis phenomenon) may be useful for development of more reliable hydrodynamic models.

1.3 Hydrodynamic impact on cohesive structures: biofilm

Biofilm is defined as a complex coherent structure of surface-attached bacteria plus cellular products or inert content such exopolysaccharides (EPS). It can be comprised by single or multiple species and is found ubiquitously in many natural, medical and industrial settings (O'Toole et al., 2000). Biofilms can be formed in any hydrated environment with proper nutrient conditions and are also able to develop on a variety of abiotic hydrophobic and hydrophilic surfaces. Due to the wide range of surfaces where it can develop, biofilm formation is often associated to "biofouling" (Melo and Flemming, 2010) and bacterial infections as well as contamination of food preparations (Costerton and Stewart, 2001). Nevertheless, biofilms have been successfully employed in the biotechnology field for wastewater treatment processes in bioreactors (Lazarova and Manem, 1994; Kwok et al., 1998).

Biofilm development, structure and population phenotype are strongly influenced by intrinsic biological properties and environmental factors like hydrodynamic conditions. The latter has major impacts on biofilm architecture, heterogeneity (Rochex et al., 2008) and metabolism of cells within (Simões et al., 2008). Hydrodynamic conditions are shown to strongly influence mass transport of cells and nutrients to the biofilm surface as well as quorum-sensing molecules by advection (Kirisits et al., 2007). Turbulent regimes are often associated to high shear stress and compression forces, which lead to structure

detachment. Besides, Simões et al. (2004) reported that biofilms formed under turbulent regime were more active and compact.

1.3.1 Mechanism of biofilm formation and cell adhesion

It was verified that bacteria primarily exist in association with surfaces rather than at planktonic state (Watnick and Colter, 2000). Biofilms represents a protection mechanism for microorganisms and allows them to survive and growth in hostile conditions. Additionally, it enables bacteria to have dynamics similar to multicellular organisms through signaling events (Waters and Bassler, 2005). Cells within biofilms possess distinct phenotype characteristics when compared to planktonic counterparts. Simões et al. (2003) noticed that *Pseudomonas fluorescens* cells at planktonic state were inactivated by antimicrobial agents at higher extent than when the cells were within biofilm. Besides that, they observed that biofilms formed under laminar conditions were more easily inactivated by antimicrobial agents, which suggests the coherent structure resilience.

The formation of biofilms can be described by the following five-step process: i) formation of a conditioning film on a given surface; ii) transport of microorganisms from the fluid to the surface, iii) adhesion of microorganisms at the interface between solid and liquid phases; iv) transport of nutrients and consumption which leads to cell replication and EPS matrix production and v) biofilm detachment as consequence of the liquid shear stress, which results in detachment force (Vieira et al., 2003). The general mechanism of biofilm formation is depicted as a cycle in Figure 1-3.

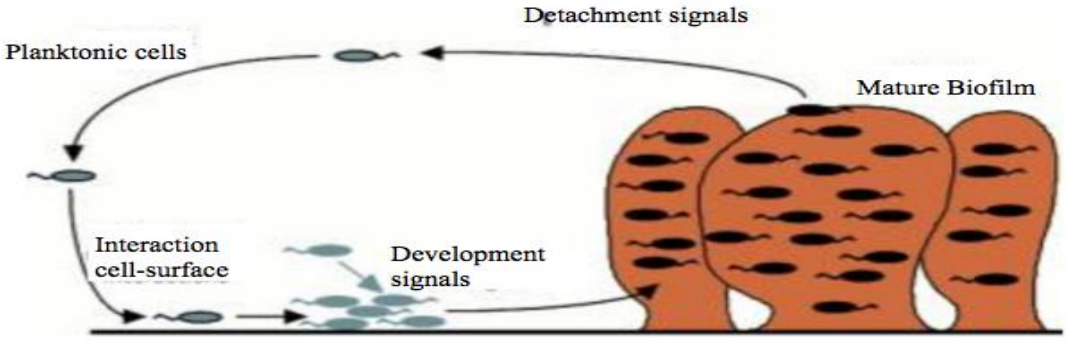

Figure 1-3: Dynamics of biofilm formation as a cycle with the most relevant aspects (adapted from O'Toole et al., 2000)

Biofilms may spread to uninfected areas depending on environmental conditions by detachment process, where detached cells re-enter a planktonic state and may adhere to another surface giving rise to a novel biofilm (O'Toole et al., 2000). The ability of the cell to attach to a given surface is carried out by specific cell surface proteins (*e.g.* appendages) and non-specific interactions (Saini, 2010). Interfacial forces like Van der Waals, electrostatic and Lewis acid-base interactions are shown to play a role on bacterial adhesion processes and are related to cell surface properties (mainly charge- and chemical composition related) (Van Oss, 1994). Basically, bacteria are theorized as colloid particles and can be included in the Derjaguin, Landau, Verwey and Overbeek (DLVO) theory, which states that bacteria attachment is the balance between the Van der Waals (attractive) and electrostatic (repulsive) forces (Goulter et al., 2009). Additionally, the self-propelling capability of bacteria through flagella is associated to biofilm forming ability (Pratt and Kolter, 1998). In general, physical (*e.g.* hydrodynamic and diffusion forces), biochemical (eg. surface dehydration) and chemical interactions (*e.g.* hydrogen bonding) are essential for adhesion and biofilm three-dimensional structure build-up (Liu et al., 2000; Calleja, 1984; Marshal, 1971). Nevertheless, the influence of hydrodynamics on cell surface properties and the consequence on interactions between cells and abiotic surfaces has not been fully understood yet.

Despite hydrodynamic conditions represent an important environmental factor, nutrient availability was also shown to influence biofilm growth, development and detachment behavior (Telgmann et al., 2004). Thus, the impact of each factor must be evaluated separately.

1.3.2 Hydrodynamics impact on biofilm structure and mechanical properties

Hydrodynamic shear force has a significant influence on biofilm steady state structures. Chang et al. (1991) observed that biofilm density increases in linear fashion with increasing shear stress, whilst biofilm thickness decreases linearly. In other words, more dense and compact biofilms are generated under higher shear stress. Pereira et al. (2002) proposed that lower thickness and higher density at higher hydrodynamic stresses are due to need of microorganisms to remain active and to be protected from external aggressions, thus microorganisms produce more EPS per unit volume which leads to an effective adhesion and reduction of void spaces. Hence, biofilms with greater cohesion are

formed in such manner. Controversially, Paramonova et al. (2009) observed that as shear stress increases, an oral biofilm thickness increased and strength decreased. This was attributed to the fact that oral biofilms comprise multi-species bacteria, which present different dynamics and higher packing under hydrodynamic stress.

According to Van Loosdrecht et al. (2002), biofilm structure is governed by a balance between detachment and outgrowth. They observed that porous structure occurs when a biofilm is strongly diffusion limited and when low shear stress is applied because detachment is not able to counteract growth of protrusions. On the other hand, Paul et al. (2012) showed the biofilm as a stratified structure, where a highly cohesive basal layer is formed under high shear stress. They hypothesized that the increase on biofilm internal strength is mainly due to compression and consolidation phenomenon. Basically, there is a shear stress limit at which biofilm thickness starts being governed by compression phenomena instead of detachments. Koerstgens et al. (2001) reported that biofilm matrix develops an intrinsic internal tension which relates to the shear stress under which biofilm was formed. Thus, biofilms developed under high shear stress will be more challenging to remove through physical techniques.

Teodósio et al. (2011) assessed *Escherichia coli* biofilm formation in a cell flow reactor system and reported that for thickness values above 400 μm the mechanical resistance to shear stress is more important than mass transfer effects. Thus, denser biofilms are formed since the need for cohesion strength seems to be more relevant than nutrient availability in these situation. By doing this, they were able to verify separately the influence of different environmental parameters on biofilm structure. In terms of microbial diversity, Rochex et al. (2008) hypothesized the high shear stress environment selects for a cell population capable of producing stronger biofilm, i.e., high shear can decrease biofilm community diversity. In addition, it was suggested that high shear stress is able to slow down biofilm maturation and keep it as a "young biofilm", which tends to present lower thickness. The fluid in movement applies forces to biofilms in many directions, which leads to several outcomes including viscoelastic deformation, rolling and development of streamers (Stewart, 2012).

From an engineering point of view, the development of models able to describe biological phenomena are crucial to have a better insight about the impact of each parameter on an observed phenomenon and to minimize number of needed experiments through *in silico* analysis. In this context, Englert (2009) developed a continuum-based mathematical model, which describes the effect of hydrodynamic conditions, more

specifically shear stress, on biofilm growth and final structure. They considered a shear-stress dependent detachment rate and that biofilm thickness is influenced by the flow velocity around it and detachment as shown by Equation 1-9:

$$\frac{dL}{dt} = u\,(t, L) - \zeta\,(\tau) \quad \text{(Equation 1-9)}$$

Where L stands for biofilm thickness, t for time and ζ for detachment rate. The relation of the detachment with shear force is given by equation 1-10, as follows:

$$\zeta = \zeta_{max}(1 - e^{-k_e \tau}) \quad \text{(Equation 1-10)}$$

Where ζ_{max} is the maximum detachment rate and k_e an empirical factor (Englert, 2009).

1.3.3 Mass transfer and signaling events

By modifying biofilm structure, mass transfer of nutrients is affected and hydrodynamic conditions must be taken into account into advection-diffusion-reaction theory of biofilms. Hydrodynamic conditions have a dual effect on mass transfer associated to biofilms (Vieira et al., 1993). Turbulent flow facilitates diffusion of substrate from fluid bulk to biofilm. On the other hand, it promotes higher shear stress, which in turn culminates in the formation of more dense biofilms and consequently, substrate internal diffusion becomes more difficult. Therefore, the real diffusion of substrate is the net result of mass transfer enhancement effects and biofilm compactness (Vieira et al., 1993; Liu and Tay, 2002). Biofilms have heterogeneous architecture and as consequence a biofilm may not have equal local mass transfer coefficients between two adjacent spots (Melo and Flemming, 2010).

Signaling mechanism is essential for cell communication in coherent structures like biofilms. Davies et al. (1998) studied the influence of cell signaling in structure of *P. aeruginosa* biofilms and observed that *N*-(3-oxododecanoyl)-L-homoserine lactone (OdDHL) was necessary for the development of complex structure. However, Stoodley et al. (1999) found no difference in structure complexity between wild type and OdDHL null mutant biofilms under same wall shear stress, but at Reynolds number higher than applied by Davies et al. (1998). They concluded that quorum sensing is also strongly influenced by mass transfer effects, which depends on hydrodynamic conditions. Hence, the architecture of biofilm is not only influenced by shear stress, but it also seems to depend on flow regime and mass transfer of nutrients and signaling molecules. It was also found in the literature that *P. aeruginosa* wild-type and quorum-sense null mutants presented identical biofilm structures under high flow conditions (Purevdorj et al., 2002). Moreover,

Kirisits et al. (2007) provided evidence that there is a signal washout under high flow rates and that the amount of biofilm required for full quorum sensing induction increased as the flow rate increased. This aspect seems plausible, since higher mass biofilms may introduce a significant mass transfer resistance to quorum sensing signals and lower dilution effects.

Lastly, Vaughan et al. (2010) reported a model which relates the fluid velocity with quorum sense influence on biofilm and observed that shape of biofilm which can be a direct impact of hydrodynamic conditions, has effect on the quorum sensing phenomenon. The relation between signaling molecule concentration and fluid velocity is given by the following governing equation:

$$\frac{\partial M}{\partial t} = D_M \nabla^2 M - u \,.\nabla M - \beta M + \mu(M) f \qquad \text{(Equation 1-11)}$$

where M stands for signaling molecule concentration; D_M is the diffusion rate of the molecule; β hydrolysis rate and u is the fluid velocity (Vaughan et al., 2010; Chopp et al., 2003).

1.3.4 Cell metabolism

According to Vieira et al. (1993), relation of shear stress or detachment force and biofilm structure was exclusively due to physical phenomenon. However, it has been observed that there is a relation between cell metabolism and shear stress, which seems to affect biofilm structure.

Liu and Tay (2001b) studied the relation between detachment force and energy metabolism of biofilm by using a conventional annular reactor at different tip velocities of rotating disk, which induced different degrees of shear stress. Moreover, they measured the dehydrogenase activity of the biofilm by monitoring the reduction of 2-(p-iodophenyl)-3-(p-nitrophenyl)-5-phenyl tetrazolium chloride (INT). They observed that as shear stress increases, cell growth yield reduces and specific INT-dehydrogenase activity increases concomitantly (Liu and Tay, 2001b). Lopez et al. (1986) showed that specific INT-dehydrogenase activity could be correlated with the electron transport system of aerobic oxidation process. Therefore, it is used to measure the respiratory activity of microorganisms and infer about their catabolic activity. A higher catabolic activity in organotrophic organisms means that more organic carbon is oxidized to carbon dioxide, and consequently electron transport system will be more active with more adenosine triphosphate (ATP) being generated through oxidative phosphorylation (Nunes, 2010).

The cell growth yield is a function of ratio between carbon directed to catabolic processes (energy production) and the one that is channeled to anabolic process (biomass formation and energy consumption). In this case, high respiratory activity implies that less biomass is formed. Bearing that in mind, the reduction of cell growth yield and the increase of INT-dehydrogenase activity reveal that there is a stimulation of catabolism over anabolism at high shear stresses.

Lertpocasombut (1991) studied the effects of high shear stress on bacterial metabolism within biofilms in terms of dissolved oxygen consumption rate (r_{O2}), total organic carbon (TOC) removal rate (r_{TOC}) and cell growth yield. This author observed that ratio r_{O2}/r_{TOC} increased linearly by increasing shear stress, which means that more oxygen was consumed per unit of TOC, hence more organic carbon was rather converted to carbon dioxide in catabolism than used in anabolism. Besides, it was shown that as ratio r_{O2}/r_{TOC} increased, cell growth yield reduced significantly which demonstrates an energy uncoupling between catabolism and anabolism when increasing shear stress is applied (Lertpocasombut, 1991).

As previously stated, adenosine triphosphate (ATP) is produced by oxidative phosphorylation process. The aerobic oxidation process involves an electron transport chain where electrons provided by substrate oxidation are transported to a final electron acceptor (*e.g.* oxygen) with formation of an electrochemical gradient through proton translocation phenomenon. Therefore, respiratory activity of microorganisms is associated to proton translocation activity and for aerobic bacteria a linkage of oxygen reduction and proton translocation was observed (Babcock and Wikstrom, 1992). With that in mind, the increasing INT-dehydrogenase and oxygen consumption rate as shear stress increases is associated to a higher extent of proton diffusion across the cell membrane, which leads to acidification of the medium, as reported by Chen and Huang (2000) for suspended cell cultures. Therefore, the catabolic activity is strongly related to proton translocation phenomenon.

The proton translocation induced by shear stress may have influence on biofilm structure and other cell aggregation phenomena, as research shows that high proton flux enhances hydrophobic interaction and surface dehydration of cells (Tay et al., 2000; Babcock and Wikstrom, 1992). Hydrophobic interactions between microbial cells are very important at the initiation of biofilm because it acts as driving force for bacteria to self-aggregate out of the liquid phase, which is hydrophilic (Rouxhet and Mozes, 1990). On the other hand, cellular surface dehydration is a biochemical force, which seems to

strength the interaction cell-cell and may lead to high-density microbial communities (Teo et al., 2000).

In terms of biofilm phenotypic characteristics, Simões et al. (2008) demonstrated that laminar flow generated biofilms presented a higher content of matrix proteins and polysaccharides per gram of biofilm than turbulent counterparts. They also observed that biofilms formed under turbulent Reynolds regime were more active as it had a higher number and density of viable cells, which had smaller radius than cells under laminar regime. These phenotypic characteristics are advantageous for microbial community in terms of resilience against antimicrobial agents (Simões et al., 2007).

1.4 Motivation and objectives

Hydrodynamics is shown to have impact at collective behavior and motions of microorganism at different scales, i.e., from micro- and meso- to macroscopic scale. Since biofilms represent one of the most common types of microbial living states and it is a result of a given microbial community dynamics, it is plausible to gather data about the effects of environmental conditions such as hydrodynamics on biofilms. Nevertheless, data about hydrodynamic effects at planktonic state would be equally important for understanding microbial dynamics.

The motivation for the study of hydrodynamic effects on bacteria at planktonic state arises from the wide range of applications involving bacteria cultivation ranging from medical and environmental applications to food industry. Therefore, hydrodynamics could be faced as an additional parameter for bioprocesses optimization. Besides, studies have demonstrated the inefficacy of several biocide-based disinfection methods of biofilms (O'Toole et al., 2000), which leads to the need for better knowledge about mechanisms underlying bacteria migration to surfaces at planktonic state and how they can be eradicated prior biofilm formation. For instance, it has been found that certain hydrodynamic conditions could be coupled to biofilm control methods in order to avoid biofilm formation, and consequently, the contamination of purified water in industrial distribution systems (Florjanic and Kristl, 2011). Another notable application relies on the increasing use of hydrodynamic cavitation method through jet nozzles to eliminate bacteria in suspensions at small scales (Loraine et al., 2012). The knowledge about the

direct influence of hydrodynamics on cell physiological behavior at planktonic state could allow the enhancement of those techniques to even larger scales.

In this context, the present study aims to investigate the influence of distinct hydrodynamic environments on growth behavior and metabolic activity of a given microorganism mainly at planktonic state. Due to crucial role of cell surface/environment interface for microorganism dynamics (cell-cell, cell-surface interactions and signaling events) and growth mode, this study will also focus on characterization at physicochemical level of cell surfaces in different hydrodynamic conditions. Furthermore, proteomic studies will allow a protein-level characterization of the cell surface and contribute to a clearer picture about the direct impact of hydrodynamics on microbial cells.

2. Materials and methods

In this chapter, a brief description of the procedures and apparatus associated to the methods employed throughout the experimental work will be given. The set of experiments were defined in order to evaluate the hypothesis that changes in hydrodynamic environment will promote a distinct cell behavior as well as changes at the cell surface level.

As described earlier, the main goals of the present study were to verify the influence of different hydrodynamic conditions on growth and collective behavior as well as on cell surface properties at the planktonic state of a selected bacterium. In order to evaluate the effects on growth, experiments involving growth curve under different agitation speeds and study of associated kinetics were performed. The impact on collective behavior was analyzed by means of auto-aggregation evaluation. On the other hand, cell surface properties were determined by a set of experiments that allowed the surface characterization at physicochemical and protein expression levels.

2.1 Bacteria isolation and identification

Acinetobacter calcoaceticus was the microorganism selected for the present study. It was isolated from a model laboratory drinking water distribution system as described by Simões et al. (2006). The bacterium was stored at -80 ºC in 50% (v/v) glycerol solution and colonies of *A. calcoaceticus* were obtained by plating on Luria-Bertani medium with Agar medium (LB-A).

2.2 Bacteria growth and distinct hydrodynamic conditions

Bacterial cells were grown in batch mode overnight at 30 ºC in Tryptic Soy Broth –TSB medium(Sigma-Aldrich, UK) in 220 mL culture medium with 280 mL hold-up (500 mL total volume flask). In order to create distinct hydrodynamic environments, cells

on each assay were grown under distinct agitation speeds. The agitation speeds employed throughout the present work were 100 rpm, 220 rpm and 375 rpm and culture flasks were agitated in a shaker/incubator (MaxQ 4450, Thermo Scientific, USA). Rotation speeds were determined by the incubator built-in tachometer. Inoculum cultures were grown under the similar conditions at 220 rpm agitation speed.

2.3 Kinetic studies

In order to observe the influence of different agitation speeds on growth behavior, growth kinetics in terms of biomass formation and reducing sugar (substrate) consumption over time were studied.

Growth curve was attained for each agitation speed through spectrophotometry at 640 nm as carried out by Tam (2002). Inoculum was diluted in sterile TSB medium to obtain an initial optical density (OD) of 0,200±0,0 determined by spectrophotometer (V-1200, VWR, Germany) in 220 mL as total volume. Following that, 2 ml aliquots were taken for OD at 640 nm measurements from 30 to 30 min in the first 2 hours and at every completed hour until total 11 hours of growth. On the following day, the same procedure was applied until stationary phase was reached. Measurements were performed in biological triplicates for each agitation speed. A relationship between optical density at 640 nm and colony-forming units (CFU) per ml was obtained for a stock culture cultivated at similar conditions under 220 rpm. Each increase of 0,1 OD unit corresponds to an increase of $2{,}5\times10^{7}$ $CFU.mL^{-1}$. Based on the growth curve obtained for each agitation speed, cell harvesting time points representing mid-exponential and stationary phases were defined for further experiments and are presented in Table 2-1.

Table 2-1: Time points for harvesting and respective growth phase for each experimental condition.

Agitation speed (rpm)	Growth phase	Time point for harvesting
100	Mid-exponential	12 h post-inoculation
	Stationary	25 h post-inoculation
220	Mid-exponential	5 h post-inoculation
	Stationary	20 h post-inoculation
375	Mid-exponential	4 h post-inoculation
	Stationary	15 h post-inoculation

Simultaneously, substrate consumption in terms of reducing sugars content was assessed by the 3,5 dinitro salicylic acid – DNS – (Sigma-Aldrich, UK) colorimetric method in a similar manner as performed by Gusakov et al. (2011). Prior analysis, cells were spinned down by centrifugation at 4500×g for 10 min. From 2 mL aliquots, 500 µL of sample was mixed with 500 µL DNS in a tube, which is placed in 100 ºC bath for 5 min in order to promote oxidation of aldehyde groups present in reducing sugars (Breuil and Saddler, 1985). The reaction leads to solution colour modification, which is analyzed by spectrophotometry. Absorbances at 540 nm were measured by the same spectrophotometer in biological triplicates for each condition and measurements were performed every 2 hours until 12 hours of growth were reached. Relationship between optical density at 540 nm and reducing sugars concentration was obtained, where each decrease of 0,1 OD corresponds to 225 mg reducing sugars.L^{-1} consumed.

Finally, specific growth rate (µ) and yield of biomass in terms of reducing sugars consumption ($Y_{X/S}$) were computed through Equation 2-1 and 2-2, respectively (Bailey and Ollis, 1986).

$$\mu = \frac{Ln\, X_f/X_i}{t} \quad \text{(Equation 2-1)}$$

$$Y_{X/S} = \frac{X_f - X_i}{S_f - S_i} \quad \text{(Equation 2-2)}$$

Where X_f represents biomass concentration at the end of exponential phase (CFU.mL^{-1}); X_i biomass concentration at beginning of exponential phase (CFU.mL^{-1}); t is time until end of exponential phase (h); S_f reducing sugars concentration at the end of exponential phase (mg.mL^{-1}) and S_i reducing sugars concentration at beginning of exponential phase (mg.mL^{-1}). The kinetic parameters were obtained to describe the exponential growth phase for each condition.

2.4 Respiratory activity assay

The respiratory activity of bacterial cells was assessed by measurement of oxygen uptake rate through a biological oxygen monitor (Model 53, Yellow Spring Instruments Inc., USA) as described by Simões et al. (2005). Firstly, cells cultivated in TSB were harvested at specific time points (see Table 2-1) by centrifugation at 4000×g for 15 min at 25 ºC. Following that, cells were washed and resuspended in 100 mM potassium chloride (VWR, Germany) until final OD at 610 nm of 0,4 was reached. Afterwards, 30 mL of

suspension were aerated for 10 min to assure oxygen saturation. After aeration, culture was placed in temperature-controlled vessels at 25 ºC attached to the biological oxygen monitor and oxygen concentration decrease was monitored over 10 min, where after initial 5 minutes 10 µL of 5 $g.L^{-1}$ glucose (Sigma-Aldrich, Germany) was injected.

According to Simões et al. (2005), the total respiration rate corresponds to the slope associated to the linear decrease of oxygen concentration in cell suspension after glucose injection. In order to compute the total respiratory activity (mg O_2.dry bacterial $mass^{-1}.min^{-1}$), dry bacterial mass by total volatile solids measurement and oxygen solubility in water at 25 ºC were obtained. Dry bacterial mass determination was performed as described by APHA, AWWA and WEF (1989). This experiment was performed in biological triplicates with technical duplicates. The experiment was performed for each agitation speed condition and growth phase (mid-exponential and stationary).

2.5 Physicochemical characterization of cell surface

2.5.1 Hydrophobicity assessment by Microbial Adhesion to Hydrocarbons (MATH) assay

The cell surface hydrophobicity was assessed by MATH assay developed by Rosenberg et al. (1980) with modifications proposed by Mukherjee et al. (2011). Briefly, cells were harvested by centrifugation at 4500×*g* for 10 min at 4ºC and washed twice with 100 mM potassium chloride. Following that, cells were suspended in a high ionic strength solution (150 mM potassium chloride at pH 7) to a final concentration of 1,000 OD at 600 nm. According to Rosenberg (2006), aqueous phase with high ionic strength tends to diminish electrostatic forces that would affect cell interaction with the organic phase, which makes cell adhesion to that phase to rely only on hydrophobic interactions.

Following that, 200 µL of *n*-hexadecane 99% (Sigma-Aldrich, Germany) were added to 1mL of suspension. Control suspension was prepared without addition of *n*-hexadecane. The mixture was vortexed for 90 s and organic phase was allowed to separate from the bacterial phase by settling the mixture for 15 min. Finally, OD at 600 nm is obtained for the aqueous phase and hydrophobicity index (H%) is computed by Equation 2-3 as follows (Mukherjee et al., 2011)

$$H(\%) = \frac{A_C - A_M}{A_C} \times 100 \quad \text{(Equation 2-3)}$$

Where A_C stands for OD at 600 nm of the control suspension and A_M is the OD at 600 nm of test suspension after mixing with *n*-hexadecane. This experiment was performed with 4 biological replicates for each tested agitation speed condition at mid-exponential and stationary phase.

2.5.2 Cell surface charge by electrophoretic mobility (EPM) measurement

This experiment was carried out in a similar manner as performed by Mukherjee et al. (2011). The bacterial electrical properties for all the agitation speed conditions at mid-exponential and stationary growth phases were attained by electrophoretic mobility measurements. The measurements were performed in a zeta potential analyzer (ZetaPALS, Brookhaven Instruments, UK) in 2 to 7 pH range. Prior analysis, the cells were washed with 100 mM potassium chloride and resuspended in the same solution until a final OD at 600 nm of 1,000 was reached. Three hundred microliters cell suspensions were diluted into 1200 µL potassium chloride solution over pH ranging from 2 to 7. Measurements were carried out with an associated electrical field of 2,5 $V.cm^{-1}$ at 2,0 Hz frequency and 5 runs with 40 cycles each were performed for each assay. Each agitation speed condition was analysed in biological triplicates for both mid-exponential and stationary growth phase.

2.5.3 Cell surface functional groups analysis through Attenuated total reflectance Fourier Transform Infrared Spectroscopy – ATR-FTIRS

The ATR-FTIRS was one of the techniques employed in the present study to characterize surface chemistry of cells grown under distinct agitation speeds (at mid-exponential and stationary growth phase) in terms of functional groups. The technique was performed in a similar manner as described by Mukherjee et al. (2011) and Jiang et al. (2004). Briefly, cells were washed twice with 0,9% sodium chloride solution (Sigma, UK) and small portion of pellet was allowed to air dry for 1h on the ATR attachment

(Pike Technologies, USA) associated to the FTIR spectrophotometer (IR Prestige-21, Shimadzu, UK). The Happ-Genzel apodisation function was used over 64 scans with resolution set to 4 cm^{-1} to obtain a FTIR spectrum between 600 and 4000 wave numbers. Spectrum processing was performed using the software IR solution provided by equipment supplier. In terms of data processing, atmospheric and baseline corrections were done to remove noise caused mainly by atmospheric water vapor and carbon dioxide. Normalization of the spectrum to intensity of the peak at 2924 cm^{-1} (related to the assymmetric stretching of C-H in $–CH_2$ according to Nauman (2006)) was carried out in order to compensate for different cell numbers loaded on the equipment across different tested conditions. That normalization procedure allowed direct comparison of spectra. For each condition, three biological replicates with three technical replicates each were performed.

Principal Component Analysis (PCA) was the multivariate statistical analysis used to attest for difference significance between spectra of cells grown under different agitation speeds. The analysis was executed by XLSTAT software (version 2013.2, Addinsoft).

2.5.4 Cell surface chemistry analysis through X-ray photoelectron spectroscopy (XPS)

The XPS analysis of the cell surface was performed in a similar manner as described by Mukherjee et al. (2011) and Ojeda et al. (2008) with slight alterations. Bacterial cells were washed three times with sterile distilled water, then 250 μL aliquot were taken and flash frozen in liquid nitrogen. Following that, cells were freeze-dried and submitted to XPS analysis.

The equipment used for the referred analysis was an Ultra Photoelectron spectrometer (Kratos Axis 165, Shimadzu, UK) at 10 kV and 20 mA with an Al Kα X-ray source. Two biological replicates were obtained for each tested hydrodynamic condition at mid-exponential and stationary growth phase. For each assay, survey scan with an associated step-size of 1,0 eV and a high resolution scan with a step-size of 0,1 eV were performed. Both scans were carried out with pass energy of 20 eV. Spectra analysis and deconvolution was performed by CasaXPS software (2.3.15 version, Casa Software). The binding energies of the survey scan peaks were assessed using the carbon (C) peak at 285

eV. On the other hand, the binding energies determination associated to high resolution scan peaks were computed using C1s peak of 284,6 eV.

The prediction of molecular composition was carried out by usage of a set of equations described by Rouxhet et al. (1994) (see Appendix D).

2.6 Auto-aggregation analysis

In order to evaluate the influence of distinct hydrodynamic conditions on auto-aggregation capability of *A. calcoaceticus*, a quantitative method based on spectrophotometry and a semi-quantitative one (visual assay) were employed for cells cultivated under distinct agitation speed at stationary phase.

2.6.1 Visual auto-aggregation assay

The visual auto-aggregation assay was performed as described by Simões et al. (2008) with minor alterations. Cells were harvested by centrifugation at 5000×g for 20 min and washed twice with sterile 100 mM potassium chloride through centrifugation cycles of 4500×g for 10 min. Following that, cells were resuspended in sterile 100 mM potassium chloride at pH 7 until final OD at 600 nm of 1,500 was attained. Then, 4 mL suspension was transferred to a test tube. After vortexing for 10 s and rolling the tube for 30 s, degree of auto-aggregation was visually assessed according to the score scheme developed by Cisar et al. (1979) at 0 h, 2 h, 24 h and 48 h after suspension preparation. The score criteria employed throughout the assay are described as follows: value 0 for suspensions with no evidence of auto-aggregation; value 1 for finely dispersed flocs; value 2 for aggregates that form immediately but remain suspended in turbid background; value 3 for aggregates that settled giving rise to slightly cloud supernatant and value 4 for rapid and complete settling of large aggregates giving rise to a clear supernatant. The experiment was performed in biological duplicates for each hydrodynamic condition tested.

2.6.2 Auto-aggregation quantification

The quantitative analysis of the auto-aggregation phenomenon was carried out as described by Phuong et al. (2008) with some alterations. Cells were washed and resuspended in 100 mM potassium chloride at pH 7 as previously described for the visual assay. Following that, 4 mL of suspension were placed in a test tube at room temperature and OD at 600 nm was measured at 0 h and 1 h after suspension preparation. The auto-aggregation index (A%) was computed by Equation 2-4 as follows:

$$A\ (\%) = \frac{A_B - A_A}{A_B} \times 100 \qquad \text{(Equation 2-4)}$$

Where A_B stands for OD at 600 nm at 0 h after suspension preparation and A_A represents the OD at 600 nm at 1 h after suspension preparation. The auto-aggregation quantification was performed in biological triplicates for each hydrodynamic condition.

2.7 Outer membrane proteins analysis – Proteomic study

In order to analyse the influence of different hydrodynamic conditions on the expression of proteins at the outer membrane of *A. calcoaceticus*, a bottom-up approach for proteins identification was carried out (Chen and Pramanik, 2009). Proteins associated to the outer membrane of cells cultivated under different agitation speeds were extracted, digested into smaller peptides and submitted to Liquid Chromatography coupled with Tandem Mass Spectrometry (LC-MS/MS) for further data processing and comparison with protein data base. The study was performed for cells at stationary phase.

2.7.1 Outer membrane protein isolation and analysis by sodium dodecyl sulphate polyacrylamide gel electrophoresis (SDS-PAGE)

The outer membrane proteins (OMP) were isolated according to the method described by Mukherjee et al. (2011) with slight alterations. After cell harvesting, cells were resuspended in 30 mL of tris(hydroxymethyl) aminomethane-hydrochloric acid (Tris-HCl) buffer adjusted to pH 7,5 with final OD at 600 nm of 1,000. Cells were washed twice with 50 mM Tris-HCl buffer and resuspended in 5 mL of the same buffer. Cell lysis occurred by sonication in ice bath comprising 6 cycles of 60 s each executed by an

ultrasonic cell disruptor (Branson 450, Emerson, UK). Non-lysed cells were removed by centrifugation at 5000×g for 10 min and obtained supernatant was submitted to centrifugation at 21000×g for 60 min. The pellet (mainly cell debris) was resuspended in 5 mL of Tris-HCl buffer and N-lauroylsarcosine sodium salt (Sigma-Aldrich, UK) was added to give final concentration of 1,5 % (v/v) in order to solubilize inner membrane proteins. The suspension is incubated for 20 min at room temperature. After incubation, suspension is centrifuged at 20000×g for 90 min. Resultant pellet containing OMP was resuspended in 1mL deionized water and stored at -20 ºC until required. Protein concentration prior SDS-PAGE analysis was assessed by NanoDrop UV-Vis spectrophotometer (2000c, Thermo Scientific, USA).

The SDS-PAGE analysis with 12% (w/v) polyacrylamide was performed as described by Laemmli (1970). Twenty micrograms of protein per sample were electrophoresed with voltages of 80V and 180V for 20 min and 45 min, respectively. The applied molecular-weight protein marker was the SigmaMarker S8445 (Sigma-Aldrich, UK), which presents molecular weights ranging from 6,5 kDa to 200 kDa. Finally, staining process was carried out by addition of Bio-Safe Coomassie blue stain (Bio-Rad, UK) to the gel. For imaging purposes, gel was destained by successive washing steps with distilled water.

2.7.2 In-gel digestion of proteins into smaller peptides

The in-gel protein digestion carried out in the present study was performed according to the method described by Shevchenko et al. (2006). Protein bands were excised, removed from the gel and placed in siliconized tube. Afterwards, protein bands were incubated with 200 μL of 100 mM ammonium bicarbonate (VWR, UK) for 30 min at room temperature with occasional vortexing and resultant supernatant was discarded. Following that, gel bands were incubated with 200 μL of 100 mM ammonium bicarbonate in 50% (v/v) acetonitrile for 30 min and that was repeated three times. This step was followed by incubation with 500 μL acetonitrile for 10 min at room temperature. Then, reduction process was performed by incubation with 100 μL of 10 mM dithiothreitol for 45 min at 56 ºC and resultant supernatant was discarded. Following an incubation with 500 μL acetonitrile for 10 min, alkylation process was carried out by incubating gel pieces with 100 μL iodoacetamide (55 mM iodoacetamide in 100 mM ammonium bicarbonate)

for 25 min in the dark and supernatant was discarded. Five hundred microliters acetonitrile were added to gel pieces and this was followed by vaccum drying at 13000×*g* for 1 min. Afterwards, 0,4 μg trypsin buffer (Promega, UK) were added to gel pieces, which were incubated at 4 ºC for 20 min. Fifty microliters of 100 mM ammonium bicarbonate were added and gel pieces saturated with trypsin were incubated overnight at 37 ºC. Following overnight incubation, supernatant was collected to a new tube and gel pieces were incubated with 60 μL of 100 mM ammonium bicarbonate for 15 min at 37 ºC and supernatant recovery was executed. For peptide extraction, gel pieces were incubated with 50 μL of 5% formic acid solution for 15 min at 37 ºC. An additional extraction step was carried out by incubation of gel pieces with 50 μL of 5% formic acid solution in acetonitrile diluted two times with water for High Performance Liquid Chromatography (HPLC water) for 15 min at 37 ºC. The supernatant obtained throughout the peptide extraction (containing peptides) was combined and dried in a vacuum centrifuge at 13000×*g* for 2 h.

2.7.3 Peptide ion sequencing of OMP by LC-MS/MS and protein identification

Tandem mass spectrometric (MS) analysis of digested peptides was performed in collision-induced dissociation (CID) mode in order to obtain fragment ions of extracted peptides as described by Bowers et al. (2008) and Mukherjee et al. (2011). Initially, dried peptides were resuspended in 20 μL Buffer A (3% (v/v) acetonitrile in HPLC water with 0,1 % (v/v) formic acid) and vortexed during 3 min. Afterwards, peptides were submitted to centrifugation at 13000 RPM for 5 min in a micro centrifuge (5418, Eppendorf, Germany) and 10 μL supernatant were transferred to LC-MS/MS vials. Initially, peptides were separated by liquid chromatography with C-18 capillary column (LC Packings PepMap, Dionex, the Netherlands) in a constant flow rate of 3 $\mu L.min^{-1}$. The elution was performed by Buffer B (97% (v/v) acetonitrile with 0,1 % (v/v) formic acid) with the following elution gradient profile: it starts with 3% (v/v) Buffer B which is constant during initial 5 min; from 5 min to 65 min Buffer B concentration increases from 3% until 40%; from 65 min to 70 min Buffer B concentration increases linearly from 40% until 90% which is kept constant from 70 min to 71 min; from 72 min to 80 min Buffer B concentration is kept constant at 3%. Following that, mass spectrometry was carried out

by Electrospray ionization-Ion trap instrument (amaZon SL, Bruker Daltonics., UK) and CID spectra were obtained. Tandem mass spectrometry was performed on peptides with +2 and +3 charge states and data acquisition was executed by Hystar Interface software (Bruker Daltonics., UK).

Tandem MS data were deconvoluted and converted to Mascot generic format (.MGF file) by Data-Analysis software (version 4.0, Bruker Daltonics., UK). The generated files were loaded on ProteinPilot software (version 4.0, AB Sciex, USA), which allows protein identification from data base searches. The protein data base loaded on the ProteinPilot software was the *Acinetobacter calcoaceticus* (strain PHEA-2) (.FASTA format file) downloaded from UniProt servers (www.uniprot.org). The cellular location of identified proteins was predicted by PSORTb online software (version 3.0.2, PSORTb, www.psort.org).

2.8 Statistical Analysis

The statistical significance of results (except the ones obtained by ATR-FTIRS) was determined by a two-tailed Wicoxon-Mann-Whitney non-parametric test with 95% confidence interval (see Appendix A). The statistical analysis was carried out by Prism 6 software (version 6.0b, GraphPad Software).

3. Results and Discussion

3.1 Growth and respiratory activity

On an initial phase, the growth kinetics and respirometry assays were carried out to study the behavior of *A. calcoaceticus* cultured under distinct agitation speeds. The bacterium used is a Gram-negative aerobe, non-motile, non-spore forming and catalase positive organism (Abbott et al., 1973). A growth kinetics study was performed as described in the previous chapter and growth curves were obtained (see Figure 3-1).

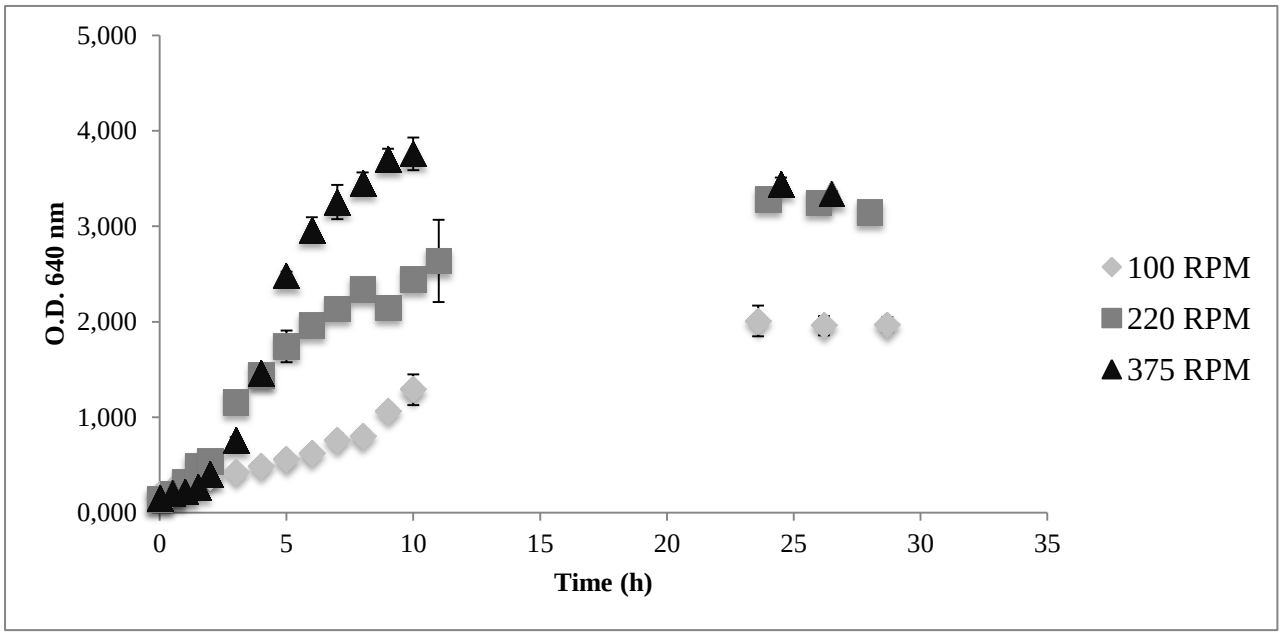

Figure 3-1: *A. calcoaceticus* growth profile at distinct agitation speeds. Cells were cultivated in TSB medium at 30ºC in batch mode. Errors bars stand for standard deviation.

A lag phase of *ca.* 2,5 h was observed for the highest agitations speeds, whereas a lag phase of *ca.* 6 h is attained at 100 rpm. The lag phase is a growth stage at which cells are adapting to the novel medium. At this point, they tend to synthesize enzymes, metabolites and other cellular components, which are important for biomass synthesis (Van Denmark and Batzing, 1987). Thus, it can be assumed that cells growing under the

lowest speed of agitation took longer to adapt to the medium and reach exponential phase. The mid-exponential phase is reached at around 4 h, 4,5 h and 10h for cultures at 375, 220 and 100 rpm, respectively. Moreover, cell density at this stage is significantly different ($p<0,05$, see Appendix A) across different agitation speeds and densities tend to be similar in the stationary phase for 100 and 220 rpm, whereas a cell density decrease is observed at 100 rpm.

In order to evaluate the growth kinetics, reducing sugars (substrate) were quantified during growth curve elaboration and the consumption over time is presented as follows (Figure 3-2).

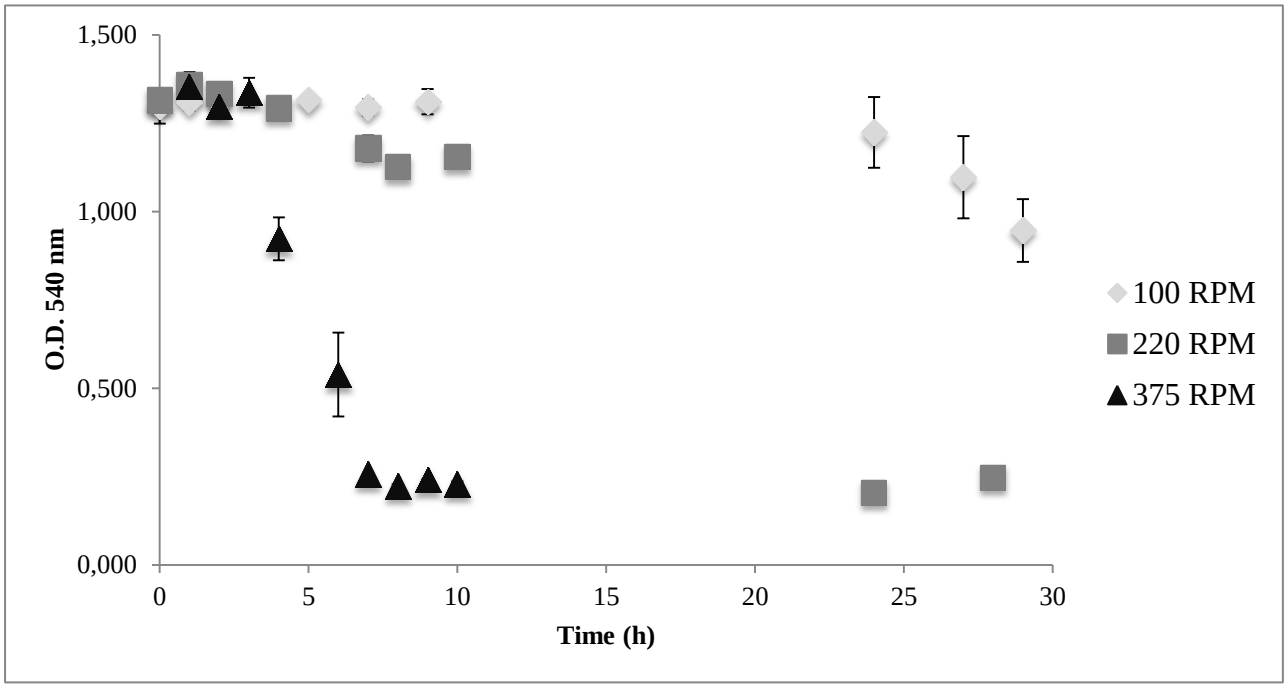

Figure 3-2: *A. calcoaceticus* reducing sugars consumption at distinct agitation speeds. Errors bars stand for standard deviation.

It is shown that in the initial 10 h post inoculation, reducing sugar consumption is significantly faster for cells cultured under 375 rpm than for the ones under different agitation speeds. That is also the period of time where major consumption of substrate is observed as cells reached the exponential phase. At this point, substrate is consumed mainly for biomass and metabolite formation as well as for cell maintenance purposes (Bailey and Ollis, 1986). Besides, substrate was almost depleted throughout the experiment, except for the assays at 100 rpm. At that agitation speed, concentration of

reducing sugars at stationary phase is significantly higher when compared to other agitation speeds, which suggests that this substrate is not the limiting one for growth at 100 rpm. Microbial cultures grow until they reach a stationary phase where substrate is only enough for cell maintenance purposes. Since the substrate consumption at this growth stage was found to be different across tested hydrodynamic conditions, it suggests that agitation speed induced changes on substrate used for cellular maintenance. For instance, Cloete and Bosch (1994) demonstrated that phosphorous uptake by *A. calcoaceticus* occurs at stationary phase with subsequent polyphosphate storage.

The differences observed so far may be mainly attributed to mass transfer effects as at lower speed, agitation tends to decrease the diffusion of substrate molecules leading to the formation of nutrient gradients. Agitation speed can be regarded as an important parameter for adequate mixing of nutrients, mass and heat transfer (Kim et al., 2003) and significantly affects bioconvection and cell swimming, which is thought to influence contact with substrate molecules (Pedley, 1992).

Acinetobacter genus can only use sugars for catabolic processes through the Entner-Doudoroff pathway, which is inoperative under anaerobic conditions (Wentzel et al. 1986). Bearing that in mind, it is possible that at lower agitation speed, mixing is not enough to promote oxygen diffusion as effectively as it occurs at higher agitation speeds, which hampers the Entner-Doudoroff pathway and, consequently, sugars consumption. The lack of oxygen in some regions of the broth may occur at an earlier stage of the growth under 100 rpm, which may explain the difference obtained for cell density at stationary phase. As a matter of fact, Du Preez et al. (1981) suggested that oxygen transfer rate may eventually become the growth limiting factor for the same organism. Nevertheless, it is important to take into account that different agitation speeds induce distinct shear stress, which may lead to distinct cell sizes (Simões et al., 2007). Since cell density determination through spectrophotometry method relies on light scattering by cells, it may happen that cells obtained at 100 rpm may scatter light in a different manner than at 375 rpm representing distinct cell number for each assay.

From the obtained data, kinetic parameters such specific growth rate (μ) and biomass yield in terms of reducing sugars consumption ($Y_{X/S}$) associated to each growth condition was computed and are presented in Table 3-1.

Table 3-1: Kinetic parameters associated to *A. calcoaceticus* cultivation in TSB at distinct agitation speeds, where μ and $Y_{X/S}$ are specific growth rate and biomass yield in terms of substrate consumption, respectively.

Speed (rpm)	μ (h^{-1})	$Y_{X/S}$ ($CFU.g^{-1} \times 10^{11}$)
100	0,098 (±0,004)	30,80 (±1,52)
220	0,132 (±0,005)	3,54 (±0,04)
375	0,322 (±0,032)	4,11 (±0,06)

Table 3-1 shows that bacteria tend to grow faster as agitation speed increases. Specific growth at lowest agitation speed is significant different ($p<0,05$) from the one obtained at highest agitation speed. Cutter and Stroot (2008) obtained a specific growth rate of 0,381 h^{-1} for the same organism cultivated at 250 rpm which is a comparable value to the ones obtained in the present study. Differences are probably due to different growth conditions like medium and aeration system.

Regarding biomass yield, a reduction of around 8 times is observed from the lowest to the highest agitation speed. The values are in the same order of magnitude for 220 and 375 rpm assays. Assuming that higher agitation speeds leads to higher shear stress, it can be stated that the results are in agreement with the literature, since it was observed that remarkable biomass yield reductions are achieved by increasing shear stress (Lertpocasombut, 1991; Liu and Tay, 2001). It was hypothesized that hydrodynamic shear force may have an impact on cell metabolic pathway as it may regulate the substrate flux flowing between catabolism and anabolism (Liu and Tay, 2002).

Aiming to verify the catabolic activity of cells grown under different agitation speeds, respirometry assays were carried out and results are presented in Figure 3-3.

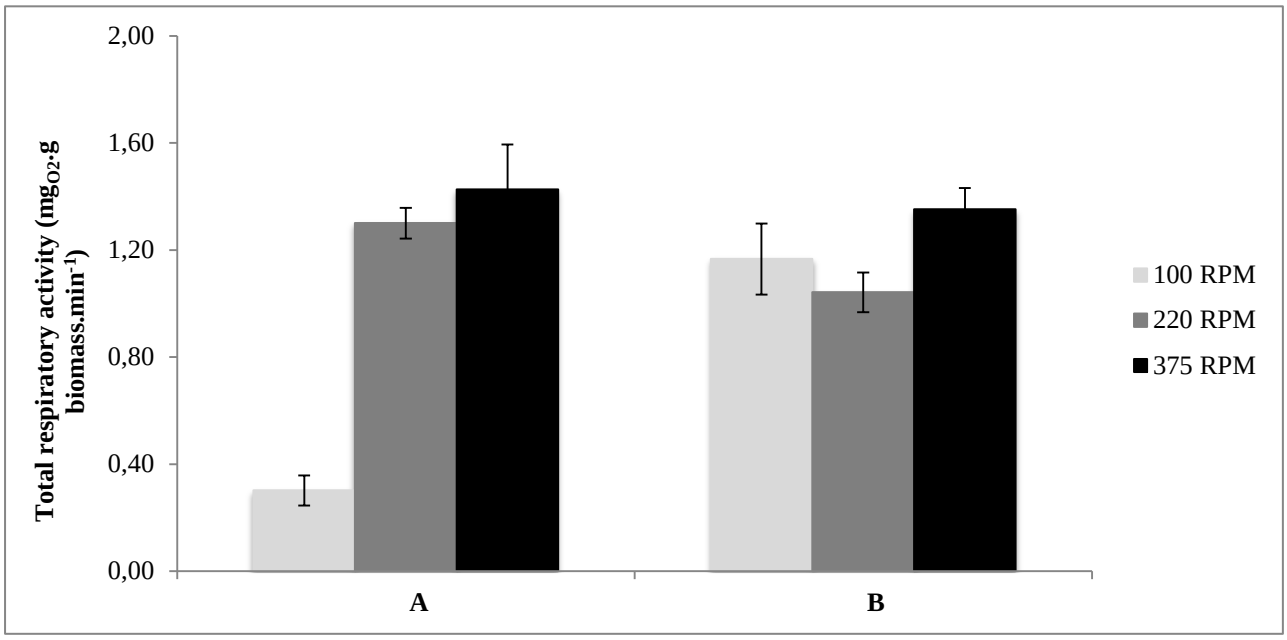

Figure 3-3: Total respiratory activity across different agitation speeds at distinct growth phases. (A) refers to mid-exponential phase and (B) mid-stationary phase. Error bars represent standard deviation.

According to Simões et al. (2005), the respirometry is a reliable method for assessing the metabolic state and respiratory activity in terms of oxygen consumption for heterotrophic aerobic bacteria. Comparison of respiratory activity at mid-exponential phase shows that bacteria grown under 100 rpm had a significantly lower metabolic activity than at higher agitation speeds ($p<0,05$). Biomass yield and specific growth rate were obtained taking into account data obtained at exponential phase, which makes correlation with total respiratory activity at the same growth phase to be possible. Therefore, it is possible to affirm that low agitation speed, consequently, lower shear stress led to high biomass yield with concomitant low respiratory activity. These results seem to be in agreement with the literature (Liu and Tay, 2002; Simões et al., 2007).

The differences between cell growth and metabolic activities across different agitation speed may be the result of interplay between physical and biological phenomena. The first is composed by mass transfer which involves bioconvection and diffusion of essential nutrients (sugars and oxygen) that could increase consumption rate in an environment with proper mixing, whereas the latter can be characterized by a stimulation of catabolism over anabolism (energy uncoupling) as shown in the literature

by proton translocation activity experiments (Liu and Tay, 2001). Moreover, Russell and Cook (1995) showed that an excess of proton translocation cycles at the cell membrane under high agitation speeds takes place when there is an imbalance between catabolic and anabolic rates and that it could be responsible for energy spilling and, consequently, lower growth efficiency.

It is noteworthy that total respiratory activities from 220 rpm to 375 rpm at stationary phase are significant different, which shows the enhancement of total respiratory activity for higher agitation speed. A significant increase of activity is also observed for the experiment at 100 rpm in stationary growth phase. It may be explained by the fact that at stationary phase bacteria does not grow any longer and substrate is channelled exclusively for maintenance purposes, *i.e.* only catabolism occurs. On the other hand, the anabolic process appears to be more active at exponential phase

3.2 Influence of hydrodynamics on cell hydrophobicity

Hydrophobicity at cell surface has been shown in the literature to play a major role on bacterial adhesion potential, which can be crucial for its physiology, cell mobility, colonization and formation of cohesive structures like granules and biofilms (Breiner et al., 2006). In terms of methods for cell hydrophobicity evaluation, MATH assay is one of the most commonly employed methods due to its relative simplicity and relation with adhesion (Phuong et al., 2009; Rosenberg and Doyle, 1990). Therefore, this method was carried out in the present study to evaluate influence of different hydrodynamic environments on bacterial cell surface hydrophobicity. The results are presented in Table 3-2**.**

Table 3-2: Hydrophobicity across different agitation speeds and growth phases obtained by MATH method.

Speed (rpm)	Growth phase	Hydrophobicity Index (%)
100	Mid-exponential	16,2 (±1,7)
	Mid-stationary	6,1(±1,6)
220	Mid-exponential	11,8(±1,2)
	Mid-stationary	1,9(±0,7)
375	Mid-exponential	7,8(±0,6)
	Mid-stationary	3,3(±0,5)

Since operational parameters applied throughout the experiment minimize electrostatic interactions effects (Rosenberg, 2006), obtained hydrophobicity index can be regarded mainly to hydrophobicity at cell surface. According to Tahmourespour et al. (2008), cell surface is regarded as hydrophobic when hydrophobicity index exceeds 50%. Hence, *A. calcoaceticus* presented mainly hydrophilic surface at all tested agitation speeds. It is shown that hydrophobicity at mid-exponential phase tends to decrease significantly ($p<0,05$) with increasing agitation speeds. It is important to notice that higher heterogeneity is observed for bacteria cultivated at 100 rpm when comparing standard deviations.

Hydrophobic interactions represent the attractive force component of the Lewis acid-base interactions, which is mainly based on electron acceptor-electron donor interactions between polar moieties (Van Oss, 1994). Taking that into account, it is plausible to affirm that the differences observed in terms of hydrophobicity along hydrodynamic condition changes may be a reflect of different chemical polar moieties at the cell surface. Hydrophobicity plays a role on cell interaction with the surrounding environment, namely cell-cell interactions and self-aggregation phenomenon. For instance, the higher hydrophobicity obtained for the lowest agitation speed would cause decrease of excess Gibbs energy associated to the cell surface. That way, cell-cell interactions would be favored in a thermodynamic point of view. Furthermore, it was reported in the literature that adhesion of cells to hydrocarbons may occur via proteins as it was shown that *A. calcoaceticus* RAG-1 adhesion occurs via fimbriae (Rosenberg et al., 1982) and *Acinetobacter spp.* A3 occurs through two proteins of 26,5 kDa and 65 kDa (Hanson et al., 1994). Based on that, it can be hypothesized that different agitation speeds

may also induce changes at cell membrane proteins expression level, which will be discussed later in this section.

Controversially, Tay et al. (2001) found that hydrophobicity of cell surface is improved by increasing shear force and that significant difference was observed prior and after granulation. The reason for the differences between these results and the ones obtained in the present work may be mainly associated to granulation extension differences (higher for Tay and Liu, 2001), different experimental set-up (aerated *vs* non-aerated system; media composition) and distinct operational parameters for MATH assay. The latter has been shown to be significantly sensitive to operational parameters like hydrocarbon-aqueous phase volume ratio, vortex duration and buffer ionic strength (Saini, 2010). Besides, it is possible that the magnitude of applied shear forces is distinct between two studies.

Finally, a hydrophobicity decrease from mid-exponential to mid-stationary phase was observed for all the assays, where less pronounced decrease was attained at 375 rpm (*ca.* 58% difference). Palmgren et al. (1998) demonstrated that oxygen limitation is generally responsible for cell surface hydrophobicity reduction. At stationary phase, dissolved oxygen is probably scarce, especially at lower agitation speeds where mixing can be affected, which may be causing the observed hydrophobicity lowering.

3.3 Hydrodynamic condition influence on cell electrophoretic mobility (EPM)

It is well known that bacteria interfacial physiology is very important for organism viability, since it tends to channel portions of its metabolic energy for synthesis and maintenance of essential macromolecules (Beveridge and Graham, 1991). The latter have an impact on the net electronegativity associated to cell surface, which has influence on cell polarity and interaction with substrates in surrounding environment (Wilson et al., 2001). The charge at cell surface is the result of pH dependent ionization of macromolecules functional groups, thus analysis of surface charge gives a hint about the chemistry on cellular interface (Hong and Brown, 2008).

Due to a significant heterogeneity at the cell surface and the fact that evaluation of electrostatic charge of colloids (such as bacteria) is a challenging task, indirect methods

like electrophoretic light scattering, which relates to bacterial electrophoretic mobility, were developed (Lytle et al., 1999). In the present study, the influence of different agitation speeds on cell interface chemical moieties and charge were investigated and results are presented in Figure 3-4 for mid-exponential and stationary phase as follows:

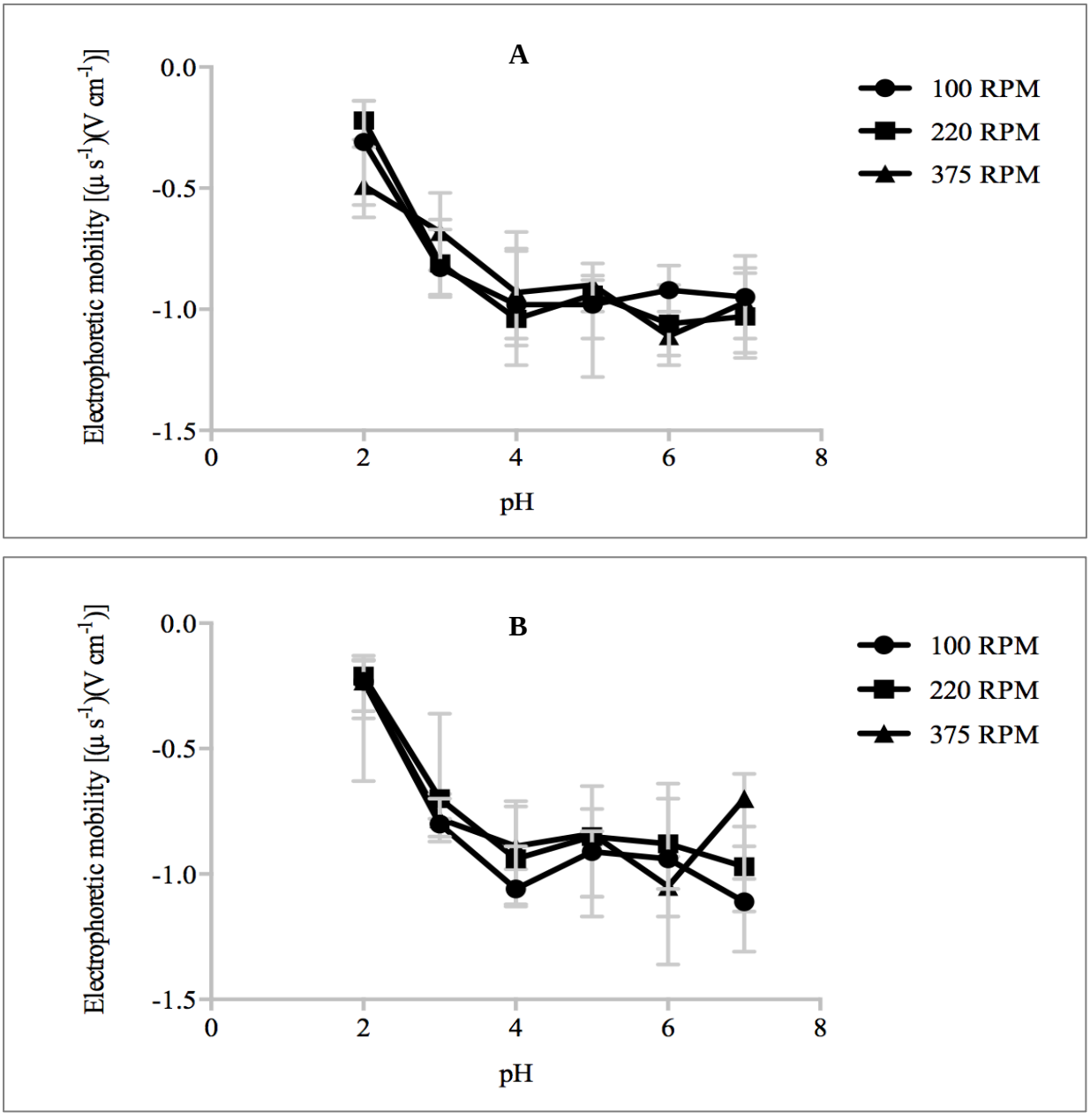

Figure 3-4: Electrophoretic mobility of *A. calcoaceticus* across pH range of 2,0 to 7,0 for distinct agitation speeds. (A) refers to mid-exponential phase and (B) stationary phase. Grey bars correspond to standard errors.

From the literature, net cell surface charge is proportional to its electrophoretic mobility (Marshal, 1976). So, it can be stated that a surface charge increase occurred for all the conditions. Higher surface charge is attained at pH 7 for every condition, except for 375 rpm at stationary phase condition, which is significantly different ($p<0,05$, see Appendix A) from the ones obtained for other agitation speeds (see Figure 3-4).

Assuming that experimental conditions apart from pH (*e.g.* ionic strength, cell density, washing step etc.) were kept constant throughout the experiment and the fact the organism under study is Gram-negative, the observed decreasing trend of electrophoretic mobility along pH can be mainly attributed to high presence of ionized phosporyl and carboxylate functional groups (characterized as anionic with acidic pKa) of lipopolyssacharides (LPS) located in the outer membrane (Rijnaarts et al. 1995; Beveridge and Graham, 1991).

Significant differences between electrophoretic mobilities ($p<0,05$) were found by comparison of 100 rpm and 375 rpm agitation speeds at pH 2 and 6 in mid-exponential phase. On the other hand, significant differences were obtained across different agitation speeds at pH 7 with cells in stationary phase. Those variations may be mainly associated to subtle differences in terms of functional group moieties type and quantity at cell surface (Hong and Brown, 2008). Moreover, interactions between charged moieties play a role as pKa of an anion is increased by anionic-anionic interactions and decreased by anionic-cationic interactions (Rijnaarts et al., 1995; Soon et al., 2011). For instance, differences found at pH 7 for cells in stationary phase can be caused by an increase of functional groups with a basic pKa (such as amines) on surface of cells grown under 375 rpm. Amines can be associated to proteins, thus observed distinct electrophoretic mobility values suggest differences in terms of protein content associated to the cell outer membrane. The cells were submitted to washing steps so extracellular polymeric substances (EPS) at the surface would be removed. Therefore, it can be assumed that differences observed were exclusively due to distinct functional groups at cell interface. From these results, it is plausible to affirm that different hydrodynamic conditions seem to have an impact on functional groups moieties, which in turn are shown to influence cell surface charge.

The electron transport system activity is strongly related to catabolic processes of microorganisms; and for aerobic organisms it has been shown that respiratory activity is coupled to proton translocation phenomenon with consequent oxygen reduction (Babcock

and Wikstrom, 1992). Basically, higher respiratory activities lead to a higher extension of protons translocated through cell membrane and acidification of the medium (Chen and Huang, 2000). Bearing that in mind, the higher accumulation of positive charge observed for bacterial cells under 375 rpm in stationary phase may also be associated to a higher proton translocation through cell membrane. This translocation phenomenon can be attributed to the stimulation of total respiratory activity as observed for bacterial cells cultivated at 375 rpm (see Figure 3-3). Difference of mobilities at pH 7 between growth phases was also evident and it can be a consequence of lipids and lipopolysaccharide conformation and composition changes (El-Khani and Stretton, 1981; Bravo et al., 2008). For example, molecular modeling suggested that LPS assumes a "bent" conformation in such manner O-antigen region covers other adjacent surface-bound molecules which could shield charged regions at the surface (Kastowsky et al., 1992; Walker et al., 2004). It is highly likely that differences at pH 7 across agitation speeds can be related to distinct LPS moieties at cell surface, which will be discussed later.

Hong and Brown (2009) showed that proton motive force across membrane and adenosine triphosphate (ATP) formation are altered by a variation of proton concentration at cell surface caused by charge regulation effects, which occurs between ionizable molecules containing surface. They reported that as bacterium approaches to a positively charged surface, pH at interface (distinct from pH at the bulk) increases and leads to an inverse pH gradient reducing the proton motive force, which would eventually cause cell death and detachment. Considering bacteria as a biotic surface, it can be hypothesized that hydrodynamic stress may also have an influence on cell adhesion potential as charge regulating phenomenon between cells and surfaces are altered by increasing proton concentration on cell interface, which in turn is promoted by high agitation speed.

Lastly, the isoelectric point (pH at which cell surface net charge is null) was not attained in the present work. Nevertheless, it can be seen that the isoelectric point is probably lower than 2,0, which suggests significant amounts of phosphate moieties at cell surface.

3.4 Influence of hydrodynamics on outer membrane chemistry – ATR-FTIR spectroscopy

Biophysical methods such as FTIR spectroscopy have been successfully used for identification and classification of bacteria as well as cell surface analysis (Naumann et al., 1991; Jing et al., 1994). Among the innumerous advantages of this method, cost- and time-effectivity, sensitivity and low biomass requirements are noteworthy (Becker et al., 2006). This method is performed at the mid-IR electromagnetic spectrum region (400-4000 cm^{-1}) and based on passage of IR radiation through a sample where specific wavelengths are absorbed causing chemical bonds vibration (stretching, bending and contracting). Since functional groups absorb in the same wavenumber in an independently manner compared to the rest of the macromolecules, correlation between band positions and functional groups in the molecule is possible (Smith, 1996).

IR spectra obtained for cells are complex and represent many superpositions of contributions from biomolecules present in a bacterial cell, which makes spectra to look similar for all bacteria but with subtle differences that are consequence of a different molecule composition often used for bacteria identification (Davis and Mauer, 2010). Besides, Jiang et al. (2004) concluded that different spectra obtained through ATR-FTIR spectroscopy are due to different properties of the cell wall and not interior of cell, which validates the method as physicochemical analysis of cell surface. Peak assignment to functional groups is a crucial step in ATR-FTIR spectroscopy analysis. Naumann (2000) described major absorbance regions for biological samples, which are highlighted in Table 3-3.

Table 3-3: Assigment of band regions commonly found in biological sample IR spectra. Adapted from Naumann (2000).

Wave number region (cm^{-1})	Assigment
1800-1500	Conformation-sensitive **amide I** and **amide II** bands
Around 1400	$-\mathbf{COO}^-$ functional groups associated to aminoacids and free fatty acids
1500-1300	$>\mathbf{CH_2}$ and $-\mathbf{CH_3}$ bending associated to proteins and lipids
1200-900	Symmetric stretching of $\boldsymbol{PO_2^-}$; **C−O−C** and **C−O−P** stretching vibration associated to oligo- and polysaccharides

In this context, ATR-FTIR spectroscopy was performed in the present study to identify specific functional groups and physicochemical properties variations associated to the cell surface in order to have a deeper insight about the influence of hydrodynamic conditions on bacteria. The spectra of *A. calcoaceticus* at stationary phase under distinct agitation speeds are shown in Figure 3-5.

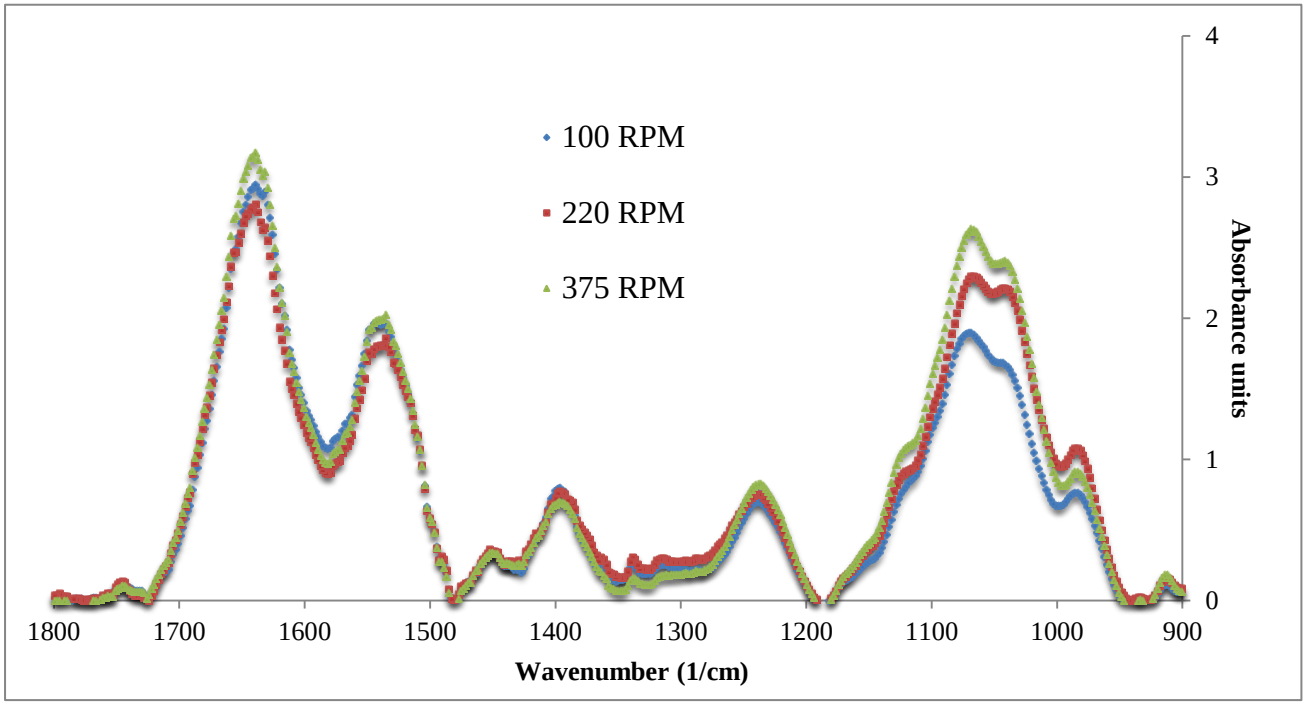

Figure 3-5: ATR-FTIR spectra for *A. calcoaceticus* grown under distinct agitation speeds at stationary growth phase. Blue line represents cells grown at 100 RPM; red line cells at 220 RPM and green line cells at 375 RPM.

From the spectra, it can be seen that cell surface differences across agitation speed are especially in amide I and amide II bands (from 1500 to 1800 cm^{-1}) and polysaccharide-associated ether functional groups (1200 to 900 cm^{-1}). Additionally, slight differences are observed in the region between 1300 and 1400 cm^{-1}, which denotes different moieties of $–CH_2$ and $–CH_3$ associated to lipids and proteins as well as amino acid side-chains and free fatty acids (Naumann, 2000).

In order to evaluate the statistical significance of the observed differences, PCA was carried out and the results are depicted in Figure 3-6. PCA is a multivariate statistical analysis tool that reduces multidimensionality of data into most relevant components and highlights variations between samples (Rodriguez-Saona et al., 2004). Over the range

between 900 to1800 cm^{-1}, it can be affirmed that first (F1) and second principal component (F2) accounted for 69,17% of total variability (29,94% and 39,23%, respectively). Clusters for each agitation speed was attained, which clearly shows that distinct agitation speeds promote significant changes on functional groups at cell surface and that cells grown at the same agitation speeds possess similarities in terms of cell surface chemical composition. From the factor analysis, it is demonstrated that the most significant differences lie in band region 1650 to 1716 cm^{-1} and 1000 to 1175 cm^{-1}, which confirms that polysaccharides and protein content at cell surface are significantly different across agitation speed (see Table C.4 in Appendix C).

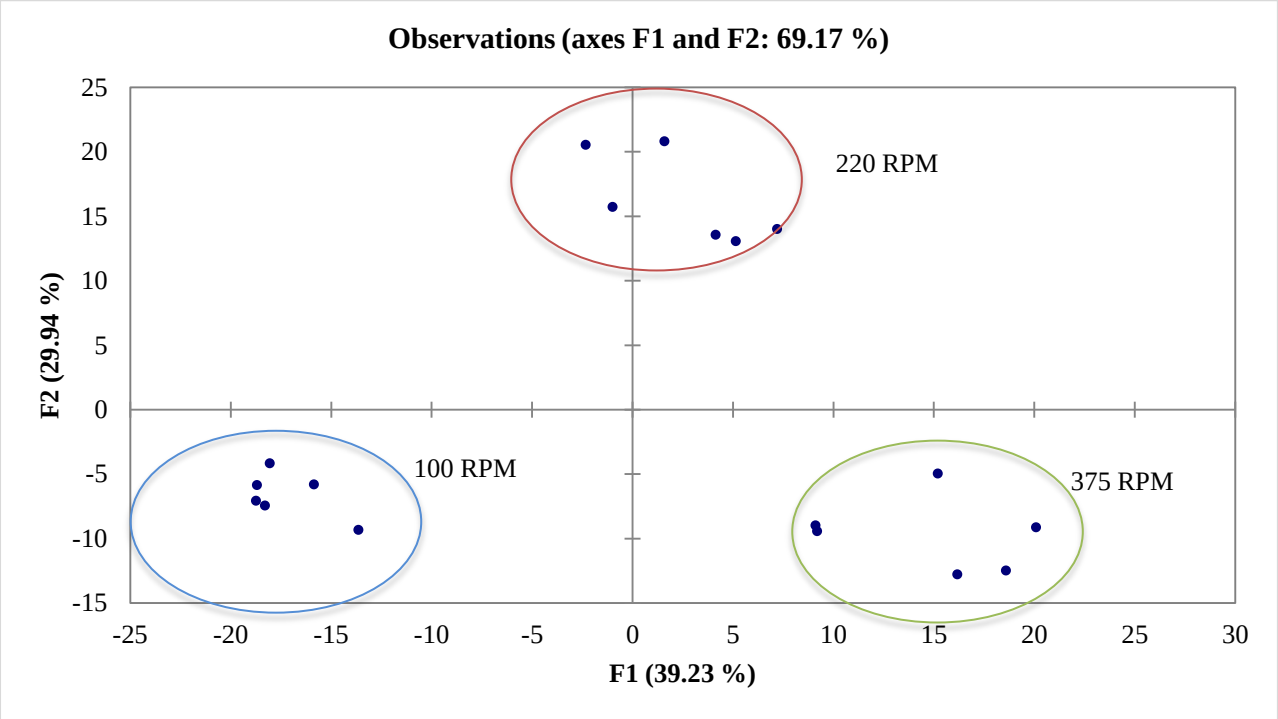

Figure 3-6: Principal Component Analysis (PCA) for *A. calcoaceticus* (at stationary growth phase) ATR-FTIR spectra.

The differences observed in band region of the spectra corresponding to polysaccharides may be attributed to an increase of LPS moieties at surface, which seems to be induced by higher agitation speeds. LPS is the major constituent of the outmost membrane of Gram-negative organism covering around 75% of membrane surface (Gronow and Brade, 2001). These macromolecules represent the primary zone of contact of bacteria with its surrounding medium. In addition, LPS has been shown in the

literature to be crucial for bacteria viability as they serve as a barrier to hydrophobic substances and are involved in the correct folding of porin PhoE (De Cock et al., 1999). LPS highly ordered structure and low fluidity are associated to bacteria mechanical stability (Brandenburg and Seydel, 1990; Lau et al., 2009). This result along the ones obtained for the EPM and MATH assay at stationary phase suggest higher presence of relatively long O-antigen structure for *A. calcoaceticus* LPS. This type of structure is associated to cell hydrophilicity (Arora, 2003) and is linked with shielding charge phenomenon when it is in "bent" conformation, which induces less electronegativity (Walker et al., 2004). Furthermore, LPS represents a highly dynamic part of bacteria as they respond to stressful environments by modifying LPS structure along with other outer membrane proteins (Ohl and Miller, 2001). It can be hypothesized that the bacterial needs for enhanced mechanical stability due to higher hydrodynamic stress may promote production of LPS with relatively long O-antigen structure as a protection mechanism and consequently, cells will be more hydrophilic and less negatively charged with increasing agitation speed.

The same method was performed for *A. calcoaceticus* at mid-exponential phase and different spectra (see Fig B.1 in Appendix B) from the Fig 3-6 was obtained across different agitation speeds. Al-Qadiri et al. (2008) reported that difference of spectra between growth phases is attributable to variations that occur in nucleic acid, protein, lipids and polysaccharide of cellular structure.

3.5 Influence of hydrodynamics on outer membrane chemistry – XPS analysis

In order to have a deeper insight on the elemental cell surface chemical components variation with hydrodynamic conditions, a XPS quantitative analysis was carried out. This method allows determination of surface chemical composition through photoelectric effect. Components are identified by measuring kinetic energies of photoelectrons, which are expelled from the samples by X-ray irradiation (Pastuszka et al., 2005). Besides that, the influence of the chemical state of the element (consequence of chemical bonds made with neighbouring elements) on detected photoelectron binding energy allows the evaluation of chemical functional groups (Ramstedt et al., 2010).

In the present study, wide survey scan and high-resolution scan were performed. The first gives rise to total amounts of elemental components at cell surface like nitrogen (N), carbon (C) and oxygen (O), whereas the latter gives rise to carbon 1s (C1s) and oxygen 1s (O1s) peaks, whose decomposition allows analysis of predominant functional groups and bonding environment analysis. The concentration of components was computed through peak area measurement. The results obtained for different agitation speeds and growth phases are shown in Table 3-4.

From the wide survey analysis presented, it can be seen that carbon and oxygen dominate the cell surface. At mid-exponential phase, it appears that total O tends to increase when agitation speed is higher than 220 rpm, whereas total N seems to lower. For both growth phases, the total carbon found at 220 rpm is the lowest one, whilst the total N is the highest, which points to differences at the surface protein expression level. The obtained results are in agreement with those found in the literature for Gram-negative cells (Mukherjee et al., 2011; Pastuszka et al. 2005).

Table 3-4: XPS result showing elemental composition of *A. calcoaceticus* for different growth phases and agitation speeds

	Binding energy (eV)	Concentration (%)					
		Mid-exponential			Stationary		
Wide survey		100 rpm	220 rpm	375 rpm	100 rpm	220 rpm	375 rpm
Total C	285	68,57 (±1,00)	67,06 (±1,05)	68,89 (±1,24)	67,67 (±0,08)	62,77 (±0,51)	65,20 (±2,46)
Total O	532	25,21 (±1,12)	25,21 (±1,77)	26,55 (±2,32)	25,73 (±0,15)	29,21 (±0,48)	27,59 (±2,62)
Total N	400	6,24 (±0,12)	7,74 (±2,82)	4,57 (±1,07)	6,60 (±0,06)	8,02 (±0,03)	7,21 (±0,16)
High resolution scan							
$\mathrm{C}-(\mathrm{C},\mathrm{H})$	284,6	48,83 (±1,55)	43,61 (±2,74)	44,81 (±3,32)	45,92 (±0,60)	32,37 (±1,05)	36,89 (±6,06)
$\bar{\mathrm{C}}-\overline{(\mathrm{O},\mathrm{N})}$	286,0	35,92 (±1,93)	39,23 (±0,88)	39,95 (±2,42)	37,97 (±1,33)	47,03 (±0,83)	44,06 (±4,48)
$\bar{\mathrm{C}}=\mathrm{O},\mathrm{O}-\underline{\mathrm{C}}-\mathrm{O}$	287,6	12,94 (±2,20)	13,87 (±0,16)	12,96 (±2,64)	13,52 (±2,46)	17,55 (±2,03)	14,74 (±2,39)
$\bar{\mathrm{C}}\mathrm{OOR}$	288,4	2,33 (±1,83)	3,30 (±2,90)	2,28 (±1,74)	2,60 (±1,73)	3,06 (±2,26)	4,32 (±3,96)
$\bar{\mathrm{C}}=\underline{\mathrm{O}},\mathrm{P}=\underline{\mathrm{O}}$	531,0	29,68 (±4,86)	30,85 (±8,10)	19,85 (±9,09)	30,16 (±1,22)	29,89 (±2,02)	27,69 (±5,54)
$\mathrm{C}-\underline{\mathrm{O}}\mathrm{H},\mathrm{C}-\underline{\mathrm{O}}-\mathrm{C},\mathrm{P}-\mathrm{OH}$	532,4	43,44 (±1,70)	60,79 (±5,44)	63,79 (±8,92)	53,21 (±3,69)	55,59 (±6,05)	52,82 (±3,21)
$\mathrm{C}\underline{\mathrm{OO}}\mathrm{R}$	532,5	26,89 (±3,17)	8,37 (±2,65)	16,37 (±0,18)	16,64 (±2,47)	14,53 (±8,07)	19,49 (±2,33)

Table 3-5: Ratio obtained from molecular fractions with respect to carbon and/or nitrogen. (A) corresponds to ratio between carbon singly bonded to heteroatom and total oxygen and nitrogen; (B) carbon doubly bonded to oxygen and total nitrogen; (C) oxygen doubly bonded to carbon and total nitrogen at cell surface and (D) total nitrogen and total carbon.

Ratio	Ratio value					
	Mid-exponential			Stationary		
	100 rpm	220 rpm	375 rpm	100 rpm	220 rpm	375 rpm
A $\frac{[\overline{C}-\overline{(O,N)}/C]}{[\frac{O}{C}+\frac{N}{C}]}$	1,14 (±0,02)	1,19 (±0,06)	1,28 (±0,03)	1,17 (±0,04)	1,26 (±0,00)	1,26 (±0,04)
B $\frac{[\overline{C}=O/C]}{[N/C]}$	2,07 (±0,31)	1,92 (±0,68)	2,99 (±1,28)	2,05 (±0,39)	2,19 (±0,26)	2,04 (±0,29)
C $\frac{[\overline{C}=\underline{O}/C]}{[N/C]}$	4,75 (±0,69)	4,07 (±0,44)	4,23 (±1,00)	4,57 (±0,22)	3,73 (±0,24)	3,83 (±0,69)
D $[N/C]$	0,09 (±0,00)	0,12 (±0,04)	0,07 (±0,01)	0,10 (±0,00)	0,13 (±0,00)	0,11 (±0,00)

The high-resolution scan pertaining to C1s and O1s allowed the evaluation of predominant functional groups at cell surface. The $(\mathrm{C}-(\mathrm{C},\mathrm{H}))$, $(\mathrm{C}-\underline{\mathrm{O}}\mathrm{H})$, $(\mathrm{C}-\underline{\mathrm{O}}-\mathrm{C})$ are predominant functional groups for all different agitation speeds at both growth phases and represent hydrocarbon-like compounds, alcohol and hemiacetal often associated to polysaccharides, respectively (Dufrêne et al., 1999). Moreover, it is noteworthy that $(\bar{\mathrm{C}}-\overline{(\mathrm{O},\mathrm{N})})$ functional group tend to increase concentration by increasing agitation speed from 100 to 220 rpm and is constant from 220 to 375 rpm. Cuperus et al. (1992) observed that $(\bar{\mathrm{C}}-\overline{(\mathrm{O},\mathrm{N})})$ indicates presence of polysaccharides at the cell surface, hence the observed trend across agitation speeds is in agreement with FTIRS results, where higher absorbance units associated to polysaccharides were attained at higher agitation speeds (see Fig. 3-5).

Regarding bonding environment of carbon and oxygen, Rouxhet et al. (1994) defined a series of plots, which shows the fraction of carbon or oxygen bonded to other elements as function of sum of total oxygen and/or total nitrogen with respect to carbon. Since the present XPS analysis was carried out in duplicates, relations between those components are shown in terms of ratios as presented in Table 3-5. (Equation A) corresponds to ratio between carbon singly bonded to heteroatom and total oxygen and nitrogen; (Equation B) is the ratio between carbon doubly bonded to oxygen and total nitrogen and (Equation C) is the oxygen doubly bonded to carbon with respect to total nitrogen.

It can be seen that all conditions presented an (Equation A) result with ratio close to 1,0, where at both growth phases ratio tends to increase along agitation speed meaning there may be higher presence of ether and acetal functional groups at higher agitation speeds. Ratios obtained by Equation B tend to increase substantially from 100 rpm to 375 rpm (*ca.* 50% variation) at mid-exponential phase, whereas at stationary phase value does not change significantly. That points to an increase in the carbonyl group (C=O) not associated to surface proteins along agitation speed at mid-exponential phase. Regarding Equation C, it reveals the bonding environment of oxygen and obtained ratios corroborate higher presence of (C=O) groups not associated with amides (Boonaert and Rouxhet, 2000).

Hamadi et al. (2008) studied the relation between functional groups at *Escherichia coli* surface and its physicochemical properties and found that as $\bar{\mathrm{C}}=\underline{\mathrm{O}}$ functional group moieties increase, electrophoretic mobility becomes more negative. The presence of

$\bar{C} = \underline{O}$ tends to be similar within 100 to 220 rpm range and decreases at 375 rpm (see Table 3-4). Thus, obtained results for XPS seems to be in agreement with the ones obtained by EPM measurements as less negative cell surface at pH 7 was attained at 375 rpm on stationary growth phase. Moreover, it is an evidence of contribution of distinct carboxyl group moieties at cell surface, which is induced by different hydrodynamic environments, to differences in terms of observed electrophoretic mobility.

The cell hydrophobicity has been associated to certain functional groups at the surface and correlation between $(\bar{C} - \overline{(O, N)})$;$\left(C - \underline{O}H, C - \underline{O} - C\right)$ and $C - (C, H)$ with hydrophobicity was established in the literature (Mozes et al., 1998; Hamadi et al., 2008). Whilst the latter has been found to be directly correlated with hydrophobicity, the first two functional groups were inversely correlated owing it to the presence of O and N, which favours hydrogen bonds. Taking that into account, it can be stated that results obtained by XPS are in agreement with the ones obtained by MATH assay in the present study. For example, increasing $(\bar{C} - \overline{(O, N)})$ functional group concentration with agitation speed observed at both growth phases can explain the decreasing hydrophobicity. Despite Marshal et al. (1994) warning regarding the errors that may be associated to relationships between XPS data and cell surface properties for Gram-negative cells, obtained results are in agreement with previous experiments.

Rouxhet et al. (1994) established that results obtained by XPS for chemical functions can be worked out further in order to predict the molecular composition associated to the cell surface. Basically, they developed a set of equations (see Appendix D) in which parameters obtained by XPS are represented as function of model constituents, such as protein (Prot), polysaccharide (Poly) and hydrocarbon-like compounds (Hydroc). By using a set of equations proposed by Rouxhet et al. (1994), the results regarding bonding environment gave rise to ratios of protein, hydrocarbon-like compounds and polysaccharides with respect to total carbon were assessed and results at distinct growth phases are shown as follows.

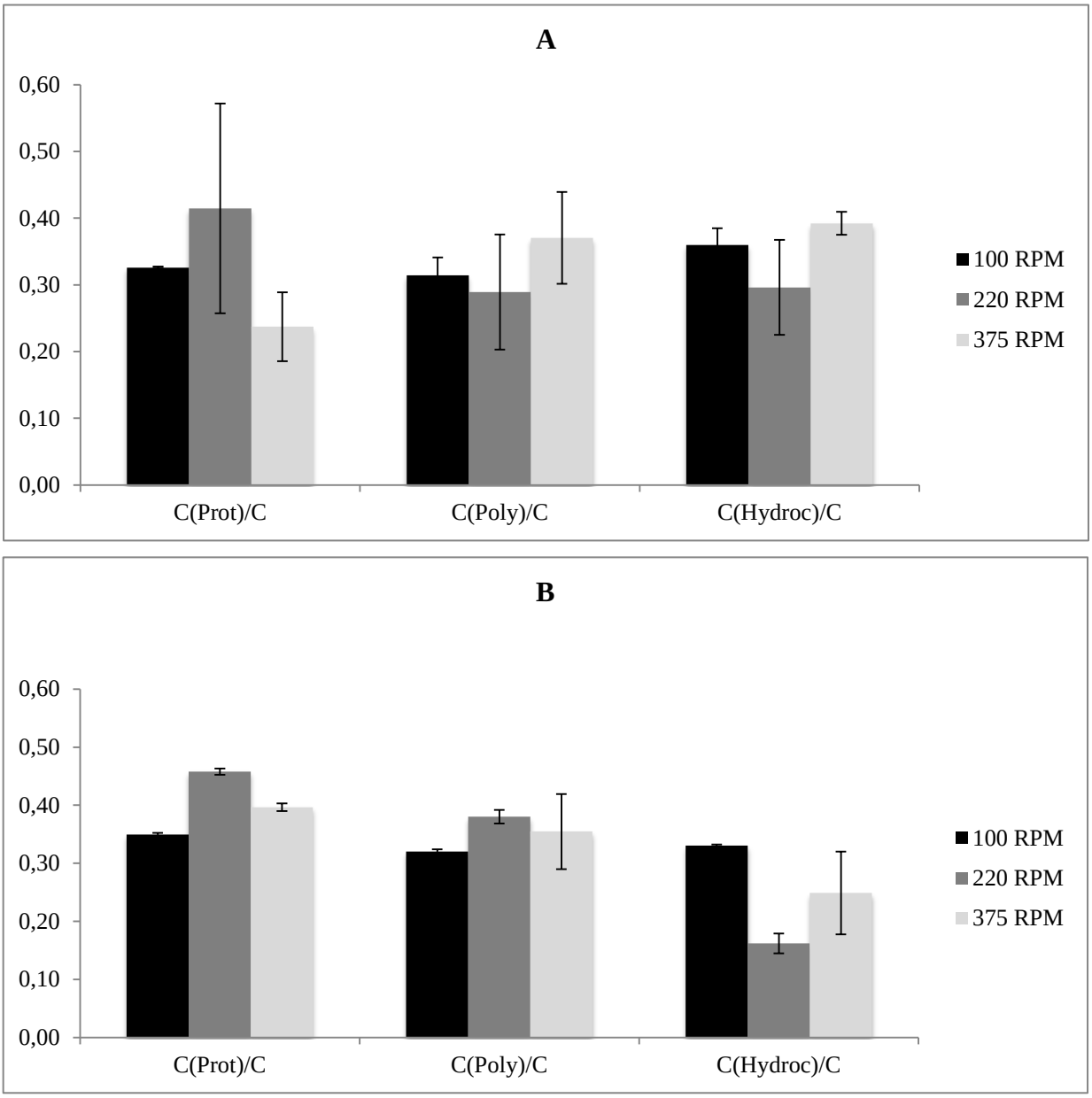

Figure 3-7: Cell surface molecular composition in terms of cell fraction occupied by cell wall main constituents. (A) refers to mid-exponential phase and (B) stationary phase.

It can be seen in Figure 3-7 that macromolecules profile is different across agitation speeds. At mid-exponential phase, the hydrocarbon-like compounds are the predominant constituents of cell surface, except at 220 rpm, which possess higher amounts of proteins. On the other hand, protein levels are much higher at stationary phase and tend to increase with agitation speed. It is noteworthy that polysaccharides tend to increase with increasing agitation speeds for both growth stages and confirms previous results presented in this section. Walker et al. (2004) reported that polysaccharides

exposed on the outer membrane represent an important factor controlling bacterial adhesion and transport, thus it can be suggested from these results that hydrodynamic environment may have an impact on cell adhesion processes not only by physical component (detachment and attachment) or force interaction with lectin-like adhesin FimH (Thomas et al., 2002), but through biological modifications in terms of macromolecules types at the surface. Similarly to these results, Tay et al. (2001b) reported that high shear stress stimulated production of cellular polysaccharide, which were shown to be associated to granulation phenomenon.

Although main constituents could be predicted by this method, it was not possible to differentiate phospholipids from other lipid compounds nor polysaccharides and lipopolysaccharides. Furthermore, it should be noticed that the cell surface composition prediction may not reflect real surfaces, since cells were submitted to freeze-drying which may change the cell surface or even lead to cell disruption.

3.6 Hydrodynamics influence on auto-aggregation capability

It is well known that *A. calcoaceticus* is an organism capable of auto- and co-aggregate as its bridging function for biofilm formation was reported (Simões et al. 2008). Auto-aggregation and co-aggregation phenomena have been shown to be important processes on coherent structure formation like biofilms and represent an important part of bacteria collective behavior. Hence, the influence of different hydrodynamic environments on aggregation feature of *A. calcoaceticus* at stationary phase was investigated through quantitative (spectrophotometric assay) and semi-quantitative (visual assay) methods. The results are shown in Table 3-6.

Table 3-6: Auto aggregation index for *A. calcoaceticus* at stationary phase cultivated under different agitation speeds along with co aggregation scores over time obtained by visual assay.

Speed (rpm)	Auto-aggregation after 1h (%)	Score after 2h	Score after 24h	Score after 48h
100	3,40 (±1,06)	2	4	4
220	2,71 (±0,74)	1	3	4
375	0,62 (±0,31)	0	2	3

It can be noted that auto-aggregation was affected by different agitation speed, since auto-aggregation index tends to reduce considerably when agitation speed is increased from 220 rpm to 375 rpm. Nevertheless, differences of auto-aggregation index among distinct agitation speeds were not significant different ($p>0,05$). The visual assay corroborates the results obtained for the auto-aggregation index as faster settleability was achieved at lower agitation speed (see also Fig B.3 in Appendix B). Although visual assay has been associated to lack of sensitivity (Elliot et al., 2006), reproducible results were obtained and are in agreement with auto-aggregation trend revealed by the spectrophotometric assay.

The capability of cells to auto- and co-aggregate is associated to its adhesion potential, which depends mainly on Van der Waal (attractive), electrostatic (repulsive) forces and Lewis acid-base interactions (hydrophobic and steric interactions) (Olofsson et al., 1998; Saini, 2010). Additionally, specific interactions that involve adhesins and complementary receptors, more specifically lectin-saccharide interactions, were shown to be crucial for the auto-aggregation process (Buswell et al., 1997). In the literature, hydrophobic interactions have been emphasized as a driving-force for cells to initiate bacterium-bacterium contact out of the liquid phase and have been correlated directly with aggregation phenomena (Liu and Tay, 2002; Phuong et al., 2009). In this context, the obtained result agrees very well with one obtained by MATH assay as cell grown at slowest agitation speed presented higher hydrophobicity and auto-aggregation index, suggesting that hydrophobicity was the predominant interaction upon auto-aggregation. It was shown by XPS that cells grown in different hydrodynamic conditions possess different surface chemistry with different amounts of proteins, polysaccharides and even hydrocarbon-like compounds. Since specific interactions between lectin and saccharide are important to auto-aggregation as well as the densities of those ligands on cell surface (Simões et al., 2008; Buswell et al., 1997), it is possible to infer that hydrodynamic environment may have an impact on the moieties and distribution of those specific ligands at cell surface.

The auto- and co-aggregation collective behavior has clear advantages to microorganisms, like ease transfer of chemical signals, exchange of genetic information and higher metabolic cooperation (Wimpenny and Colasanti, 2004). Lower agitation speed is associated to lower mass transfer of important metabolites and formation of nutrient gradients. Therefore, it can be hypothesized that higher auto-aggregation

extension for cells cultivated at 100 rpm is part of mechanism by which cells undergo in order to overcome mass transfer issues.

3.7 Outer membrane protein (OMP) variations with distinct hydrodynamic conditions

Proteome is part of a dynamic system by which cells use to adapt to different environments. Proteins represent cellular building blocks that show potential function of genes through cellular processes ranging from enzymatic catalysis to molecular signaling (Yates et al., 2009).

In this study, the outer membrane proteins (OMP) of cells grown under different agitation speeds at stationary phase were separated and identified by LC/MS in bottom-up approach. Extracted proteins were submitted to SDS-PAGE analysis prior separation and result is presented in Figure B.2 (in Appendix B). It is noteworthy that protein profile is comparable among agitation speeds, where major differences are only in terms of band intensity in the region ranging from 29 kDa to 20 kDa. Since lanes represent duplicates for each condition, differences between duplicates within a condition may represent certain heterogeneity in terms of protein expression, in this case, higher heterogeneity was attained for cells cultivated at 100 rpm.

Further analysis through LC/MS separation and direct search against *A. calcoaceticus* protein database allowed identification of extracted proteins. Identified OMP with respective accession number for each tested condition are found in Appendix C. For 100 rpm, 220 rpm and 375 rpm conditions, 17%, 26% and 27% of total identified proteins were OMP, respectively. This result seems to agree well with the prediction carried out through XPS analysis as at 100 RPM less proteins were found at the cell surface. The number of OMP and respective functions were obtained for each condition and are presented in Figure 3-8.

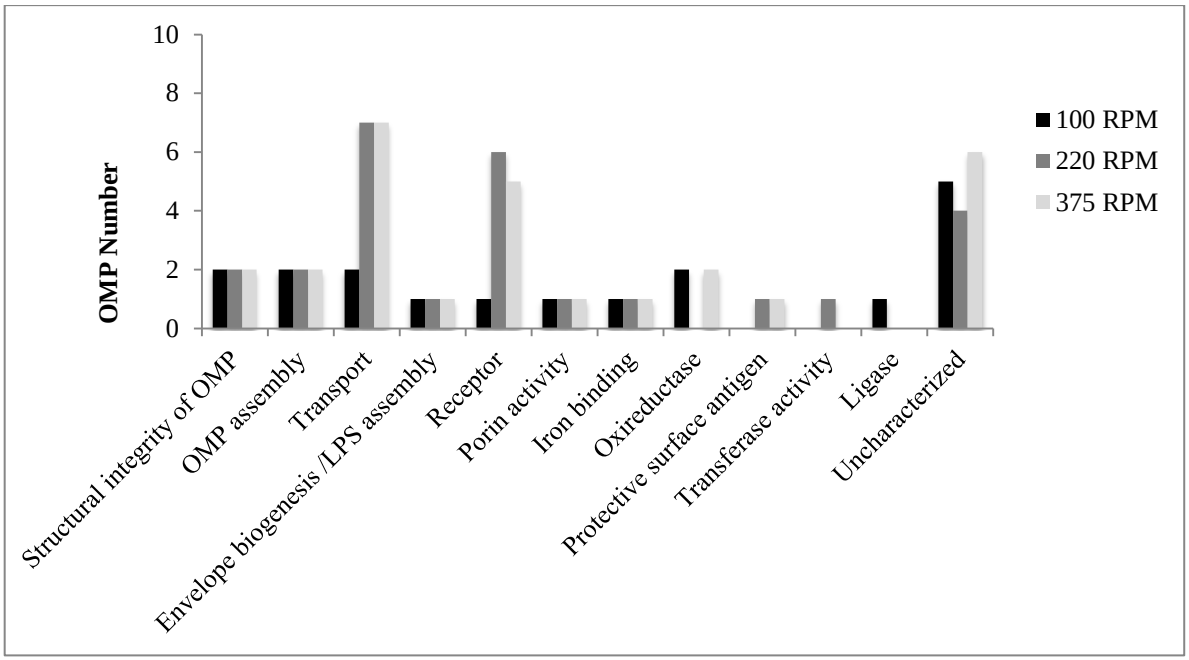

Figure 3-8: Number of OMP with respective function identified for *A. calcoaceticus* grown under different agitation speed at stationary phase.

Apart from uncharacterized proteins, it is noticeable that major differences among agitation speeds rely on proteins that have transport and receptor functions. Bacterial cells cultivated at higher agitation speeds showed a higher number of those proteins compared to 100 rpm condition. It is known that transport processes play an important role in cellular metabolism, since uptake of nutrients, excretion of toxic metabolites and maintenance of ion concentration depend on it (Burkovski and Kraemer, 2002). Receptor proteins bind to specific molecules, which lead to conformation changes and control of a multitude of cellular activities, i.e., receptor proteins represent a connection between cell internal and external environments (Mitchel, 2013). Therefore, it seems that cells grown under higher agitation speeds have more complete apparatus to sense the environment, which may yield to rapid metabolic responses to environmental stress.

TonB-dependent receptor (F0KNU8_ACICP); putative hemolysin activator (F0KPM4_ACICP); putative outer membrane copper receptor (F0KJZ1_ACICP) were receptor/transport proteins only found for 220 and 375 rpm conditions. The first protein is associated to TonB-dependent transport, which involves a TonB complex that transduces proton motive forces of the cytoplasm to energize transport of rare nutrients such as vitamin B_{12}, iron and nickel transport across the outer membrane (Schauer et al., 2008; Schauer et al., 2007). This complex is often associated to pathogenicity factor because

bacteria survival chances in their hosts will rely on the ability to compete for micronutrients (Miethke and Marahiel, 2007). Apart from TonB role on molecules transportation, it was found that TonB complex is also involved in recognition and binding of cells to fibronectin, which allows effective colonization of niches in a given host (Pauer et al., 2009). Putative hemolysin activator is a protein predicted by bioinformatics tools, which are thought to be involved in transport mechanism that is associated to transcription activation of hemolysin, prototype of homologous RTX family of toxins secreted by Gram-negative bacteria (UniProt Consortium, 2013; Langston et al., 2004). The putative outer membrane copper receptor was also predicted to be part of TonB complex and can be regarded as fibronectin binding protein, which has been shown to be crucial for bacteria adhesion to fibronectin surfaces and pathogenicity of *Acinetobacter baumanii* (Smani et al., 2012). In general, it is plausible to affirm that those proteins are strongly involved with cell pathogenicity, adaptation and survival. Hence, it corroborates results found in the literature where higher activity and more diverse metabolic mechanisms were suggested for cell cultivated under turbulent regimes (Liu and Tay, 2002; Simões et al. 2007).

Zhan et al. (2011) reported that *A. calcoaceticus* PHEA-2 acquired many genes associated to cell adaptation through horizontal gene transfer. Furthermore, Hendrickx et al. (2000) showed that *A. calcoaceticus* BD413 subjected to high shear stress displayed higher transformation frequency in terms of ratio of cells transformed to recipient cells. Bearing that in mind, it can be hypothesized that lack of most transport/receptor proteins at 100 rpm may be associated to low horizontal gene transfer due to low shear stress and mass transfer effects and clearly it has an impact on cell survival dynamics.

In terms of oxireductases, two proteins were identified at 100 rpm and 375 rpm and none at 220 rpm. Electron transfer flavoprotein alpha-subunit (F0KL87_ACICP) and Malate dehydrogenase (F0KPX6_ACICP) were the identified proteins. The first is a soluble heterodimeric FAD-containing protein which functions as electron carrier between diverse flavoprotein dehydrogenases and are strongly associated to membrane-bound respiratory activity (Toogood et al. 2007). The latter is an enzyme involved in the reversible catalysis of reversible oxidation of malate to oxaloacetate, which is part of tricarboxylic acid cycle associated to aerobic respiration pathway (Eprintsev et al. 2004). According to Trémoulet et al. (2002), malate dehydrogenase is highly regulated in order to adapt to different growth conditions and is involved in biofilm growth. Shin et al. (2009) demonstrated that proteins involved in metabolism like malate dehydrogenase are

up-regulated when *Acinetobacter baumannii* 1656-2 undergo biofilm formation. Therefore, the fact that those proteins were only identified for 100 rpm and 375 rpm conditions (both regarded as stress conditions) may be due to an up-regulation of those proteins caused by cell trend to form biofilm. In this case, a biofilm formation study in a flow cell reactor with hydrodynamic environments similar to the ones applied in this study would represent a huge asset. Interestingly, the presence of those proteins involved in cellular respiration is in agreement with results obtained for respirometry assay (see Figure 3-3) because higher respiration activities were attained at stationary phase for 100 RPM and 375 rpm conditions (as opposed to mid-exponential phase).

Proteins exclusive to each condition were identified and are presented in Table 3-7 as follows.

Table 3-7: Proteins identified exclusively for each condition.

Speed (rpm)	Accession number	Protein	PSORTb score for outer-membrane location
100	F0KLX8_ACICP	Succinyl-CoA ligase [ADP-forming] subunit beta	0,05
220	F0KPM3_ACICP	Putative member of ShlA/HecA/FhaA exoprotein family	9,95
	F0KGT9_ACICP	Ferric enterobactin receptor	10
375	F0KHB5_ACICP	Putative ferric siderophore receptor	10

It is shown that proteins identified for 220 rpm and 375 rpm are associated to iron metabolism of cells as Gram-negative bacteria acquire iron through elaboration of chelating agents (*e.g.* ferric siderophores) and uptake of the ferric complex by specific receptors, which are TonB-dependent outer membrane receptor proteins (Cae et al., 2000; Payne et al. 1997). Differences in terms of iron metabolism can be inferred, which seems to be influenced by the agitation speed. The iron metabolism is often associated to pathogenicity of bacteria, thus it is highly probable that bacteria cultivated under higher speed agitations are more pathogenic and, consequently, more metabolically active.

On the other hand, the protein identified only for 100 rpm condition catalyzes a reversible reaction of succinyl-CoA to succinate, which is important for substrate-level

phosphorylation step of tricarboxylic acid cycle (Nishimura, 1986). Despite being known as cytoplasmic protein, Thomas (1974) observed that diglyceride kinase activity of isolated *E. coli* vesicles at cell membrane is mediated by succinyl CoA synthetase, which can appear at the inner membrane. Diglyceride kinase is an enzyme involved in the biosynthesis of membrane phospholipids (Raetz and Newman, 1979). It can be suggested that cells at 100 rpm may also differ from the ones grown at higher agitation speeds in terms of inner membrane phospholipids formation dynamics, which can even contribute to distinct cell mechanical stability.

In order to have a clearer picture about the influence of different hydrodynamic conditions on bacteria proteome and their metabolic pathways, it would be interesting to perform quantitative proteomic studies not only at the level of outer membrane, but at cytoplasmic level as well.

4. Conclusions and future work perspectives

The outcomes of hydrodynamic conditions on bacteria behavior have been extensively studied in the literature mainly at cohesive structure formation level. In order to have a clear picture about hydrodynamics impact on cell growth, physiology and dynamics, the present study focused on the influence of different agitation speeds on bacteria at planktonic state growth and metabolic activity as well as on cell surface properties.

In terms of growth kinetics and metabolic activity, it was observed that cells grown under lower agitation speed had lower growth rate with lower reducing consumption and total respiratory activity. Those results were in agreement with the ones found in the literature and confirm that hydrodynamics have influence on cell catabolism and anabolism, as microbial cells cultivated under 100 rpm seemed to direct carbon mainly to anabolic pathways, which gives rise to higher biomass yield in terms of reducing sugars consumption with concomitant lower respiratory activity. The observed uncoupling between anabolic and catabolic processes can be regarded as one of the evidences that attest for biological component associated to hydrodynamics.

Microbial cell surface represents a crucial interaction interface between cells and biotic/abiotic surfaces and as such, possess important roles on microbial cell growth dynamics. This study showed that cell surface present different chemistry for different hydrodynamic environments, which may contribute to observed differences in terms of cell surface hydrophobicity and surface charge. Since those properties are assumed to be relevant for cell interactions, it can be concluded that cells may present distinct interactions with its surroundings depending on the hydrodynamic conditions. Differences in terms of macromolecules moieties at the surface were mainly associated to polysaccharides, which were shown to increase significantly with increasing agitation speed conditions. Due to the fact LPS is a major constituent of Gram-negative cells outer membrane, differences in polysaccharide content can be associated to different moieties of LPS at outer membrane, which may impart different features to cell surface.

Furthermore, LPS was hypothesized as part of protection mechanism of Gram-negative bacteria against mechanical stress that is promoted at higher agitation speeds. This study showed that hydrodynamics may have an impact on cell adhesion and cohesive structure formation processes not only by a physical component (associated to shear stress and detachment) but through biological modifications of macromolecules at the cell surface. In this context, the observed differences with respect to bacteria auto aggregation capability can be explained as the final product of cell-cell interaction dynamics, which are affected by different moieties of macromolecules promoted by distinct hydrodynamic conditions.

Regarding the outer membrane proteome, it was verified that bacteria cultivated under higher agitation speeds present higher number of proteins associated to cellular transport and reception mechanisms. Since those mechanisms represent an important connection between cells internal and external environments, the result points to a higher capability of cell under higher agitation speeds to sense the environment and respond quickly to variations at metabolic level. This can lead to more resilient and dynamic bacterial cells. Additionally, some proteins identified for cells at higher agitation speed (*eg.* TonB-dependent receptor and copper receptor) are associated to pathogenicity factors and cell survival capability in wider range of environments, which suggests that hydrodynamics can influence cell surface protein content, and consequently, microbial cell metabolic versatility and activity. In order to have a clearer picture on the direct influence of hydrodynamics on cell proteins and metabolic pathways, it would be interesting to perform a quantitative proteomics analysis not only at the outer membrane level, but at the cytoplasmic level as well.

Finally, in engineering point of view it is important to have a deeper understanding of the mechanisms by which hydrodynamics influence cell metabolism and the outcomes predicted by complete mathematical models of a certain set of conditions. In this context, the mathematical characterization of hydrodynamic environment and realization of the set of experiments performed throughout this project at higher scales in a wider range of agitation speed conditions would represent a huge asset for hydrodynamics influence on bacteria behavior modeling process.

5.References

Abbott, B.; Laskin, A. and McCoy, C. (1973). Growth of *Acinetobacter calcoaceticus* on ethanol. Applied Microbiology. Vol. 25, pp: 787-792.

Adler, J. (1966). Chemotaxis in bacteria. Science 153:708-716.

Al-Qadiri, H.; Alami, N.; Lin, M. et al. (2008). Studying of the bacterial growth phases using Fourier transform infrared spectroscopy and multivariate analysis.Journal of Rapid Methods and Automation in Microbiology. Vol. 16, pp: 73-89.

APHA;AWWA; and WPCF. (1989). Standard methods for the examination of water and wastewater 17th edition. American Public Health Association. Washington DC, USA.

Armitage, J. and Schmitt, R. (1997). Bacterial chemotaxis: *Rhodobacter sphaeroide* and *Sinorhizobium meliloti*-variations on a theme ?. Microbiology. Vol. 143, pp.: 3671-3682.

Arora, B. (2003). Detection of polysaccharide on a bacterial cell surface using atomic force microscopy. Worcester Polytechnic Institute. Worcester, United Kingdom.

Atlas, R. and Bartha, R.. (1987). Chapter 8: Effects of abiotic factors on microorganisms. In Microbial Ecology. Second Edition. Benjamin/Cummings Publications. California, United States of America.

Babcock, G.; Wikstrom, M. (1992). Oxygen activation and the conservation of energy in cell respiration. Nature. Vol. 356, pp: 301-309.

Bailey, J. and Ollis, D. (1986). Biochemical Engineering Fundamentals. McGraw-Hill. New York, United States of America.

Becker, K.; Al Laham, N. and von Eiff, C. (2006). Fourier-transform infrared spectroscopic analysis is a powerful tool for studying the dynamic changes in *Staphylococcus aureus* small-colony variants. Journal of Clinical Microbiology. Vol. 44, pp: 3274-3278.

Berke, A.; Turner, L.; Berg, C. et al. (2008). Hydrodynamic Attraction of Swimming Microorganisms by Surfaces. Physical Review Letters. Vol. 101, pp.: 1-4.

Beveridge, T. and Graham, L. (1991). Surface layers of bacteria. Microbiology Review. Vol. 55, pp: 684-705.
Blake, J. (1971). A note on the image system for a stokeslet in a no-slip boundary. Cambridge Philosophical Society. Vol. 70, pp.: 303.

Boonaert, C. and Rouxhet, P. (2000). Surface of lactic acid bacteria: relationship between chemical composition and physicochemical properties. Applied Environmental Microbiology. Vol. 66, pp: 2548-2554.

Bowers, J.; Liu, J.; Gunawardena, H. et al. (2008). Protein identification via ion-trap collision-induced dissociation and examination of low-mass product ions. Journal of Mass Spectrometry. Vol. 43, pp: 23-34.

Brandenburg, K. and Seydel, U. (1990). Investigation into the fluidity of lipopolysaccharide and free lipid A membrane systems by Fourier-transform infrared spectroscopy and differential scanning calorimetry. European Journal of Biochemistry. Vol.191, pp: 229-236.

Bravo, D.; Silva, C.; Carter, J. et al. (2008). Growth-phase regulation of lipopolysaccharide O-antigen chain length influences serum resistance in serovars of *Salmonella*. Journal of Medical Microbiology. Vol. 57, pp: 938-946.

Breiner, J.; Anderson, M., Tom, H. et al. (2006). Properties of surface-modified colloidal particles. Clay and Clays Minerals. Vol. 54, pp: 12-24.

Brennen, C. and Winet, H. (1977). Fluid mechanics of propulsion by cilia and flagella. Annual Review of Fluid Mechanics. Vol. 9, pp.: 339-398.
Breuil, C. and Saddler, J. (1985). Comparison of the 3,5-dinitrosalicylic acid and Nelson-Somogyi methods of assaying for reducing sugars and determining cellulose activity. Enzyme and Microbial Technology. Vol. 7, pp: 327-332.

Burkovski, A. and Kraemer, R. (2002). Bacterial amino acid transport proteins: occurrence, functions, and significance for biotechnological applications. Applied Microbiology and Biotechnology. Vol. 58, pp: 265-274.

Buswell, C.; Herlihy, Y.; Marsh, P. et al. (1997). Co-aggregation amongst aquatic biofilm bacteria. Journal of Applied Microbiology. Vol. 83, pp: 477-484.

Calleja, G. (1984). Microbial aggregation. CRC Press. Florida, United States of America.

Cao, Z.; Qi, Z.; Sprencel, C. et al. (2000). Aromatic components of two ferric enterobactin binding sites in *Escherichia coli* FepA. Molecular Microbiology. Vol. 37, pp: 1306-1317.

Chang, H.; Rittmann, B.; Amar, D.; Heim, R.; Ehrlinger, O.; Lesty, Y. (1991). Biofilm detachment mechanisms in a liquid fluidized bed. Biotechnology and Bioengineering. Vol. 38, pp: 409-506.

Chen, S.; Huang, S. (2000). Shear stress effects on cell growth and L-DOPA production by suspension culture of *Stizolobium hassjoo* cells in an agitated bioreactor. Bioprocess Engineering. Vol. 22, pp.: 5-12.

Chen, G. and Pramanik, B. (2009). Application of LC/MS to proteomics studies: current status and future prospects. Drug Discovery Today. Vol. 14, pp.: 465-471.

Chopp, D.; Kirisits, M.; Moran, M. et al. (2003). The dependence of quorum sensing on the depth of a growing biofilm. Bulletin of Mathematical Biology. Vol. 65, pp.: 1053-1079.

Cisar, J.; Kolenbrander, O. and McIntire, F. (1979). Specificity of coaggregation reactions between human oral Streptococci and strains of *Actinomyces viscosus* or *Actinomyces naeslundii*. Infection and Immunity. Vol. 24, pp: 742-752.

Cloete, T. and Bosch, M. (1994). Acinetobacter cell biomass, growth stage and phosphorous uptake from activated sludge mixed liquor. University of Pretoria. Pretoria, South Africa.
Copeland, M. and Weibel, D. (2009) Bacterial swarming: A model system for studying dynamic self-assembly. Soft Matter. Vol. 5, pp.:1174–1187.

Costerton, J. and Stewart, P. (2001). Battling biofilms - the war is against bacterial colonies that cause some of the most tenacious infections known. The weapon is the knowledge of enemy's communication system. Scientific American. Vol. 285, pp.: 74-81.

Cuperus, P.; Van der Mei, H.; Reid, G. et al. (1993). Physicochemical surfaces characteristics of urogenital and poultry lactobacilli. Journal of Colloid Interfaces Science. Vol. 156, pp: 319-324.

Cutter, M. and Stroot, P. (2008). Determination of specific growth rate by measurement of specific rate of ribosome synthesis in growing and non-growing cultures of *Acinetobacter calcoaceticus*. Applied and Environmental Microbiology. Vol. 74, pp: 901-903.

Davies, D.; Parsek, M.; Pearson, J.; Iglewski, B.; Costerton, J.; Greenberg, E. (1998). The involvement of cell-to-cell signals in the development of a bacterial biofilm. Science. Vol. 280, pp: 295-298.

Davis, R. and Mauer, L. (2010). Current research, technology and education topics in applied microbiology and microbial biotechnology. Formatex. Badajoz, Spain.

De Campos, J. (2003). Apontamentos da Unidade Curricular de Mecânica dos Fluidos. Universidade do Porto. Porto, Portugal.

De Cock, H.; Brandenburg, K.; Wiese, A. et al. (1999). Non-lamellar structure and negative charges of lipopolysaccharides required for efficient folding of outer membrane protein PhoE of *Escherichia coli*. Journal of Biological Chemistry. Vol. 274, pp: 5114-5119.

Drescher, K.; Dunkel, J.; Cisneros, L. et al. (2011). Fluid dynamics and noise in bacterial cell-cell and cell-surface scattering. PNAS. Vol. 108, pp.: 10940-10945.

Du Preez, J.; Toerien, D. and Lategan, P. (1981). Growth parameters of *Acinetobacter calcoaceticus* on acetate and ethanol. European Journal of Applied Microbiology and Biotechnology. Vol. 13, pp: 45-53.

Dufrêne, Y.; Boonaert, C. and Rouxhet, P. (1999). Surface analysis by X-ray photoelectron spectroscopy in study of bioadhesin and biofilms. Methods in Enzymology. Vol. 310, pp: 375-389.

El-Khani, M. and Stretton, R. (1981). Effect of growth medium on the lipid composition of log and stationary phase cultures of *Salmonella typhimurium*. Microbios. Vol. 31, pp: 161-169.
Elliot, R.; Wilson, M.; Buckley, C. et al. (2006). Aggregative behavior of bacteria isolated from canine dental plaque. Applied Environmental Microbiology. Vol. 72, pp: 5211-5217.

Englert, D. (2009). Microfluidic systems for investigating bacterial chemotaxis and colonization. Texas A&M University. Texas, United States of America.

Eprintsev, A.; Falaleeva, M.; Klimova, M. et al. (2004). Isolation and properties of malate dehydrogenase from meso- and thermophilic bacteria. Applied Biochemistry and Microbiology. Vol. 42, pp: 241-245.

Florjanic, M.; and Kristl, J. (2011). The control of biofilm formation by hydrodynamics of purified water in industrial distribution system. International Journal of Pharmaceutics. Vol. 405, pp: 16-22.

Goulter, R.; Gentle, I. and Dykes, G. (2009). Issues in determining factors influencing bacterial attachment: a review using the attachment of *Escherichia coli* to abiotic surfaces as an example. Letters in Applied Microbiology. Vol. 49, pp: 1-7.

Gronow, S. and Brade, H. (2001). Lipolysaccharide biosynthesis: which steps do bacteria need to survive ?. Journal of Endotoxin Research. Vol. 7, pp: 3-23.

Gusakov, A.; Kondratyeva, E. and Sinitsyn, A. (2011). Comparison of two methods for assaying reducing sugars in the determination of carbohydrase activities. International Journal of Analytical Chemistry. Vol. 2011, pp: 1-4.

Hamadi, F.; Latrache, H.; Zahir, H. et al. (2008). The relation between *Escherichia coli* surface functional groups composition and their physicochemical properties. Brazilian Journal of Microbiology. Vol. 39, pp: 10-15.

Hanson, K.; Vikram, G.; Kale, C. et al. (1994). The possible involvement of cell surface and outer membrane proteins of *Acinetobacter sp.* A3 in crude oil degradation. FEMS Microbiology Letters. Vol. 122, pp: 275-280.

Hendrickx, L.; Hausner, M. and Wuertz, S. (2000). In situ monitoring of natural genetic transformation of *Acinetobacter calcoaceticus* BD413 in monoculture of biofilms. Water Science Technology. Vol. 41, pp: 155-158.

Hernandez-Ortiz, J.; Stoltz, C. and Graham, M. (2005). Transport and Collective Dynamics in Suspensions of Confined Swimming Particles. Physical Review Letters. Vol. 95, pp.: 1-4.

Hong, Y. and Brown, D. (2008). Electrostatic behavior of the charge-regulated bacterial cell surface. Langmuir. Vol. 24, pp: 5003-5009.

Hong, Y. and Brown, D. (2009). Alteration of bacterial surface electrostatic potential and pH upon adhesion to a solid surface and impacts to cellular bioenergetics. Biotechnology and Bioengineering. Vol. 105, pp: 965-972.

Ishikawa, T. and Hota, M. (2006a). Interaction of two swimming Paramecia. The Journal of Experimental Biology. Vol. 209, pp.: 4452-4463.

Ishikawa, T.; Sekiya, G.; Imai, Y. et al. (2007). Hydrodynamic Interactions between Two Swimming Bacteria. Biophysical Journal. Vol. 93, pp.: 2217-2225.

Ishikawa, T.; Simmonds, M. and Pedley, T. (2006b). Hydrodynamic interaction of two swimming model microorganisms. Journal of Fluid Mechancics. Vol. 568, pp.: 119-160.

Jiang, W.; Saxena, A.; Song, B. et al. (2004). Elucidation of functional groups on gram-positive and gram-negative bacterial surfaces using infrared spectroscopies. Langmuir. Vol., pp: 11433-11442.

Kastowsky, M.; Gutberlet, T. and Bradaczek, H. (1992). Molecular modeling of the three-dimensional structure and conformational flexibility of bacterial lipopolysaccharide. Journal of Bacteriology. Vol. 14, pp: 4798-4806.

Kim, S. and Karilla, J. (1991). Microhydrodynamics: Principles and selected applications. Butterworth-Heinemann. Boston, United States of America.

Kim, S.; Hwang, H.; Xu, C. et al. (2003). Effect of aeration and agitation on the production of mycelial biomass and exopolysaccharides in an enthomopathogenic fungus *Paecilomyces sinclairii*. Letters in Applied Microbiology. Vol. 36, pp: 321-326.

Kirisits, M.; Margolis, J.; Purevdorj-Gage, B. et al. (2007). Influence of the Hydrodynamic Environment on Quorum Sensing in *Pseudomonas aeruginosa* Biofilms. Journal of Bacteriology. Vol. 189, pp.: 8357-8360.

Koerstgens, V.; Flemming, H., Windeger, J. et al. (2001). Uniaxial compression measurement device for investigation of the mechanical stability of biofilms. Journal of Microbiological Methods. Vol. 46, pp.: 9-17.

Kwok, W.; Picioreanu, C.; Ong, S.et al. (1998). Influence of biomass production and detachment force on biofilm structures in a biofilm airlift suspension reactor. Biotechnology and Bioengineering. Vol. 58, pp.: 400-407.

Laemmli, U. (1970). Cleavage of structural proteins during the assembly of the head of bacteriophage T4. Nature. Vol. 227, pp: 680-685.

Langston, K.; Worsham, L.; Earls, L. et al. (2004). Activation of hemolysin toxin: relationship between two internal protein sites of acylation. Biochemistry. Vol. 43, pp: 4338-4346.

Lau, P.; Lindhout, T.; Beveridge, T. et al. (2009). Differential lipopolysaccharide core capping leads to quantitative and correlated modifications of mechanical and structural properties in *Pseudomonas aeruginosa* biofilms. Journal of Bacteriology. Vol. 191, pp: 6618-6631.

Lazarova, V. and Manem, J. (1994). Advances in biofilm aerobic reactors ensuring effective biofilm activity control. Water Science Technology. Vol. 29, pp.: 319-327.

Lecuyer, S.; Rusconi, R.; Shen, Y. (2011). Shear Stress Increases the Residence Time of Adhesion of *Pseudomonas aeruginosa*. Biophysical Journal. Vol. 100, pp.: 341-350.

Lega, J. and Passot, T. (2003). Hydrodynamics of bacterial colonies: A model. Physical Review. Vol. 67, pp.: 1-18.

Lertopocasombut, K. (1991). Epuration carbonée par film biologique mince dans un réacteur à lit fluidisé triphasique. Institut National des Sciences Appliquées. Toulouse, France.

Liu, Y.; Tay, J. (2001a). Detachment forces and their influence on the structure and metabolic behaviour of biofilms. World Journal of Microbiology & Biotechnology. Vol. 17, pp.: 111-117.

Liu, Y.; Tay, J. (2001b). Metabolic response of biofilm to shear stress in fixed-film culture. Journal of Applied Microbiology. Vol. 90, pp.: 337-342.

Liu, Y.; Tay, J. (2002). The essential role of hydrodynamic shear force in the formation of biofilm and granular sludge. Water Research. Vol.36, pp: 1653-1665.

Liu, Y.; Zhao, Q. and Zheng, X. (2000). Biofilm technology for wastewater treatment. Chinese Building Industry Press. Beijing, People's Republic of China.

Lopez, J.; Koopman, B.; Bitton, G. (1986). INT-dehydrogenase test for activated sludge process control. Biotechnology and Bioengineering. Vol. 28, pp.: 1080-1085.

Loraine, G.; Chahine, G.; Hsiao, C. et al. (2012). Disinfection of Gram-negative and Gram-positive using *Dynajets* hydrodynamic cavitating jets. Ultrasonics and Sonochemistry. Vol. 19, pp: 710-717.

Lytle, D.; Rice, E.; Johnson, C. et al. (1999). Electrophoretic mobilities of *Escherichia coli* 0157:H7 and wild-type *Escherichia coli* strains. Applied Environmental Microbiology. Vol. 65, pp: 3222:3225.

Madigan, M., Martinko, J. and Parker, J. (2000). Brock Microbiology of Microorganisms. Ninth Edition. Prentice Hall. New Jersey, United States of America.

Marshal, K. (1976). Interfaces in microbial ecology. Harvard University Press. Cambridge, United States of America.
Marshall, K.; Pembrey, R. and Schneider, R. (1994). The relevance of X-ray photoelectron spectroscopy for analysis of microbial cell surfaces: a critical review. Colloids and Surfaces B Biointerfaces. Vol. 2, pp: 371-376.

Marshall, K.; Stout, R. and Mitchell, S. (1971). Mechanism of initial events in the adsorption of marine bacteria to surface. Journal of General Microbiology. Vol. 68, pp.: 337-348.

Melo, L. and Flemming, H. (2010). Mechanistic aspects of heat exchanger and membrane biofouling and prevention. The science and technology of industrial water treatment. Taylor & Francis. Brecksville, United States of America.

Metcalfe, A.; Pedley, T. and Thingstad, T. (2004). Incorporating of turbulence into a plankton foodweb model. Journal of Marine Systems. Vol. 49, pp.: 105-122.

Metzger, B. and Butler, J. (2010). Irreversibility and chaos: Role of long-range hydrodynamic interactions in sheared suspensions. Physical review E. Vol. 82, pp.: 82-86.

Miethke, M. and Marahiel, M. (2007). Siderophore-based iron acquisition and pathogen control. Microbiology and Molecular Biology Reviews. Vol. 71, pp: 413-451.

Mitchel, H. (2013). Basic features of biological membranes and the function of membrane proteins. Max-Planck Institut fuer Biophysik. Frankfurt, Germany.

Mozes, N.; Léonard, A. and Rouxhet, P. (1988). On the relation between elemental surface composition of yeast and bacteria and their charge and hydrophobicity. Biochimica et Biophysica Acta. Vol. 945, pp: 324-334.

Najafi, A.; Golestanian, R. (2010) Coherent hydrodynamic coupling for stochastic swimmers. Europhysics Letters. Vol. 90, pp.: 68003.-68011.

Naumann, D. (2000). Infrared spectroscopy in Microbiology: In Encyclopedia of analytical chemistry. John Wiley & Sons. Chichester, United Kingdom.

Naumann, D.; Helm, D. and Labischinski, H. (1991). Microbiological characterizations by FT-IR spectroscopy. Nature. Vol. 351, pp: 81-82.

Nicolella, C.; van Loosdrecht, M.; Heijnen, J. (2000). Wastewater treatment with particulate biofilm reactors. Journal of Biotechnology. Vol. 80, pp: 1-33.

Nishimura, J. (1986). Succinyl-CoA synthetase structure-function relationships and other considerations. Advanes in Enzymoloy and Related Areas of Molecular Biology. Vol. 58, pp: 142-146.

Nunes, O. (2010). Apontamentos teóricos da Unidade Curricular Bioquímica Microbiana. Universidade do Porto. Porto, Portugal.

O'Toole, G.; Kaplan, H. and Kolter, R. (2000). Biofilm formation as microbial development. Annual Review in Microbiology. Vol. 109, pp.: 31-43.

Ohl, M. and Miller, S. (2001). *Salmonella*: a model for bacterial pathogenesis. Annual Review of Medicine. Vol. 52, pp: 259-274.

Ojeda, J.; Romero-González, M.; Bachmann, R. et al. (2008). Characterization of the cell surface and cell wall chemistry of drinking water bacteria by combining XPS, FTIR spectroscopy, modeling and potentiometric titrations. Langmuir. Vol. 24, pp: 4032-4040.

Olofsson, A.; Zita, A. and Hermansson, M. (1998). Floc stability and adhesion of green-fluorescent-protein-marked bacteria to flocs in activated sludge. Microbiology. Vol. 144, pp: 519-528.

Palmgren, R.; Jorand, F.; Nielsen, P. et al. (1998). Influence of oxygen limitation on the cell surface properties of bacteria activated sludge. Water Science and Technology. Vol. 37, pp: 349-352.

Paramonova, E.; Kalmykowa, H.; van der Mei, H. et al. (2009). Impact of Hydrodynamics on Oral Biofilm Strength. Journal of Dental Research. Vol. 88, pp.: 922-926.

Pastuszka, J.; Talik, E.; Hacura, A. et al. (2005). Chemical characterization of airborne bacteria using X-ray photoelectron microscopy (XPS) and Fourier transform infrared spectroscopy (FTIRS). Aerobiologia. Vol. 21, pp: 181-192.

Pauer, H.; de Oliveira Ferreira, E.; dos Santos-Filho, J. et al. (2009). A TonB-dependent outer membrane protein as a *Bacteroides fragilis* fibronectin-binding molecule. FEMS Immunology & Medical Microbiology. Vol. 55, pp: 388-395.

Pault, E.; Ochoa, J.; Pechaud, Y. et al. (2012). Effect of shear stress and growth conditions on detachment and physical properties of biofilms. Water Research. Vol. 46, pp.: 5499-5508.

Payne, M.; Igo, J.; Cao, Z. et al. (1997). Biphasic binding kinetics between FepA and its ligands. Journal of Biological Chemistry. Vol. 272, pp: 21950-21955.

Pedley, T. (1992). Hydrodynamic phenomena in suspension of swimming microorganisms. Annual Review of Fluid Mechanics. Vol. 24, pp: 313-358.

Pedley, T. and Kessler, J. (1992). Hydrodynamic Phenomena in Suspension of Swimming Microorganisms. Annual Review of Fluid Mechanics. Vol. 24, pp.: 313-358.

Pereira, M.; Kuehn, M.; Wuertz, S. et al. (2002). Effect of flow regime on the architecture of a *Pseudomonas fluorescens* biofilm. Biotechnology and Bioengineering. Vol. 78, pp.: 164-171.

Phan-Thien, N.; Tran-Cong, T. and Ramia, M. (1987). A boundary-element analysis of flagellar propulsion. Journal of Fluid Mechanics. Vol. 184, pp.: 533-549.
Phuong, K.; Kakii, K. and Nikata, T. (2009). Intergeneric coaggregation of non-flocculating *Acinetobacter spp.* isolates with other sludge-constituting bacteria. Journal of Bioscience and Bioengineering. Vol. 107, pp: 394-400.

Phuong, K.; Kakii,K. and Nikata, T. (2009). Intergeneric coaggregation of non-flocculating *Acinetobacter* spp. isolates with other sludge-constituting bacteria. Journal of Bioscience and Bioengineering. Vol. 107, pp: 394-400.

Pratt L.; Kolter, R. (1998). Genetic analysis of E. coli biofilm formation: roles of flagella, motility, chemotaxis and type I pili. Molecular Microbiology. Vol. 30, pp.:285–293.

Purevdorj, B.; Costerton, J. and Stoodley, P. (2002). The influence of hydrodynamics and cell signaling on the Structure Behavior of *Pseudomonas aeruginosa* Biofilms. Applied and Environmental Microbiology. Vol. 68, pp.: 4457-4464.

Raetz, C. and Newman, K. (1979). Diglyceride kinase mutants of *Escherichia coli*: inner membrane association of 1,2-Diglyceride and its relation to synthesis of membrane-derived oligosaccharides. Journal of Bacteriology. Vol. 137, pp: 860-868.

Ramia, M.; Tullock, D. and Phan-Thien, N. (1993). The role of hydrodynamic interaction in the locomotion of microorganisms. Biophysics Journal. Vol. 65, pp.: 755-778.

Ramstedt, M.; Nakao, R.; Nyunt Wai, S. et al. (2010). Monitoring surface chemical changes in the bacterial cell wall. Journal of Biological Chemistry. Vol. 286, pp: 12389-12396.

Rijnaarts, H.; Norde, W.; Lyklema, J. et al. (1995). The isoelectric point of bacteria as an indicator for the presence of cell surface polymers that inhibit adhesion. Colloids and Surfaces B: Biointerfaces. Vol. 4, pp: 191-197.

Rochex, A., Godon, J.; Bernet, N. et al. (2008). Role of shear stress on composition, diversity and dynamics of biofilm bacterial communities. Water research. Vol. 42, pp.: 4915-4922.

Rodriguez-Saona, L.; Khambaty, F.; Fry, F. et al. (2004). Detection and identification of bacteria in a juice matrix with Fourier transform-near infrared spectroscopic and multivariate analysis. Journal of Food Protection. Vol. 67, pp: 2555-2559.

Rosenberg, M and Doyle, R. (1990). Microbial cell surface hydrophobicity: history, measurement and significance. ASM. Washington DC, United States of America.

Rosenberg, M; Bayer, E.; Delarea, J. et al. (1982). Role of thin fimbriae in adherence and growth of *Acinetobacter calcoaceticus* RAG-1 on hexadecane. Applied and Environmental Microbiology. Vol. 44, pp: 929-937.

Rosenberg, M. (2006). Microbial adhesion to hydrocarbons: twenty-five years of doing MATH. FEMS Microbiology Letters. Vol. 262, pp: 129-134.

Rosenberg, M.; Gutnick, D. and Rosenberg, E. (1980). Adherence of bacteria to hydrocarbons: a simple method for measuring cell-surface hydrophobicity. FEMS Microbiology Letters. Vol. 9, pp: 29-33.

Rouxhet P.; Mozes N. (1990). Physical chemistry of the interaction between attached microorganisms and their support. Water Science Technology. Vol. 22, pp.: 1–16.

Rouxhet, P.; Mozes, N.; Dengis, P. et al. (1994). Application of X-ray photoelectron spectroscopy to microorganisms. Colloids and Surfaces B. Bionterfaces. Vol. 2, pp: 347-369.

Russell, J. and Cook, G. (1995). Energetics of bacterial growth: balance of anabolic and catabolic reactions. Microbiology Review. Vol. 59, pp: 48-62.

Saini, G. (2010). Bacterial hydrophobicity: Assessment techniques, applications and extension to colloids. Oregon State University. Oregon, United States of America.

Schauer, K.; Gouget, B.; Carrière, M. et al. (2007). Novel nickel transport mechanism across the bacterial outer membrane energized by the TonB/ExbB/ExbD machinery. Molecular Microbiology. Vol. 63, pp: 1054-1068.

Schauer, K.; Rodionov, D. and de Reuse, H. (2008). New substrate for TonB-dependent transport: do we only see the "tip of the iceberg"?. Trends in Biochemical Science. pp: 1-9.

Shevchenko, A.; Tomas, H.; Havlis, J. et al. (2006). In-gel digestion for mass spectrometric characterization of proteins and proteomes. Nature Protocols. Vol. 1, pp: 2856-2860.

Shin, J.; Lee, H.; Kim, S. et al. (2009). Proteomic analysis of *Acinetobacter baumannii* in biofilm and planktonic growth mode. The Journal of Microbiology. Vol. 47, pp: 728-735.
Simões, L.; Azevedo, N.; Pacheco, A. et al. (2006). Drinking water biofilm assessment of total and culturable bacteria under different operating conditions. Biofouling. Vol. 22, pp: 91-99.

Simões, L.; Simões, M. and Vieira, M. (2008). Intergeneric coaggregation among drinking water bacteria: evidence of a role for *Acinetobacter calcoaceticus* as a bridging bacterium. Applied and Environmental Microbiology. Vol. 74, pp: 1259-1263.

Simões, L.; Simões, M.; Oliveira, R. et al. (2007). Potential of the adhesion of bacteria isolated from drinking water to materials. Journal of Basic Microbiology. Vol. 47, pp: 174-183.

Simões, M.; Pereira, M. and Vieira, J. (2005). Validation of respirometry as a short-term method to assess the efficacy of biocides. Biofouling. Vol. 21, pp: 9-17.

Simões, M.; Pereira, M. and Vieira, M. (2004). Cellular changes due to biofilm formation - influence of flow regime. International Conference: Biofilms 2004. Las Vegas, United States of America, pp.: 105-109.

Simões, M.; Pereira, M.; Sillankorva, S.; et al. (2007). The effect of hydrodynamic conditions on the phenotype of *Pseudomonas fluorescens* biofilms. Biofouling. Vol. 23, pp.: 249-258.

Simões, M.; Pereira, M.and Vieira, M. (2003). Monitoring the effects of biocide treatment of *Pseudomonas fluorescens* formed under different flow regimes. Water Science Technology. Vol. 47, pp.: 217-223.

Simões, M.; Simões, L. and Vieira, M. (2008). Physiology and behavior of *Pseudomonas fluorescens* single and dual strain biofilms under diverse hydrodynamic stresses. International Journal of Food Microbiology.Vol. 128, pp.: 309-316.

Smani, Y.; McConnell, M. and Pachón, J. (2012). Role of fibronectin in the adhesion of *Acinetobacter baumanii* to host cells. PLOS One. Vol. 7, pp: 1-7.

Smith, B. (1996). Fundamentals of Fourier transform infrared spectroscopy. CRC Press. Washington DC, United States of America.

Soon, R.; Nation, R.; Cockram, S. et al. (2011). Different surface charge of colistin-susceptible and –resistant *Acinetobacter baumanii* cells measured with zeta potential as a function of growth phase and colistin treatment. Journal of Antimicrobial Chemotherapy. Vol. 66, pp: 126-133.

Stewart, P. (2012). Mini-review: Convection around biofilms. Biofouling. Vol. 28, pp.: 187-198.

Stoodley, P.; Jorgensen, F.; Williams, P.; et al. (1999). The Role of hydrodynamics and AHL signaling molecules as determinants of the structure of *Pseudomonas aeruginosa* biofilms. "Biofilms: The Good, The Bad, and The Ugly" - 4th meeting of the Biofilm Club. Gregynog, United Kingdom.

Tam, K. (2002). Removal of multiple substrates in a mixed culture process for the treatment of brewery wastewater. McGill University. Montréal, Canada.

Tay, J.; Liu, Q. and Liu, Y. (2001). The effects of shear force on the formation, structure and metabolism of aerobic granules. Applied Microbiology and Technology. Vol. 57, pp: 227-233.

Tay, J.; Liu, Q. and Liu, Y. (2001b). The role of cellular polysaccharides in the formation and stability of aerobic granules. Letters in Applied Microbiology. Vol. 33, pp: 222-226.

Tay, J.; Xu, H. and Teo, K. (2000). Molecular mechanism of granulation. I: H+ translocation-dehydration theory. Journal of Environmental Engineering. Vol. 126, pp.: 403-410.

Telgmann, U.; Horn, H. and Morgenroth, E. (2004). Influence of growth history on sloughing and erosion from biofilms. Water Research. Vol. 38, pp.: 3671-3684.

Teo, K.; Xu, H.; Tay, J. (2000). Molecular mechanism of granulation. II: Proton translocating activity. Journal of Environmental Engineering. Vol. 126, pp.: 411-418.

Teodósio, J.; Simões, M.; Melo, L. and Mergulhão, F. (2011). Flow cell hydrodynamics and their effects on *E. coli* biofilm formation under different nutrient conditions and turbulent flow. Biofouling. Vol 27, pp.: 1-11.

Thomas, E. (1974). Studies on the metabolism of ATP by isolated bacterial membranes: role of succinyl CoA synthetase in diglyceride kinase activity. Archives of Biochemistry and Biophysics. Vol. 163, pp: 530-536.
Thomas, W.; Trintchina, E.; Forero, M. et al. (2002). Bacterial adhesion to target cells enhanced by shear force. Cell. Vol. 109, pp: 913-923.

Toogood, H.; Leys, D. and Scrutton, N. (2007). Dynamics driving function – new insights from electron transferring flavoproteins and partner complexes. The FEBS Journal. Vol. 274, pp: 5481-5504.

Trémoulet, F.; Duché, O.; Namane, A. et al. (2002). A proteomic study of *Escherichia coli* O157:H7 NCTC12900 cultivated in biofilm or in planktonic growth mode. FEMS Microbiology Letters. Vol. 215, pp: 7-14.

Uniprot Consortium. (2013). www.uniprot.org. Date of access: July-2013.

Van Denmark, P. and Batzing, B. (1987). The Microbes: An Introduction to Their Nature and Importance. Benjamin/Cummings Publishing. California, United States of America.

Van Loosdrecht, M.; Picioreanu, C. and Heijnen, J. (1997). A more unifying hypothesis for the structure of microbial biofilms. FEMS Microbiology Ecology. Vol. 24, pp.: 181-183.

Van Oss, C. (1994). Interfacial forces in aqueous media. Marcel Dekker Inc.. Florida, United States of America.

Vaughan, B.; Smith, B. and Chopp, D. (2010). The Influence of Fluid Flow on Modeling Quorum Sensing in Bacterial Biofilms. Bulletin of Mathematical Biology. Vol. 72, pp.: 1143-1165.

Vicsek, T.; Czirok, A.; Ben-Jacob, E. et al. (1995). Novel type of phase transition in a system of self-driven particles. Physics Review Letters. Vol. 75, pp.: 1226-1229.

Vieira, M.; Melo, L. and Pinheiro, M. (1993). Biofilm formation: Hydrodynamic effects on internal diffusion and structure. Vol. 7, pp.: 67-80.

Walker, S.; Redman, J. and Elimelech, M. (2004). Role of cell surface lipopolysaccharides in *Escherichia coli* K12 adhesion and transport. Langmuir. Vol. 20, pp: 7736-7746.

Waters CM, Bassler BL (2005) Quorum sensing: cell-to-cell communication in bacteria. Annu Rev Cell Dev Biol 21:319–346.

Waters, C. and Bassler, B. (2005). Quorum sensing: cell-to-cell communication in bacteria. Annual Review of Cell and Developmental Biology. Vol. 21, pp.: 319-346.

Watnick, P. and Kolter, R. (2000). Biofilm, city of microbes. Journal of Bacteriology. Vol. 182, pp.: 2675-2679.

Wentzel, M.; Loetter, L.; Loewenthal, R. et al. (1986). Metabolic behavior of *Acinetobacter spp.* in enhanced biological phosphorous removal – a biochemical model. Water SA. Vol. 12, pp: 209-224.

Wessa, P. (2013). Free Statistics Software. Office for Research, development and education, URL http://www.wessa.net/

Wilson, W.; Wade, M.; Holman, S. et al. (2001). Status of methods for assessing bacterial cell surface charge properties based on zeta potential measurements. Journal of Microbiological Methods. Vol. 43, pp: 153-164.

Wimpenny, J. and Colasanti, R. (2004). A simple automaton model for coaggregation. Biofilms. Vol. 1, pp: 369-375.
Yates, J.; Ruse, C. and Nakorchevsky, A. (2009). Proteomics by mass spectrometry: approaches, advances, and applications. Annual Review of Biomedical Engineering. Vol. 11, pp: 49-79.

Youngren, G. and Acrivos, A. (1975). Stokes flow past a particle of arbitrary shape: a numerical method of solution. Journal of Fluid Mechanics. Vol. 69, pp.: 377-403.

Zhan, Y.; Yan, Y.; Zhang, W. et al. (2011). Comparative analysis of the completgenome of an *Acinetobacter calcoaceticus* strain adapted to a phenol-polluted environment. Research in Microbiology. pp: 1-8.

Appendix A – Statistical analysis

The Wicoxon-Mann-Whitney test was the statistical test applied throughout the present study to evaluate the statistical significance associated to differences between two independent samples. It is a non-parametric test, which is commonly applied as an alternative to *t*-Student for samples with small dimension, heterogeneous variances and non-normal distributions. The statistical hypothesis associated to the bilateral test are described as follows: i) null hypothesis (H_0): differences between two independent samples are not significant ($p>0,05$) and ii) alternative hypothesis (H_1): differences between two independent samples are significant ($p<0,05$) (Wessa, 2013).

The probe values (95% confidence) associated to experiments results, for which Wicoxon-Mann-Whitney test was relevant, are shown as follows.

A.1 Analysis on specific growth rate difference

Table A.1: Probe values associated to non-parametric test for analysis of specific growth rate differences between agitation speeds conditions.

Samples under analysis	P-value
100 RPM *vs* 220 RPM	0,0014
220 RPM *vs* 375 RPM	0,0075
100 RPM *vs* 375 RPM	0,0060

A.2 Analysis on total respiratory activity difference

Table A.2: Probe values associated to non-parametric test for analysis of total respiration activity differences between agitation speeds conditions in mid-exponential and stationary growth phases.

Growth phase	Samples under analysis	P-value
Mid-exponential	100 RPM *vs* 220 RPM	0,0471
	220 RPM *vs* 375 RPM	0,400
	100 RPM *vs* 375 RPM	0,0286
Stationary	100 RPM *vs* 220 RPM	0,1714
	220 RPM *vs* 375 RPM	0,0286
	100 RPM *vs* 375 RPM	0,3143

A.3 Analysis on hydrophobicity index difference

Table A.3.1: Probe values associated to non-parametric test for hydrophobicity index differences between agitation speeds conditions at mid-exponential and stationary growth phases.

Growth phase	Samples under analysis	P-value
Mid-exponential	100 RPM *vs* 220 RPM	0,1623
	220 RPM *vs* 375 RPM	0,1320
	100 RPM *vs* 375 RPM	0,0022
Stationary	100 RPM *vs* 220 RPM	0,0022
	220 RPM *vs* 375 RPM	0,0087
	100 RPM *vs* 375 RPM	0,0021

Table A.3.2: Probe values associated to non-parametric test for hydrophobicity index differences between distinct growth phases across different agitation speeds conditions.

Samples under analysis	P-value
100 RPM exponential *vs* 100 RPM stationary	0,0022
220 RPM exponential *vs* 220 RPM stationary	0,0023
375 RPM exponential *vs* 375 RPM stationary	0,0022

A.4 Analysis on electrophoretic mobility medians at pH 7 difference

Table A.4: Probe values associated to non-parametric test for electrophoretic mobility differences between agitation speeds conditions at pH 7 in mid-exponential and stationary growth phases.

Growth phase	Samples under analysis	P-value
Mid-exponential	100 RPM *vs* 220 RPM	0,9918
	220 RPM *vs* 375 RPM	0,6750
	100 RPM *vs* 375 RPM	0,6453
Stationary	100 RPM *vs* 220 RPM	0,3833
	220 RPM *vs* 375 RPM	0,0458
	100 RPM *vs* 375 RPM	0,0089

A.4.1 Analysis on electrophoretic mobility medians at pH 2 and 6 in mid-exponential growth phase

Table A.4.1: Probe values associated to non-parametric test for electrophoretic mobility differences between agitation speeds conditions at pH 2 and 6 in mid-exponential growth phases.

pH	Samples under analysis	P-value
6	100 RPM *vs* 220 RPM	0,0463
	220 RPM *vs* 375 RPM	0,4925
	100 RPM *vs* 375 RPM	0,0416
2	100 RPM *vs* 220 RPM	0,1339
	220 RPM *vs* 375 RPM	<0,0001
	100 RPM *vs* 375 RPM	0,0013

A.5 Analysis of auto aggregation index difference

Table A.5: Probe values associated to non-parametric test for analysis of auto aggregation index differences between agitation speeds conditions in stationary growth phase.

Samples under analysis	P-value
100 RPM *vs* 220 RPM	0,400
220 RPM *vs* 375 RPM	0,100
100 RPM *vs* 375 RPM	0,100

Appendix B – Figures

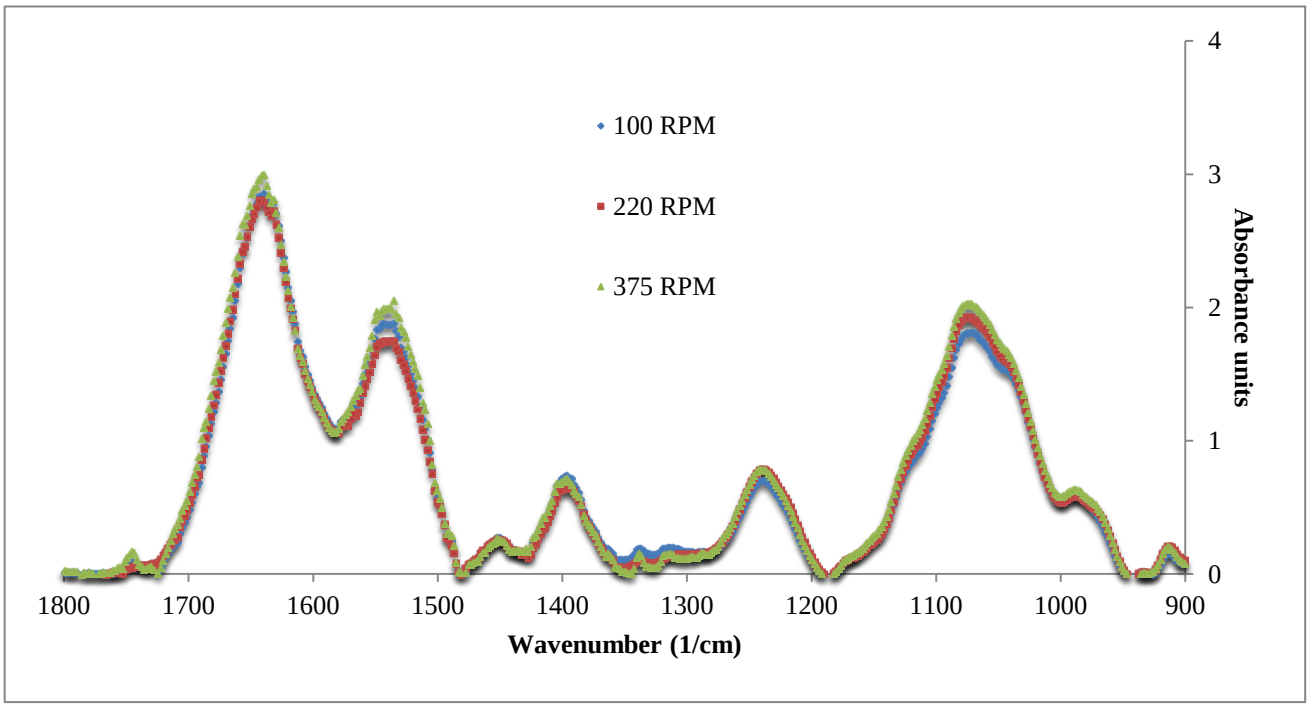

Figure B.1: ATR-FTIR spectra for *A. calcoaceticus* grown under distinct agitation speeds at mid-exponential growth phase. Blue line represents cells grown at 100 rpm; red line cells at 220 rpm and green line cells at 375 rpm.

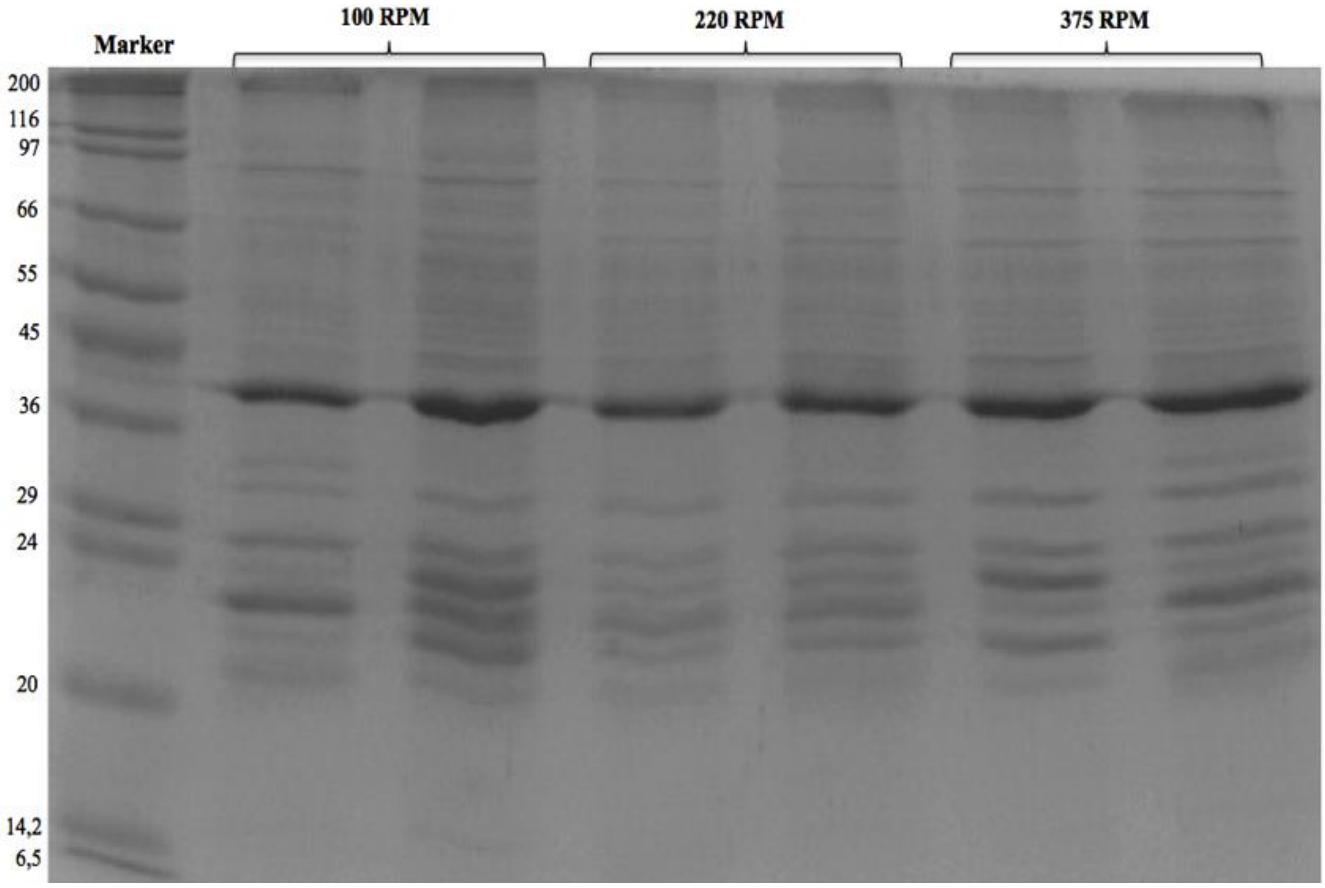

Figure B.2: SDS-PAGE analysis of outer membrane proteins extracted from *A. calcoaceticus* cultivated under distinct agitation speeds at stationary growth phase. Numbers on the left side represent molecular weigth (in kDa).

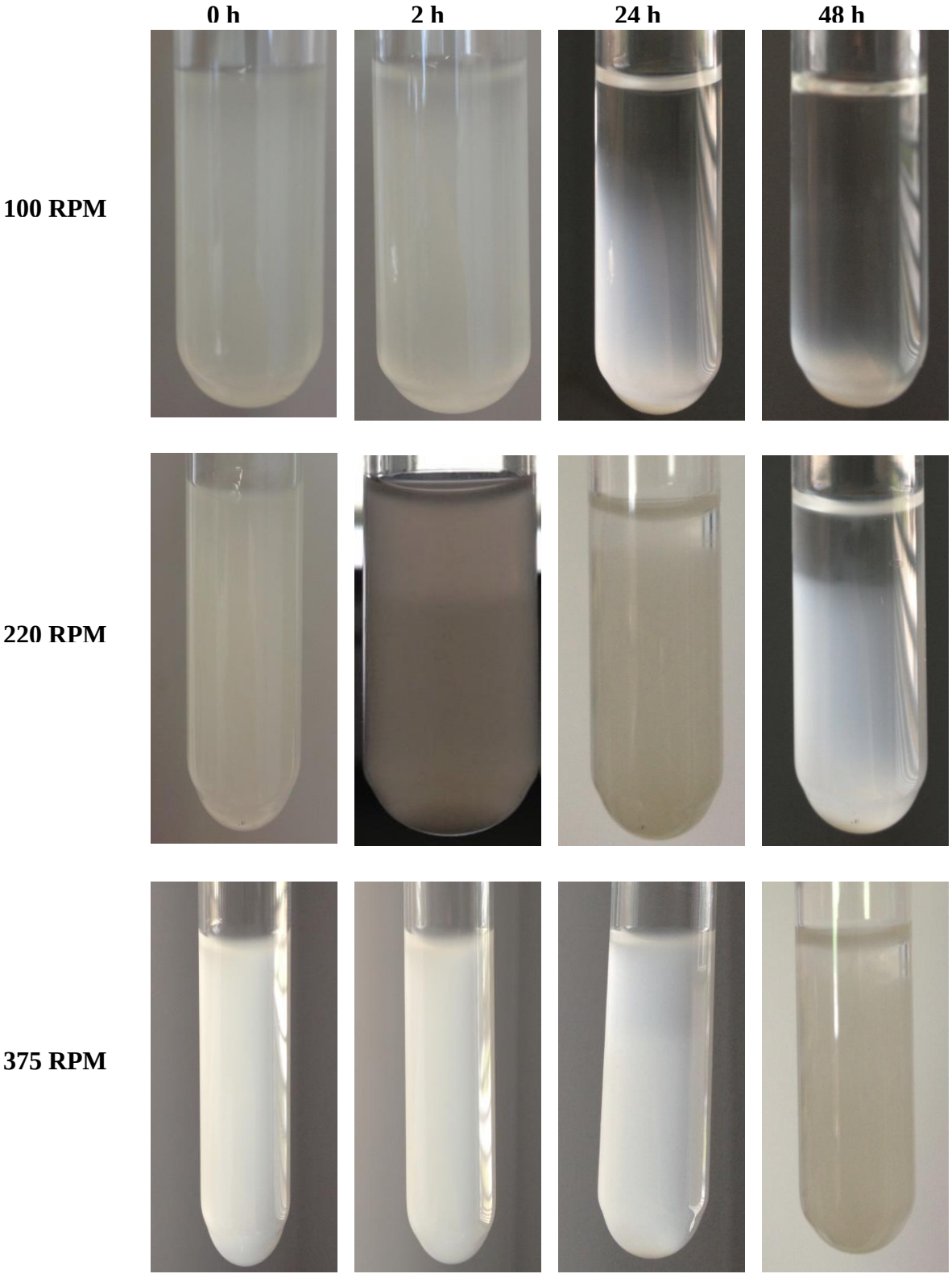

Figure B.3: Auto aggregation analysis by visual assay of *A. calcoaceticus* cultivated under different agitation speeds at stationary phase. Numbers on the upper part represent time elapsed after auto aggregation suspension preparation.

Appendix C - Tables

C.1 Identified OMP from *A. calcoaceticus* cultivated under 100 rpm agitation speed

Table C.1: Identified OMP from *A. calcoaceticus* cultivated under 100 rpm agitation speed with respective OM localization score and accession number. Protein functions were obtained from UniProt Consortium.

Protein	Accession Number	Score for localization at OM	Function
Putative outer membrane protein (OmpA-like) OS=Acinetobacter calcoaceticus (strain PHEA-2) GN=ompA PE=3 SV=1	F0KNA3_ACICP	10	Structural integrity of OMP
Outer membrane protein assembly factor BamA OS=Acinetobacter calcoaceticus (strain PHEA-2) GN=yaeT PE=3 SV=1	F0KGC9_ACICP	10	OMP assembly
Peptidoglycan-associated lipoprotein OS=Acinetobacter calcoaceticus (strain PHEA-2) GN=pal PE=3 SV=1	F0KL58_ACICP	10	Bacterial survival/pathogenesis
Outer membrane factor, OMF family OS=Acinetobacter calcoaceticus (strain PHEA-2) GN=oprM PE=4 SV=1	F0KMH8_ACICP	10	Transport
Uncharacterized protein OS=Acinetobacter calcoaceticus (strain PHEA-2) GN=BDGL_002439 PE=4 SV=1	F0KPI2_ACICP	2,5	Uncharacterized
Uncharacterized protein OS=Acinetobacter calcoaceticus (strain PHEA-2) GN=BDGL_002225 PE=4 SV=1	F0KML6_ACICP	9,52	Uncharacterized
Uncharacterized protein OS=Acinetobacter calcoaceticus (strain PHEA-2) GN=BDGL_002763 PE=4 SV=1	0KGS8_ACICP	9,52	Uncharacterized
Electron transfer flavoprotein alpha-subunit OS=Acinetobacter calcoaceticus (strain PHEA-2) GN=etfA PE=4 SV=1	F0KL87_ACICP	2	Oxireductase
P Uncharacterized protein OS=Acinetobacter calcoaceticus (strain PHEA-2) GN=BDGL_002006	F0KL34_ACIC	9,52	Uncharacterized

PE=4 SV=1			
OmpA domain protein OS=Acinetobacter calcoaceticus (strain PHEA-2) GN=yiaD PE=3 SV=1	F0KFL4_ACICP	10	Structural integrity of OMP
Putative porin for vanillate trafficking OS=Acinetobacter calcoaceticus (strain PHEA-2) GN=vanP PE=4 SV=1	F0KHN9_ACICP	10	Porin activity
Uncharacterized protein OS=Acinetobacter calcoaceticus (strain PHEA-2) GN=BDGL_002510 PE=4 SV=1	F0KQ01_ACICP	2	Uncharacterized
Malate dehydrogenase OS=Acinetobacter calcoaceticus (strain PHEA-2) GN=mdh PE=3 SV=1	F0KPX6_ACICP	2	Oxireductase
Succinyl-CoA ligase [ADP-forming] subunit beta OS=Acinetobacter calcoaceticus (strain PHEA-2) GN=sucC PE=3 SV=1	F0KLX8_ACICP	0,01	Ligase
Polysaccharide export protein OS=Acinetobacter calcoaceticus (strain PHEA-2) GN=wza PE=4 SV=1	F0KIQ6_ACICP	9,92	Transport
LPS-assembly protein LptD OS=Acinetobacter calcoaceticus (strain PHEA-2) GN=lptD PE=3 SV=1	F0KMB2_ACICP	10	Envelope biogenesis /LPS assembly
P Putative ferric siderophore receptor protein OS=Acinetobacter calcoaceticus (strain PHEA-2) GN=bfrD PE=3 SV=1	F0KM61_ACIC	9,95	Receptor/Iron binding
Outer membrane protein assembly factor BamD OS=Acinetobacter calcoaceticus (strain PHEA-2) GN=comL PE=3 SV=1	F0KFH3_ACICP	9,92	OMP assembly

C.2 Identified OMP from *A. calcoaceticus* cultivated under 220 rpm agitation speed

Table C.2: Identified OMP from *A. calcoaceticus* cultivated under 220 rpm agitation speed with respective OM localization score and accession number. Protein functions were obtained from UniProt Consortium.

Protein	Accession Number	Score for localization at OM	Function
Putative outer membrane protein (OmpA-like) OS=Acinetobacter calcoaceticus (strain PHEA-2) GN=ompA PE=3 SV=1	F0KNA3_ACICP	10	Structural integrity of OMP
Outer membrane protein assembly factor BamA OS=Acinetobacter calcoaceticus (strain PHEA-2) GN=yaeT PE=3 SV=1	F0KGC9_ACICP	10	OMP assembly
Peptidoglycan-associated lipoprotein OS=Acinetobacter calcoaceticus (strain PHEA-2) GN=pal PE=3 SV=1	F0KL58_ACICP	10	Bacterial survival/pathogenesis
Outer membrane factor, OMF family OS=Acinetobacter calcoaceticus (strain PHEA-2) GN=oprM PE=4 SV=1	F0KMH8_ACICP	10	Transport
Putative member of ShlA/HecA/FhaA exoprotein family OS=Acinetobacter calcoaceticus (strain PHEA-2) GN=fhaB PE=4 SV=1	F0KPM3_ACICP	9,95	Transferase activity
Polysaccharide export protein OS=Acinetobacter calcoaceticus (strain PHEA-2) GN=wza PE=4 SV=1	F0KIQ6_ACICP	9,92	Transport
OmpA domain protein OS=Acinetobacter calcoaceticus (strain PHEA-2) GN=yiaD PE=3 SV=1	F0KFL4_ACICP	10	Structural integrity of OMP
Putative ferric siderophore receptor protein OS=Acinetobacter calcoaceticus (strain PHEA-2) GN=bfrD PE=3 SV=1	F0KM61_ACICP	9,95	Transporter/Receptor/Iron binding
Acriflavine resistance protein A OS=Acinetobacter calcoaceticus (strain PHEA-2) GN=acrA PE=4 SV=1	F0KMH5_ACICP	4,69	Transport
Uncharacterized protein OS=Acinetobacter calcoaceticus (strain PHEA-2) GN=BDGL_002225 PE=4 SV=1	F0KML6_ACICP	9,52	Uncharacterized
Putative outer membrane copper receptor OS=Acinetobacter calcoaceticus (strain PHEA-2) GN=oprC PE=3 SV=1	F0KJZ1_ACICP	10	Transporter/Receptor
Putative TonB-dependent receptor protein OS=Acinetobacter calcoaceticus (strain PHEA-2)	F0KN91_ACICP	9,49	Transport/Receptor

GN=yncD PE=3 SV=1			
Uncharacterized protein OS=Acinetobacter calcoaceticus (strain PHEA-2) GN=BDGL_002763 PE=4 SV=1	F0KGS8_ACICP	9,52	Uncharacterized
Surface antigen (D15) OS=Acinetobacter calcoaceticus (strain PHEA-2) GN=ytfM PE=4 SV=1	F0KHR0_ACICP	10	Protective surface antigen
Outer membrane protein assembly factor BamD OS=Acinetobacter calcoaceticus (strain PHEA-2) GN=comL PE=3 SV=1	F0KFH3_ACICP	9,92	OMP assembly
Uncharacterized protein OS=Acinetobacter calcoaceticus (strain PHEA-2) GN=BDGL_002510 PE=4 SV=1	F0KQ01_ACICP	2	Uncharacterized
Uncharacterized protein OS=Acinetobacter calcoaceticus (strain PHEA-2) GN=BDGL_002650 PE=4 SV=1	F0KG05_ACICP	2	Uncharacterized
Putative hemolysin activator OS=Acinetobacter calcoaceticus (strain PHEA-2) GN=shlB PE=4 SV=1	F0KPM4_ACICP	10	Transport
LPS-assembly protein LptD OS=Acinetobacter calcoaceticus (strain PHEA-2) GN=lptD PE=3 SV=1	F0KMB2_ACICP	10	Envelope biogenesis /LPS assembly
TonB-dependent receptor OS=Acinetobacter calcoaceticus (strain PHEA-2) GN=btuB PE=3 SV=1	F0KNU8_ACICP	9,93	Receptor
Ferric enterobactin receptor OS=Acinetobacter calcoaceticus (strain PHEA-2) GN=pfeA PE=3 SV=1	F0KGT9_ACICP	10	Receptor
Putative porin for vanillate trafficking OS=Acinetobacter calcoaceticus (strain PHEA-2) GN=vanP PE=4 SV=1	F0KHN9_ACICP	10	Porin activity
Putative ferric siderophore receptor protein OS=Acinetobacter calcoaceticus (strain PHEA-2) GN=foxA PE=3 SV=1	F0KHD1_ACICP	10	Receptor

C.3 Identified OMP from *A. calcoaceticus* cultivated under 375 rpm agitation speed

Table C.3: Identified OMP from *A. calcoaceticus* cultivated under 375 rpm agitation speed with respective OM localization score and accession number. Protein functions were obtained from UniProt Consortium.

Protein	Accession Number	Score for localization at OM	Function
Putative outer membrane protein (OmpA-like) OS=Acinetobacter calcoaceticus (strain PHEA-2) GN=ompA PE=3 SV=1	F0KNA3_ACICP	10	Structural integrity of OMP
Outer membrane protein assembly factor BamA OS=Acinetobacter calcoaceticus (strain PHEA-2) GN=yaeT PE=3 SV=1	F0KGC9_ACICP	10	Assembly of beta barrel proteins
Outer membrane factor, OMF family OS=Acinetobacter calcoaceticus (strain PHEA-2) GN=oprM PE=4 SV=1	F0KMH8_ACICP	10	Lipid binding/transporter
Peptidoglycan-associated lipoprotein OS=Acinetobacter calcoaceticus (strain PHEA-2) GN=pal PE=3 SV=1	F0KL58_ACICP	10	Bacterial survival/pathogenesis
Uncharacterized protein OS=Acinetobacter calcoaceticus (strain PHEA-2) GN=BDGL_002763 PE=4 SV=1	F0KGS8_ACICP	9,52	Unchracterized
Uncharacterized protein OS=Acinetobacter calcoaceticus (strain PHEA-2) GN=BDGL_002225 PE=4 SV=1	F0KML6_ACICP	9,52	Uncharacterized
Putative hemolysin activator OS=Acinetobacter calcoaceticus (strain PHEA-2) GN=shlB PE=4 SV=1	F0KPM4_ACICP	10	Transport
LPS-assembly protein LptD OS=Acinetobacter calcoaceticus (strain PHEA-2) GN=lptD PE=3 SV=1	F0KMB2_ACICP	10	Envelope biogenesis /LPS assembly
Acriflavine resistance protein A OS=Acinetobacter calcoaceticus (strain PHEA-2) GN=acrA PE=4 SV=1	F0KMH5_ACICP	4,69	Transport
Putative TonB-dependent receptor protein OS=Acinetobacter calcoaceticus (strain PHEA-2) GN=yncD PE=3 SV=1	F0KN91_ACICP	9,49	Transporter/Receptor
Putative porin for vanillate trafficking OS=Acinetobacter calcoaceticus (strain PHEA-2) GN=vanP PE=4 SV=1	F0KHN9_ACICP	10	Porin activity

Putative outer membrane copper receptor OS=Acinetobacter calcoaceticus (strain PHEA-2) GN=oprC PE=3 SV=1	F0KJZ1_ACICP	10	Transporter/Receptor
Putative ferric siderophore receptor protein OS=Acinetobacter calcoaceticus (strain PHEA-2) GN=bfrD PE=3 SV=1	F0KM61_ACICP	9,95	Transporter/Receptor/Iron binding
Malate dehydrogenase OS=Acinetobacter calcoaceticus (strain PHEA-2) GN=mdh PE=3 SV=1	F0KPX6_ACICP	2	Oxireductase
Polysaccharide export protein OS=Acinetobacter calcoaceticus (strain PHEA-2) GN=wza PE=4 SV=1	F0KIQ6_ACICP	9,92	Transporter
OmpA domain protein OS=Acinetobacter calcoaceticus (strain PHEA-2) GN=yiaD PE=3 SV=1	F0KFL4_ACICP	10	Structural integrity of OMP
Uncharacterized protein OS=Acinetobacter calcoaceticus (strain PHEA-2) GN=BDGL_002006 PE=4 SV=1	F0KL34_ACICP	9,52	Uncharacterized
Surface antigen (D15) OS=Acinetobacter calcoaceticus (strain PHEA-2) GN=ytfM PE=4 SV=1	F0KHR0_ACICP	10	Protective surface antigen
Uncharacterized protein OS=Acinetobacter calcoaceticus (strain PHEA-2) GN=BDGL_002439 PE=4 SV=1	F0KPI2_ACICP	2,5	Uncharacterized
TonB-dependent receptor OS=Acinetobacter calcoaceticus (strain PHEA-2) GN=btuB PE=3 SV=1	F0KNU8_ACICP	9,93	Receptor
Uncharacterized protein OS=Acinetobacter calcoaceticus (strain PHEA-2) GN=BDGL_003217 PE=4 SV=1	F0KKS6_ACICP	2	Uncharacterized
Uncharacterized protein OS=Acinetobacter calcoaceticus (strain PHEA-2) GN=BDGL_002650 PE=4 SV=1	F0KG05_ACICP	2	Uncharacterized
Electron transfer flavoprotein alpha-subunit OS=Acinetobacter calcoaceticus (strain PHEA-2) GN=etfA PE=4 SV=1	F0KL87_ACICP	2	Oxireductase
Outer membrane protein assembly factor BamD OS=Acinetobacter calcoaceticus (strain PHEA-2) GN=comL PE=3 SV=1	F0KFH3_ACICP	9,92	OMP assembly
Putative ferric siderophore receptor protein OS=Acinetobacter calcoaceticus (strain PHEA-2) GN=foxA PE=3 SV=1	F0KHB5_ACICP	10	Receptor

C.4 Factor analysis associated to Principal Component Analysis (PCA)

Table C.4: Square cosines associated to Principal Component Analysis (PCA) of ATR-FTIR spectrum obtained for *A. calcoaceticus* at stationary growth phase. The values in bold represent variables to the factor for which squared cosine is the largest

Wave number (1/cm)	F1	F2	F3	F4
898,828256	0,006	0,213	**0,564**	0,000
900,757072	0,019	0,217	**0,536**	0,001
902,685888	0,079	0,208	**0,517**	0,001
904,614704	0,338	0,110	**0,398**	0,003
906,54352	**0,577**	0,027	0,289	0,006
908,472336	**0,721**	0,010	0,182	0,007
910,401152	**0,801**	0,004	0,128	0,006
912,329968	**0,849**	0,000	0,096	0,003
914,258784	**0,860**	0,003	0,081	0,002
916,1876	**0,842**	0,005	0,084	0,003
918,116416	**0,793**	0,005	0,114	0,003
920,045232	**0,707**	0,001	0,169	0,005
921,974048	**0,535**	0,006	0,273	0,006
923,902864	0,346	0,041	**0,354**	0,002
925,83168	0,206	0,082	**0,409**	0,000
927,760496	0,131	0,131	**0,407**	0,002
929,689312	0,061	0,139	**0,453**	0,009
931,618128	0,009	0,153	**0,473**	0,014
933,546944	0,002	0,150	**0,485**	0,012
935,47576	0,009	0,190	**0,428**	0,009
937,404576	0,013	0,293	**0,334**	0,007
939,333392	0,004	0,303	**0,336**	0,002
941,262208	0,000	**0,358**	0,318	0,000
943,191024	0,014	**0,443**	0,233	0,000
945,11984	0,037	**0,512**	0,181	0,000
947,048656	0,084	**0,554**	0,122	0,000
948,977472	0,121	**0,566**	0,101	0,001
950,906288	0,190	**0,531**	0,094	0,002
952,835104	0,281	**0,477**	0,078	0,004
954,76392	0,354	**0,451**	0,051	0,007
956,692736	0,418	**0,418**	0,034	0,007
958,621552	**0,480**	0,377	0,024	0,007
960,550368	**0,506**	0,362	0,018	0,008
962,479184	**0,528**	0,345	0,016	0,009
964,408	**0,513**	0,360	0,017	0,010
966,336816	**0,486**	0,388	0,016	0,011
968,265632	**0,461**	0,419	0,016	0,014
970,194448	0,431	**0,464**	0,014	0,015
972,123264	0,410	**0,496**	0,013	0,018
974,05208	0,394	**0,523**	0,012	0,019
975,980896	0,379	**0,549**	0,011	0,018
977,909712	0,369	**0,569**	0,010	0,016

979,838528	0,364	**0,582**	0,009	0,014
981,767344	0,369	**0,582**	0,008	0,012
983,69616	0,362	**0,591**	0,008	0,011
985,624976	0,351	**0,602**	0,009	0,009
987,553792	0,334	**0,616**	0,012	0,009
989,482608	0,314	**0,632**	0,014	0,008
991,411424	0,304	**0,640**	0,017	0,009
993,34024	0,318	**0,626**	0,018	0,009
995,269056	0,353	**0,593**	0,018	0,011
997,197872	0,403	**0,547**	0,017	0,013
999,126688	0,464	**0,491**	0,016	0,015
1001,055504	**0,536**	0,421	0,014	0,018
1002,98432	**0,602**	0,356	0,013	0,021
1004,913136	**0,670**	0,290	0,011	0,024
1006,841952	**0,730**	0,229	0,010	0,026
1008,770768	**0,780**	0,180	0,009	0,027
1010,699584	**0,820**	0,140	0,009	0,028
1012,6284	**0,848**	0,113	0,008	0,028
1014,557216	**0,872**	0,089	0,008	0,029
1016,486032	**0,891**	0,070	0,008	0,028
1018,414848	**0,906**	0,057	0,007	0,027
1020,343664	**0,917**	0,048	0,007	0,025
1022,27248	**0,924**	0,043	0,007	0,024
1024,201296	**0,931**	0,038	0,007	0,023
1026,130112	**0,934**	0,034	0,007	0,022
1028,058928	**0,939**	0,032	0,006	0,020
1029,987744	**0,944**	0,030	0,006	0,018
1031,91656	**0,949**	0,027	0,005	0,016
1033,845376	**0,954**	0,024	0,005	0,016
1035,774192	**0,956**	0,021	0,005	0,016
1037,703008	**0,960**	0,019	0,004	0,015
1039,631824	**0,963**	0,016	0,004	0,014
1041,56064	**0,964**	0,015	0,004	0,014
1043,489456	**0,966**	0,013	0,004	0,015
1045,418272	**0,966**	0,012	0,004	0,015
1047,347088	**0,968**	0,010	0,005	0,015
1049,275904	**0,970**	0,008	0,005	0,015
1051,20472	**0,973**	0,005	0,004	0,014
1053,133536	**0,976**	0,002	0,004	0,014
1055,062352	**0,978**	0,000	0,004	0,014
1056,991168	**0,979**	0,000	0,004	0,013
1058,919984	**0,979**	0,000	0,004	0,013
1060,8488	**0,980**	0,001	0,004	0,011
1062,777616	**0,980**	0,002	0,004	0,011
1064,706432	**0,977**	0,003	0,004	0,012
1066,635248	**0,976**	0,006	0,004	0,012
1068,564064	**0,974**	0,009	0,004	0,010
1070,49288	**0,973**	0,012	0,004	0,009
1072,421696	**0,969**	0,016	0,004	0,008
1074,350512	**0,964**	0,022	0,004	0,008

1076,279328	**0,958**	0,028	0,004	0,007
1078,208144	**0,951**	0,037	0,003	0,006
1080,13696	**0,943**	0,045	0,003	0,004
1082,065776	**0,935**	0,055	0,003	0,003
1083,994592	**0,931**	0,060	0,002	0,003
1085,923408	**0,928**	0,064	0,002	0,002
1087,852224	**0,925**	0,066	0,002	0,002
1089,78104	**0,925**	0,065	0,002	0,001
1091,709856	**0,923**	0,067	0,003	0,001
1093,638672	**0,920**	0,069	0,003	0,001
1095,567488	**0,914**	0,074	0,003	0,001
1097,496304	**0,906**	0,081	0,004	0,001
1099,42512	**0,899**	0,088	0,004	0,000
1101,353936	**0,889**	0,095	0,005	0,000
1103,282752	**0,883**	0,098	0,007	0,000
1105,211568	**0,875**	0,103	0,008	0,000
1107,140384	**0,865**	0,107	0,009	0,000
1109,0692	**0,855**	0,114	0,010	0,000
1110,998016	**0,845**	0,121	0,012	0,000
1112,926832	**0,845**	0,123	0,011	0,000
1114,855648	**0,846**	0,127	0,009	0,000
1116,784464	**0,860**	0,117	0,008	0,000
1118,71328	**0,889**	0,095	0,006	0,000
1120,642096	**0,915**	0,073	0,005	0,000
1122,570912	**0,934**	0,057	0,004	0,000
1124,499728	**0,950**	0,043	0,003	0,000
1126,428544	**0,967**	0,028	0,002	0,000
1128,35736	**0,978**	0,018	0,001	0,000
1130,286176	**0,984**	0,012	0,001	0,000
1132,214992	**0,989**	0,006	0,001	0,000
1134,143808	**0,992**	0,002	0,001	0,000
1136,072624	**0,993**	0,000	0,001	0,000
1138,00144	**0,992**	0,000	0,001	0,000
1139,930256	**0,988**	0,002	0,001	0,000
1141,859072	**0,981**	0,006	0,002	0,000
1143,787888	**0,974**	0,008	0,002	0,001
1145,716704	**0,966**	0,011	0,004	0,002
1147,64552	**0,961**	0,013	0,004	0,003
1149,574336	**0,954**	0,015	0,004	0,004
1151,503152	**0,946**	0,020	0,003	0,005
1153,431968	**0,937**	0,022	0,002	0,008
1155,360784	**0,931**	0,020	0,001	0,011
1157,2896	**0,920**	0,019	0,000	0,015
1159,218416	**0,903**	0,019	0,000	0,021
1161,147232	**0,878**	0,024	0,000	0,030
1163,076048	**0,859**	0,019	0,000	0,042
1165,004864	**0,829**	0,012	0,000	0,054
1166,93368	**0,782**	0,007	0,000	0,076
1168,862496	**0,727**	0,007	0,000	0,101
1170,791312	**0,648**	0,005	0,000	0,138

1172,720128	**0,535**	0,006	0,000	0,172
1174,648944	**0,371**	0,007	0,000	0,229
1176,57776	0,165	0,007	0,003	0,322
1178,506576	0,032	0,016	0,006	0,368
1180,435392	0,004	0,021	0,005	0,365
1182,364208	0,058	0,018	0,001	0,319
1184,293024	0,097	0,032	0,000	0,268
1186,22184	0,085	0,048	0,000	0,230
1188,150656	0,059	0,069	0,001	0,223
1190,079472	0,032	0,060	0,004	0,244
1192,008288	0,013	0,046	0,006	0,247
1193,937104	0,001	0,042	0,008	0,239
1195,86592	0,006	0,028	0,008	0,224
1197,794736	0,060	0,023	0,008	0,194
1199,723552	0,186	0,010	0,013	0,166
1201,652368	0,396	0,000	0,014	0,115
1203,581184	**0,581**	0,003	0,012	0,074
1205,51	**0,693**	0,008	0,012	0,053
1207,438816	**0,746**	0,017	0,010	0,040
1209,367632	**0,781**	0,027	0,010	0,030
1211,296448	**0,804**	0,039	0,006	0,019
1213,225264	**0,820**	0,052	0,006	0,017
1215,15408	**0,820**	0,070	0,007	0,017
1217,082896	**0,828**	0,079	0,005	0,014
1219,011712	**0,836**	0,080	0,005	0,013
1220,940528	**0,846**	0,080	0,004	0,011
1222,869344	**0,867**	0,066	0,003	0,007
1224,79816	**0,879**	0,057	0,002	0,006
1226,726976	**0,885**	0,054	0,001	0,007
1228,655792	**0,892**	0,050	0,002	0,009
1230,584608	**0,897**	0,045	0,002	0,010
1232,513424	**0,898**	0,041	0,002	0,012
1234,44224	**0,894**	0,042	0,002	0,016
1236,371056	**0,901**	0,035	0,001	0,020
1238,299872	**0,907**	0,024	0,001	0,024
1240,228688	**0,907**	0,020	0,002	0,024
1242,157504	**0,913**	0,011	0,001	0,026
1244,08632	**0,915**	0,003	0,002	0,032
1246,015136	**0,913**	0,000	0,002	0,038
1247,943952	**0,901**	0,007	0,004	0,039
1249,872768	**0,878**	0,028	0,004	0,037
1251,801584	**0,833**	0,068	0,005	0,039
1253,7304	**0,775**	0,124	0,005	0,039
1255,659216	**0,700**	0,203	0,005	0,038
1257,588032	**0,618**	0,288	0,005	0,032
1259,516848	**0,544**	0,372	0,003	0,023
1261,445664	**0,460**	0,452	0,005	0,028
1263,37448	0,391	**0,513**	0,009	0,036
1265,303296	0,323	**0,587**	0,008	0,032
1267,232112	0,266	**0,647**	0,008	0,030

1269,160928	0,210	**0,710**	0,006	0,026
1271,089744	0,162	**0,756**	0,006	0,028
1273,01856	0,130	**0,769**	0,011	0,044
1274,947376	0,101	**0,776**	0,018	0,061
1276,876192	0,067	**0,798**	0,020	0,069
1278,805008	0,041	**0,822**	0,018	0,072
1280,733824	0,022	**0,834**	0,020	0,076
1282,66264	0,011	**0,829**	0,021	0,089
1284,591456	0,003	**0,844**	0,016	0,087
1286,520272	0,001	**0,873**	0,008	0,067
1288,449088	0,000	**0,881**	0,005	0,062
1290,377904	0,000	**0,849**	0,011	0,089
1292,30672	0,001	**0,817**	0,014	0,113
1294,235536	0,004	**0,808**	0,014	0,120
1296,164352	0,009	**0,815**	0,011	0,111
1298,093168	0,021	**0,782**	0,012	0,128
1300,021984	0,037	**0,745**	0,014	0,144
1301,9508	0,060	**0,706**	0,013	0,158
1303,879616	0,091	**0,679**	0,010	0,158
1305,808432	0,130	**0,659**	0,007	0,147
1307,737248	0,169	**0,650**	0,002	0,127
1309,666064	0,203	**0,624**	0,001	0,121
1311,59488	0,223	**0,660**	0,006	0,063
1313,523696	0,211	**0,688**	0,016	0,044
1315,452512	0,240	**0,674**	0,007	0,040
1317,381328	0,229	**0,673**	0,028	0,032
1319,310144	0,261	**0,639**	0,021	0,037
1321,23896	0,271	**0,614**	0,000	0,076
1323,167776	0,277	**0,576**	0,001	0,105
1325,096592	0,265	**0,580**	0,002	0,110
1327,025408	0,253	**0,596**	0,001	0,105
1328,954224	0,242	**0,614**	0,001	0,099
1330,88304	0,244	**0,615**	0,001	0,100
1332,811856	0,256	**0,598**	0,001	0,104
1334,740672	0,272	**0,626**	0,001	0,064
1336,669488	0,278	**0,579**	0,098	0,004
1338,598304	0,212	**0,591**	0,162	0,000
1340,52712	0,268	**0,592**	0,096	0,007
1342,455936	0,353	**0,448**	0,003	0,139
1344,384752	**0,379**	0,368	0,006	0,178
1346,313568	0,370	**0,422**	0,002	0,153
1348,242384	0,319	**0,508**	0,001	0,125
1350,1712	0,276	**0,570**	0,000	0,109
1352,100016	0,230	**0,629**	0,000	0,099
1354,028832	0,184	**0,704**	0,000	0,074
1355,957648	0,137	**0,756**	0,000	0,069
1357,886464	0,098	**0,808**	0,001	0,058
1359,81528	0,053	**0,876**	0,010	0,029
1361,744096	0,034	**0,890**	0,036	0,009
1363,672912	0,017	**0,913**	0,025	0,010

1365,601728	0,004	**0,905**	0,008	0,042
1367,530544	0,003	**0,903**	0,001	0,028
1369,45936	0,008	**0,890**	0,000	0,022
1371,388176	0,003	**0,900**	0,011	0,009
1373,316992	0,000	**0,869**	0,064	0,001
1375,245808	0,001	**0,849**	0,069	0,001
1377,174624	0,009	**0,833**	0,044	0,002
1379,10344	0,022	**0,782**	0,055	0,001
1381,032256	0,008	**0,733**	0,100	0,005
1382,961072	0,002	**0,659**	0,148	0,009
1384,889888	0,033	**0,566**	0,254	0,001
1386,818704	0,123	**0,405**	0,355	0,003
1388,74752	0,200	0,339	**0,339**	0,000
1390,676336	0,258	0,195	**0,311**	0,003
1392,605152	**0,416**	0,102	0,381	0,001
1394,533968	0,387	0,099	**0,403**	0,003
1396,462784	0,417	0,068	**0,418**	0,005
1398,3916	**0,453**	0,048	0,400	0,004
1400,320416	**0,596**	0,008	0,289	0,000
1402,249232	**0,550**	0,018	0,220	0,001
1404,178048	**0,516**	0,008	0,306	0,004
1406,106864	**0,369**	0,000	0,234	0,002
1408,03568	0,276	0,051	0,162	0,000
1409,964496	0,162	0,020	0,152	0,000
1411,893312	0,067	0,005	0,107	0,002
1413,822128	0,023	0,010	0,079	0,008
1415,750944	0,041	**0,341**	0,267	0,009
1417,67976	0,012	**0,452**	0,196	0,003
1419,608576	0,011	**0,541**	0,039	0,001
1421,537392	0,110	**0,465**	0,004	0,004
1423,466208	0,119	**0,589**	0,002	0,000
1425,395024	**0,359**	0,312	0,090	0,005
1427,32384	**0,377**	0,249	0,151	0,015
1429,252656	0,258	**0,478**	0,054	0,020
1431,181472	0,267	**0,475**	0,047	0,027
1433,110288	0,260	**0,442**	0,046	0,038
1435,039104	0,148	**0,552**	0,010	0,082
1436,96792	0,153	**0,504**	0,018	0,125
1438,896736	0,211	**0,316**	0,074	0,173
1440,825552	0,213	0,008	0,102	**0,360**
1442,754368	0,151	0,003	0,081	**0,434**
1444,683184	0,126	0,012	0,022	**0,416**
1446,612	0,025	**0,428**	0,112	0,175
1448,540816	0,023	**0,387**	0,128	0,194
1450,469632	0,000	0,100	0,128	**0,243**
1452,398448	0,043	0,173	**0,611**	0,025
1454,327264	0,021	0,161	**0,344**	0,211
1456,25608	0,003	0,186	0,177	**0,332**
1458,184896	0,005	0,207	0,054	**0,398**
1460,113712	0,082	0,084	0,052	**0,428**

1462,042528	0,099	0,006	**0,396**	0,294
1463,971344	0,011	0,043	0,145	**0,486**
1465,90016	0,015	0,025	0,269	**0,429**
1467,828976	0,009	0,003	0,236	**0,513**
1469,757792	0,114	0,050	0,034	**0,489**
1471,686608	0,212	0,219	0,074	**0,258**
1473,615424	0,188	**0,319**	0,072	0,194
1475,54424	0,094	**0,558**	0,029	0,113
1477,473056	0,000	**0,466**	0,147	0,169
1479,401872	**0,313**	0,177	0,005	0,187
1481,330688	**0,303**	0,192	0,010	0,190
1483,259504	0,275	0,049	0,022	**0,296**
1485,18832	**0,189**	0,147	0,159	0,115
1487,117136	0,049	0,265	**0,500**	0,005
1489,045952	0,034	0,204	**0,678**	0,006
1490,974768	0,019	0,181	**0,674**	0,000
1492,903584	0,059	0,000	**0,612**	0,067
1494,8324	0,010	0,092	0,252	**0,269**
1496,761216	0,001	0,015	**0,700**	0,051
1498,690032	0,029	0,078	**0,558**	0,084
1500,618848	0,008	0,017	**0,871**	0,001
1502,547664	0,002	0,130	**0,799**	0,000
1504,47648	0,022	0,164	**0,702**	0,017
1506,405296	0,014	0,006	**0,902**	0,022
1508,334112	0,016	0,000	**0,891**	0,044
1510,262928	0,021	0,000	**0,881**	0,052
1512,191744	0,035	0,058	**0,827**	0,021
1514,12056	0,031	0,048	**0,834**	0,032
1516,049376	0,047	0,030	**0,837**	0,038
1517,978192	0,066	0,104	**0,755**	0,019
1519,907008	0,074	0,190	**0,669**	0,009
1521,835824	0,086	0,249	**0,604**	0,005
1523,76464	0,088	0,312	**0,543**	0,002
1525,693456	0,081	0,346	**0,522**	0,002
1527,622272	0,084	0,408	**0,461**	0,000
1529,551088	0,081	**0,540**	0,337	0,001
1531,479904	0,057	**0,498**	0,414	0,000
1533,40872	0,048	**0,532**	0,380	0,001
1535,337536	0,066	**0,548**	0,327	0,000
1537,266352	0,015	**0,699**	0,248	0,011
1539,195168	0,013	**0,701**	0,239	0,012
1541,123984	0,008	**0,720**	0,222	0,014
1543,0528	0,001	**0,726**	0,223	0,014
1544,981616	0,000	**0,750**	0,198	0,021
1546,910432	0,000	**0,822**	0,104	0,040
1548,839248	0,005	**0,739**	0,187	0,020
1550,768064	0,011	**0,695**	0,216	0,015
1552,69688	0,022	**0,770**	0,150	0,028
1554,625696	0,036	**0,738**	0,162	0,038
1556,554512	0,049	**0,727**	0,157	0,047

1558,483328	0,062	**0,703**	0,165	0,052
1560,412144	0,076	**0,709**	0,124	0,075
1562,34096	0,088	**0,717**	0,030	0,119
1564,269776	0,142	**0,651**	0,150	0,035
1566,198592	0,176	**0,614**	0,157	0,037
1568,127408	0,169	**0,620**	0,135	0,067
1570,056224	0,187	**0,603**	0,119	0,083
1571,98504	0,225	**0,577**	0,130	0,060
1573,913856	0,225	**0,594**	0,092	0,081
1575,842672	0,227	**0,580**	0,091	0,092
1577,771488	0,242	**0,563**	0,082	0,101
1579,700304	0,278	**0,526**	0,079	0,101
1581,62912	0,285	**0,508**	0,066	0,118
1583,557936	0,278	**0,505**	0,065	0,125
1585,486752	0,262	**0,509**	0,068	0,132
1587,415568	0,239	**0,526**	0,074	0,132
1589,344384	0,210	**0,547**	0,088	0,129
1591,2732	0,171	**0,580**	0,093	0,130
1593,202016	0,132	**0,613**	0,096	0,134
1595,130832	0,098	**0,654**	0,091	0,134
1597,059648	0,071	**0,683**	0,074	0,145
1598,988464	0,052	**0,711**	0,063	0,147
1600,91728	0,037	**0,735**	0,067	0,141
1602,846096	0,028	**0,758**	0,071	0,127
1604,774912	0,024	**0,777**	0,062	0,123
1606,703728	0,021	**0,792**	0,065	0,110
1608,632544	0,016	**0,813**	0,056	0,104
1610,56136	0,015	**0,825**	0,043	0,107
1612,490176	0,015	**0,836**	0,032	0,106
1614,418992	0,005	**0,859**	0,024	0,104
1616,347808	0,001	**0,868**	0,022	0,101
1618,276624	0,000	**0,876**	0,014	0,101
1620,20544	0,002	**0,894**	0,031	0,069
1622,134256	0,000	**0,885**	0,024	0,083
1624,063072	0,005	**0,881**	0,020	0,087
1625,991888	0,012	**0,886**	0,017	0,078
1627,920704	0,033	**0,864**	0,015	0,080
1629,84952	0,058	**0,837**	0,008	0,086
1631,778336	0,077	**0,820**	0,011	0,082
1633,707152	0,091	**0,790**	0,016	0,089
1635,635968	0,149	**0,736**	0,014	0,085
1637,564784	0,211	**0,681**	0,016	0,077
1639,4936	0,286	**0,615**	0,005	0,074
1641,422416	0,291	**0,611**	0,004	0,074
1643,351232	0,268	**0,631**	0,009	0,074
1645,280048	0,296	**0,574**	0,008	0,094
1647,208864	0,369	**0,502**	0,007	0,090
1649,13768	0,379	**0,494**	0,006	0,089
1651,066496	0,378	**0,483**	0,003	0,101
1652,995312	**0,447**	0,408	0,001	0,102

1654,924128	**0,504**	0,350	0,001	0,100
1656,852944	**0,579**	0,294	0,002	0,081
1658,78176	**0,626**	0,248	0,000	0,077
1660,710576	**0,596**	0,253	0,002	0,099
1662,639392	**0,692**	0,164	0,000	0,089
1664,568208	**0,777**	0,094	0,000	0,074
1666,497024	**0,783**	0,091	0,000	0,071
1668,42584	**0,817**	0,062	0,002	0,064
1670,354656	**0,846**	0,038	0,002	0,060
1672,283472	**0,860**	0,023	0,001	0,061
1674,212288	**0,869**	0,012	0,001	0,062
1676,141104	**0,881**	0,004	0,000	0,060
1678,06992	**0,901**	0,001	0,000	0,042
1679,998736	**0,899**	0,004	0,037	0,017
1681,927552	**0,908**	0,004	0,014	0,029
1683,856368	**0,908**	0,005	0,004	0,037
1685,785184	**0,905**	0,006	0,000	0,042
1687,714	**0,917**	0,020	0,008	0,018
1689,642816	**0,914**	0,039	0,003	0,008
1691,571632	**0,925**	0,017	0,001	0,022
1693,500448	**0,872**	0,017	0,005	0,061
1695,429264	**0,882**	0,023	0,000	0,053
1697,35808	**0,891**	0,023	0,000	0,047
1699,286896	**0,878**	0,027	0,001	0,054
1701,215712	**0,852**	0,027	0,005	0,070
1703,144528	**0,873**	0,024	0,003	0,058
1705,073344	**0,872**	0,018	0,000	0,063
1707,00216	**0,843**	0,012	0,013	0,081
1708,930976	**0,869**	0,009	0,011	0,050
1710,859792	**0,840**	0,002	0,017	0,066
1712,788608	**0,729**	0,015	0,000	0,169
1714,717424	**0,559**	0,071	0,004	0,264
1716,64624	**0,398**	0,129	0,036	0,330
1718,575056	0,272	0,154	0,111	**0,355**
1720,503872	0,190	0,135	0,267	**0,314**
1722,432688	0,121	0,114	0,320	**0,347**
1724,361504	0,048	0,086	0,302	**0,439**
1726,29032	0,002	0,100	0,342	**0,448**
1728,219136	0,007	0,269	0,136	**0,470**
1730,147952	0,007	0,327	0,004	**0,517**
1732,076768	0,021	0,309	0,019	**0,522**
1734,005584	0,023	0,276	0,036	**0,540**
1735,9344	0,018	0,245	0,101	**0,524**
1737,863216	0,038	0,214	0,070	**0,558**
1739,792032	0,049	0,122	0,018	**0,645**
1741,720848	0,079	0,010	0,151	**0,508**
1743,649664	0,026	0,117	**0,728**	0,000
1745,57848	0,004	0,165	**0,691**	0,012
1747,507296	0,001	0,227	**0,643**	0,007
1749,436112	0,004	0,253	**0,583**	0,001

1751,364928	0,002	0,261	**0,356**	0,097
1753,293744	0,006	0,080	0,080	**0,330**
1755,22256	0,000	**0,292**	0,126	0,150
1757,151376	0,010	0,208	0,104	0,234
1759,080192	0,001	0,063	0,060	0,358
1761,009008	0,040	0,071	0,060	0,305
1762,937824	0,050	0,018	0,011	0,337
1764,86664	0,127	0,024	0,000	0,346
1766,795456	0,118	0,078	0,105	0,197
1768,724272	0,125	0,071	0,150	0,152
1770,653088	0,135	0,044	0,122	0,153
1772,581904	0,142	0,040	0,090	0,143
1774,51072	0,158	0,030	0,064	0,163
1776,439536	0,190	0,030	0,050	0,152
1778,368352	0,204	0,082	0,072	0,121
1780,297168	0,157	0,161	0,142	0,082
1782,225984	0,158	0,128	0,068	0,130
1784,1548	0,152	0,200	0,063	0,109
1786,083616	0,130	0,032	0,169	**0,284**
1788,012432	**0,291**	0,063	0,006	0,145
1789,941248	0,084	**0,497**	0,136	0,013
1791,870064	0,080	**0,515**	0,121	0,017
1793,79888	0,089	**0,496**	0,089	0,031
1795,727696	0,014	**0,717**	0,110	0,001
1797,656512	0,028	**0,565**	0,167	0,002
1799,585328	0,057	**0,550**	0,134	0,010
1801,514144	0,058	**0,553**	0,129	0,012

Appendix D - Equations

In order to predict the macromolecular composition of bacteria cell surface through XPS data, the following set of equations was used.

$$\frac{\bar{C}=O}{C} = 0{,}279\left(\frac{C_{Prot}}{C}\right) + 0{,}167\left(\frac{C_{Poly}}{C}\right) \quad \text{(Equation D.1)}$$

$$\frac{\bar{C}-(O,N)}{C} = 0{,}293\left(\frac{C_{Prot}}{C}\right) + 0{,}833\left(\frac{C_{Poly}}{C}\right) \quad \text{(Equation D.2)}$$

$$\frac{\bar{C}-(C,H)}{C} = 0{,}428\left(\frac{C_{Prot}}{C}\right) + 1{,}000\left(\frac{C_{Hydroc}}{C}\right) \quad \text{(Equation D.3)}$$

Where $\left(\frac{C_{Prot}}{C}\right)$ represents the ratio between carbons associated to proteins and total carbon; $\left(\frac{C_{Poly}}{C}\right)$ carbons associated to polysaccharides and total carbon and $\left(\frac{C_{Hydroc}}{C}\right)$ carbons associated to hydrocarbons and total carbon.